IntechOpen

Metamorphic Rocks as the Key to Understanding Geodynamic Processes

Edited by Károly Németh

Metamorphic Rocks as the Key to Understanding Geodynamic Processes

Edited by Károly Németh

Published in London, United Kingdom

Metamorphic Rocks as the Key to Understanding Geodynamic Processes
http://dx.doi.org/10.5772/intechopen.1000289
Edited by Károly Németh

Contributors
Harel Thomas, Haritabh Rana, Haroun A. Mohamed, Károly Németh, Rafat Zaki, Shehata Ali, Sándor Józsa, Tamás Sági, Tarek Sedki, Vladimir Shchiptsov

First published in London, United Kingdom, 2024 by IntechOpen
IntechOpen is the global imprint of INTECHOPEN LIMITED, registered in England and Wales, registration number: 11086078, 167-169 Great Portland Street, London, W1W 5PF, United Kingdom

British Library Cataloguing-in-Publication Data
A catalogue record for this book is available from the British Library

Additional hard and PDF copies can be obtained from orders@intechopen.com

Metamorphic Rocks as the Key to Understanding Geodynamic Processes
Edited by Károly Németh
p. cm.
Print ISBN 978-0-85466-494-8
Online ISBN 978-0-85466-493-1
eBook (PDF) ISBN 978-0-85466-495-5

Meet the editor

Károly Németh is an expert at the Saudi Geological Survey working on volcanology, geohazard, and geoheritage of volcanic fields of the Arabian Peninsula. He is also a senior researcher at the Institute of Earth Physics and Space Science, Hungary; Adjunct Professor of Volcanic Risk Solutions, Massey University, New Zealand; and a research affiliate at the National Institute of Geophysics and Volcanology, Italy. He was a member of the Executive Committee of the International Association of Volcanology and Chemistry of Earth Interior, leading its Volcaniclastic Sediments, Monogenetic Volcanism and Volcanic Geoheritage commissions. Currently, he is a vice president of the International Association of Sedimentologists and chair of the International Union of Geological Sciences' Sub-commission on Geological Heritage Sites.

Contents

Preface

Metamorphic Rocks as the Key to Understanding Geodynamic Processes provides a snapshot of current advances in metamorphic geology research. As a traditional field-based geology subject, metamorphic geology has evolved dramatically in the last decades. This book offers thorough overviews of some key aspects of metamorphic geology, including geothermobarometric methods and metamorphic processes such as metasomatism and ophiolite belts. In general, metamorphic geology research is strongly represented in the literature, with a steady stream of publications appearing within bibliometric databases such as Scopus. Keyword searches within titles, abstracts, and keywords for "metamorphic geology" and "metamorphism" yielded 2602 publications (as of 27 February 2024) since 1906, with marked step-like increases in the early 2000s and around 2019. Earth and planetary sciences are still the main disciplines where metamorphic geology research outputs are classified, indicating its strong standing as a basic geological subject of research (**Figure 1**).

Chapter 1 provides an introduction to new advances in metamorphic geology.

Chapter 2 offers a comprehensive overview of garnet, one of the most common minerals used for geothermobarometry within metamorphic petrogenesis. This seemingly narrow subject, according to bibliometric data, occupies a wide segment of metamorphic geology research, indicating the valid claim of the chapter in which it is discussed that the use of garnet in geothermobarometry should be included as an important

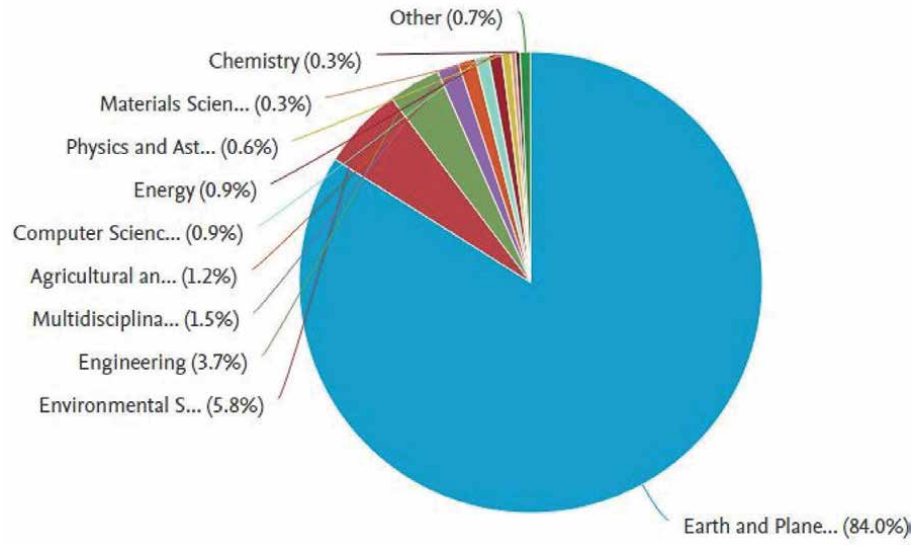

Figure 1.
Subject areas of published papers identified under metamorphic geology and metamorphism search categories in Scopus (1909-2024).

research field within metamorphic geology. The chapter is based on direct research experience and provides critical summaries.

Chapter 3 discusses the formation of sillimanite minerals in the Fennoscandian Shield, a segment of the Earth's crust.

Chapters 4 and 5 examine the geodynamically important subject of ophiolites. While ophiolites are considered thrust sheets of ancient oceanic crust and the upper part of mantle rocks that have been uplifted and exposed above sea level and often emplaced on top of the continental lithosphere, they represent important geotectonic belts with diverse and unique rock assemblages associated with metamorphic processes. In this sense, ophiolite belts are commonly associated with specific zonation of rock units formed in various types of metamorphism, such as those recorded in iconic locations in Oman. Within these unique rock zones, there are economically significant areas with specific mineralization as well as formation of rocks such as various types of "greenstones" that also play key roles in geocultural developments such as the pounamu in New Zealand.

Overall, this book offers insight into developments across the broad and diverse field of metamorphic geology. Although the variety of trends and major research directions are far larger than represented within this book, we hope that this volume is useful and will inspire future research.

This book would have not been possible without the support of many individuals. I would like to thank the staff at IntechOpen as well as my colleagues who provided expert advice.

Károly Németh
Massey University,
Palmerston North, New Zealand

Saudi Geological Survey,
Jeddah, Kingdom of Saudi Arabia

Institute of Earth Physics and Space Science,
Sopron, Hungary

The Geoconservation Trust Aotearoa Pacific,
Opotiki, New Zealand

Chapter 1

Introductory Chapter: Introduction to New Advances in Metamorphic Geology

Károly Németh

1. Introduction

1.1 Metamorphic geology as the core of traditional field geology

Metamorphism in the context of geology (https://opengeology.org/petrology/9-intro-to-metamorphism/ – accessed on 25 February 2024) is a process that changes the mineralogy, microstructure, texture, and chemical compositions of any rocks, normally over long time scale (millions of years) and in a dominantly solid state [1]. Fluid-driven transition of rock textures and compositions are commonly viewed as a special part of metamorphism (or not even included at all within metamorphism) normally associated with some fluid migration controlled by magmatism such as metasomatism on a sea floor in small or lithospheric scales, including ophiolites [2–7]. In general, metamorphism is understood as a process that forms rock assemblages directly in response to gradually changing physical and chemical conditions. Metamorphism can be considered to begin when the original rock (protolith) faces new and persistent physical or chemical conditions markedly different from its original environment, or better to say the difference can be considered in a significant scale (https://geologyglasgow.org.uk/minerals-rocks-fossils/metamorphic-rocks/ - accessed on 25 February 2024). The classical view on metamorphism is based on the physical-chemical parameters to define the metamorphic environment including the temperature and pressure being the most important ones (https://www.geolsoc.org.uk/ks3/gsl/education/resources/rockcycle/page3576.html – accessed on 25 February 2024). In contrast, fluid availability and nature as well as the nature of the tectonic stress field are other aspects to view metamorphism [8, 9]. These categories almost automatically determine the main approaches metamorphic geology follow. Most importantly and traditionally, the most abundant method is the chemical characterization of the processes (e.g., petrography and petrology), following geochemical methods such as bulk chemical study of the metamorphic products or mineral-level documentation of the chemical (and textural) changes [10]. These methods are the most obvious ones one can think of about metamorphic geology.

2. Advances in scale to track steps of metamorphism

The main advances in this field are centered around the application of new chemical systematics to follow mineral phase changes and link them to a geological process. High-resolution microchemistry is commonly performed to lower the

potential resolution of time scales of the metamorphic events recognizable; hence, a strong drive is visible for developing new techniques to determine the ages of various metamorphic events in the micromineralogy level [11–14]. As metamorphism may occur over a wide range of temperature and pressure conditions, the applicable chemical techniques to define these conditions have formed a great variety of research avenues over the past decades. In this perspective, there is a clear and gradual transition from experts focusing on the primary rocks such as sedimentary successions specialized to recognize the early stages of solid phase transition of the original mineral constitutes of sediments and sedimentary rocks to experts clearly dealing with the metamorphic products from the sedimentary protoliths [15–20]. It is also a common approach that the metamorphism starts when the diagenesis completed. While this sounds a trivia, to "capture" the distinct line between diagenesis and metamorphism is not simple. This fuzzy boundary between diagenesis and metamorphism naturally generated various schools following different distinctive parameters since the early 70s in the dawn of metamorphic geology. As in regional sense, these boundaries follow some temperature-pressure conditions, and it is not a surprise that the boundaries are also not fixed as they are also heavily dependent on the actual region geothermal gradients; hence, the limits are different in regions with high geothermal gradients such as orogenic belts [21–23].

3. Temperature-pressure concept of metamorphism

In the other end of the temperature-pressure spectrum, a similar problem exists as great variations known among suggested barriers. In extreme high temperature and/or pressure, the rock starts to behave as melt and shows similar features expected with igneous rocks. Melting itself in this context is not considered to be a metamorphic process, and we are entering to the unsharp boundary between metamorphic and magmatic processes. However, as melting considered in a rock when the temperature exceeds its wet solidus that is normally around 650°C for most metasediments and metabasites, the beginning of melting does not mean the end of metamorphism. There is a stage when potential melting through the metamorphic grades can take place, but it is hardly ever occurred in *en mass* and large scale; instead, following stages and pulses is likely associated with some external forcing mechanism as tectonism. Some research groups hence favor to delineate a fine line between metamorphic melting and igneous melting. The extracted melts form purely igneous intrusions within the crust normally shallower than the melting anomaly. In contrast, in situ *restites* that are the solid mineral assemblages after melt segregation may form gneisses or granulites of high metamorphic grade, or form migmatites [24] together with the locally segregated melts [25, 26]. Thermobarometer revealed that igneous intrusions at shallow crustal level indicate much lower temperatures from high-grade metamorphic rocks in the source region. The highest measured granulite formation temperatures suggest about 1000–1100°C considered to be the highest metamorphic temperatures [27]. It is obvious that metamorphic geology advanced significantly in recent years to refine these boundaries, or better to say look at metamorphic processes withing the broader geological context without implying the need to follow strict boundaries among processes. To explore the spectrum of pressure conditions within metamorphic processes opened new research directions and recognition of characteristic diagnostic minerals to look for. Ultra-high pressures of metamorphism [28, 29] have been recognized from rocks suspected to be subducted over the depth of

300 km followed by rapid uplift and preservation. These findings determine also new research directions to locate rocks that can be viewed as messengers of extreme and long sustained conditions.

4. Texture recognition techniques from micro to landscape scale

New techniques and modeling are also emerged just as more refined textural analysis of metamorphic fabric. The new mineral phases generated by metamorphic processes on the expenses of original minerals generate typical metamorphic textures extensively studied. The recognition of major textural changes is characteristic for the major physical-chemical condition changes. This means that, in metamorphic geology, the recognition of rock textures, such as metamorphic fabric, is a critical aspect of research and a field where new advances achieved due to the rapid development

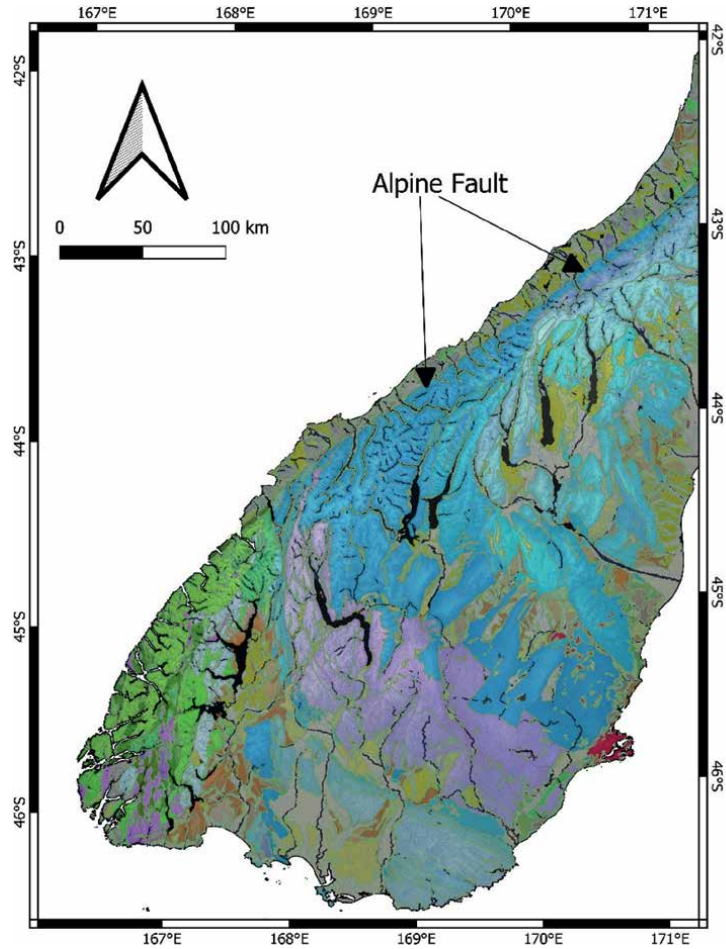

Figure 1.
The South Island of New Zealand 1 to 1 million scale geological map overlaid on the 8 m resolution digital terrain model (LINZ) demonstrating well the connection between the structural elements and morphology of the region. The metamorphic grade increases toward the main active fault (Alpine Fault) within the Permo-Triassic Eastern Province's Rakaia Terrain. Higher grade greenschist zones marked by purple grades are already part of another terrain, the Triassic Eastern Provinces' Caples Terrain. For clarity, large lakes are marked with black fields.

and availability of advanced technologies such as image analysis and remote sensing techniques of microlevel identification of various phases [30–32]. The combination of remote sensing techniques, Geographic Information Systems (GIS), modeling with microanalytical techniques successfully applied within classical igneous petrology, but in recent times, metamorphic geology also follows these trends to benefit from the seemingly distant disciplines.

Metamorphic geology is also closely linked to structural geology (**Figure 1**). Most of the metamorphic textures are the most complex 3D textural and structural assemblages from landscape to microscales (**Figures 2** and **3**). While traditional mapping is still the key for recording and interpreting such complex textures in micro to landscape scales, the fusion of various high resolution digital elevation modeling, including LiDAR and structure for motions (SfM) photogrammetry tools allowing us to reach mm-scale resolution of 3D models capable to capture fine details earlier, was nearly impossible [33–35]. While the combination of metamorphic and structural geology is still in its infantry by application, the advanced technologies, the direction is clear. Other than visible light sensors, multispectral analysis or laser scanning are just among few main tracks, and high-resolution structural analysis is possible. Combining the high-resolution spatial data from micro to landscape scale with the advanced chemical tools through machine learning and AI will clearly provide a revolution within metamorphic geology to understand the evolution of various lithosphere segments and identify key patterns.

Metamorphic geology is also just in the first steps to be more known within geoheritage and geodiversity research [36–38]. As our planet facing with global and planetary changes, metamorphism is one fundamental aspect of geology that produced numerous geoheritages where dedicated metamorphic geology heritage sites should be systematically explored. We will likely experience an explosion of the

Figure 2.
Higher grade greenschist along the Alpine Fault in the South Island of New Zealand.

Figure 3.
Strong deformation along the Alpine Fault in the outcrop scale offering perfect opportunity to use high-resolution advanced technologies including applied remote sensing of mapping the link between structural patterns and metamorphic zones.

number of such research in the future. Overall, metamorphic geology has experienced dramatic advances in recent times, and the recognition of these steps is important in recurrent scientific report such as this InTech book.

Author details

Károly Németh[1,2,3,4]

1 Massey University, Palmerston North, New Zealand

2 Saudi Geological Survey, Jeddah, Kingdom of Saudi Arabia

3 Institute of Earth Physics and Space Science, Sopron, Hungary

4 The Geoconservation Trust Aotearoa Pacific, New Zealand

*Address all correspondence to: knemeth69@gmail.com

IntechOpen

References

[1] Gillen C. Metamorphic Geology: An Introduction to Tectonic and Metamorphic Processes. Dordrecht: Springer Science & Business Media; 1982. p. 146. DOI: 10.1007/978-94-011-5978-4. Print ISBN 978-0-04-551058-0, Online ISBN 978-94-011-5978-4

[2] Lesher CE, Spera FJ. Chapter 5 - thermodynamic and transport properties of silicate melts and magma. In: Sigurdsson H, editor. The Encyclopedia of Volcanoes (Second Edition). Amsterdam: Academic Press; 2015. pp. 113-141

[3] Ran Q et al. Chapter 3 – Volcanic reservoir mode. In: Ran Q et al., editors. Development of Volcanic Gas Reservoirs. Elsevier Science & Technology. San Diego: Petroleum Industry Press; 2018(2019). pp. 115-266. DOI: 10.1016/B978-0-12-816132-6.00003-X. Print ISBN – 9780128161326, Online ISBN – 9780128163061

[4] Eriksson PG et al. Chapter 3 - tectonism and mantle plumes through time. In: Eriksson PG et al., editors. Developments in Precambrian Geology. Dordrecht: Elsevier; 2004. pp. 161-270. DOI: 10.1016/S0166-2635(04)80005-7

[5] Zhang C et al. Spatial-temporal distribution, metallogenic mechanisms and genetic types of nephrite jade deposits in China. Frontiers in Earth Science. 2023:11. DOI: 10.3389/feart.2023.1047707

[6] Ábalos B, Puelles P, Gil Ibarguchi JI. Polyphase tectonic reworking of serpentinites and chlorite-tremolite-talc rocks (SW Spain) from the subduction forearc to intracontinental emplacement. Journal of Metamorphic Geology. 2023;**41**(4):491-523

[7] Nicolas A. 27 - ophiolites and oceanic lithosphere. In: Roberts DG, Bally AW, editors. Regional Geology and Tectonics: Principles of Geologic Analysis. Amsterdam: Elsevier; 2012. pp. 820-835

[8] Holder RM, Viete DR. The metamorphic rock record through Earth's history. In: Reference Module in Earth Systems and Environmental Sciences. Dordrecht: Elsevier; 2023. DOI: 10.1016/B978-0-323-99762-1.00002-4

[9] Holder RM, Viete DR. The metamorphic rock record through Earth's history. In: Reference Module in Earth Systems and Environmental Sciences. Elsevier; 2023

[10] Engi M, Lanari P. Composition effects on metamorphic mineral assemblages. In: Alderton D, Elias SA, editors. Encyclopedia of Geology (Second Edition). Oxford: Academic Press; 2021. pp. 502-512

[11] Paradis S et al. Impact of deformation and metamorphism on sphalerite chemistry – Element mapping of sphalerite in carbonate-hosted Zn-Pb sulfide deposits of the Kootenay arc, southern British Columbia, Canada and northeastern Washington, USA. Ore Geology Reviews. 2023;**158**. Article no.: 105482. DOI: 10.1016/j.oregeorev.2023.105482

[12] Wei QD et al. In situ U-Pb geochronology of vesuvianite by LA-SF-ICP-MS. Journal of Analytical Atomic Spectrometry. 2022;**37**(1):69-81

[13] Harlov DE et al. Zircon as a recorder of trace element changes during high-grade metamorphism of Neoarchean lower crust, Shevaroy block, eastern Dharwar craton, India. Journal of

Petrology. 2022;**63**(5). Article no.:egac036. DOI: 10.1093/petrology/egac036

[14] Igami Y, Kuribayashi T, Miyake A. Determination of Al/Si order in sillimanite by high angular resolution electron channeling X-ray spectroscopy, and implications for determining peak temperatures of sillimanite. American Mineralogist. 2018;**103**(6). Article no.: 944-951

[15] Wang H et al. Diagenesis and very low grade metamorphism in a 7,012 m-deep well Hongcan 1, eastern Tibetan plateau. Swiss Journal of Geosciences. 2012;**105**(2):249-261

[16] Henry DJ, Dutrow BL. Tourmaline at diagenetic to low-grade metamorphic conditions: Its petrologic applicability. Lithos. 2012;**154**:16-32

[17] Bozkaya Ö, Yalçın H, Göncüoğlu MC. Diagenetic and very low-grade metamorphic characteristics of the Paleozoic series of the Istanbul terrane (NW Turkey). Swiss Journal of Geosciences. 2012;**105**(2):183-201

[18] Abad I et al. Diagenesis to metamorphism transition in an episutural basin: The late Paleozoic St. Mary's basin, Nova Scotia, Canada. Canadian Journal of Earth Sciences. 2010;**47**(2):121-135

[19] Bozkaya Ö, Yalçin H. Diagenesis and very low-grade metamorphism of the Antalya unit: Mineralogical evidence of Triassic rifting, Alanya-Gazipaşa, central Taurus belt, Turkey. Journal of Asian Earth Sciences. 2005;**25**(1):109-119

[20] Bauluz B, Fernandez-Nieto C, Gonzalez Lopez JM. Diagenesis - very low-grade metamorphism of clastic Cambrian and Ordovician sedimentary rocks in the Iberian range (Spain). Clay Minerals. 1998;**33**(2-3):373-393

[21] Weller OM et al. The metamorphic and magmatic record of collisional orogens. Nature Reviews Earth & Environment. 2021;**2**(11):781-799

[22] Frisch W, Meschede M, Blakey R. Old orogens. In: Frisch W, Meschede M, Blakey RC, editors. Plate Tectonics: Continental Drift and Mountain Building, Springer. Berlin Heidelberg: Berlin, Heidelberg; 2011. pp. 159-170

[23] Hyndman RD. Origin of regional Barrovian metamorphism in hot Backarcs prior to orogeny deformation. Geochemistry, Geophysics, Geosystems. 2019;**20**(1):460-469

[24] Yakymchuk C. Migmatites. In: Alderton D, Elias SA, editors. Encyclopedia of Geology (Second Edition). Oxford: Academic Press; 2021. pp. 492-501

[25] Nicollet C et al. Eocene ultra-high temperature (UHT) metamorphism in the Gruf complex (Central Alps): Constraints by LA-ICPMS zircon and monazite dating in petrographic context. Journal of the Geological Society. 2018;**175**(5):774-787

[26] Tichomirowa M, Whitehouse MJ, Nasdala L. Resorption, growth, solid state recrystallisation, and annealing of granulite facies zircon - a case study from the Central Erzgebirge, bohemian massif. Lithos. 2005;**82**(1-2 SPEC. ISS):25-50

[27] Harley SL. Refining the P–T records of UHT crustal metamorphism. Journal of Metamorphic Geology. 2008;**26**(2):125-154

[28] Liou JG, Zhang R-Y. Ultrahigh-pressure metamorphic rocks. In: Meyers RA, editor. Encyclopedia of Physical Science and Technology (Third Edition). New York: Academic Press; 2003. pp. 227-244

[29] Chetty TRK, Kehelpannala KVW. Chapter 4 - Proterozoic orogens of southern Africa. In: Chetty TRK, Kehelpannala KVW, editors. Atlas of Deformed and Metamorphosed Rocks from Proterozoic Orogens. Dordrecht: Elsevier; 2022. pp. 237-313. DOI: 10.1016/B978-0-12-817978-9.00005-6

[30] Blandine KTA et al. Geological mapping and structural interpretation of the Dschang-Santchou-escarpment (west, Cameroon), using Landsat 8 OLI/TIRS sensors/SRTM and field observations. Geological Journal. 2023;**58**(3):1111-1130

[31] Moradpour H et al. Landsat-7 and ASTER remote sensing satellite imagery for identification of iron skarn mineralization in metamorphic regions. Geocarto International. 2022;**37**(7):1971-1998

[32] Ali-Bik MW et al. The late Neoproterozoic pan-African low-grade metamorphic ophiolitic and island-arc assemblages at Gebel Zabara area, central Eastern Desert, Egypt: Petrogenesis and remote sensing - based geologic mapping. Journal of African Earth Sciences. 2018;**144**:17-40

[33] Le Gall B et al. LiDAR offshore structural mapping and U/Pb zircon/monazite dating of Variscan strain in the Leon metamorphic domain, NW Brittany. Tectonophysics. 2014;**630**(C):236-250

[34] Zheng YF. Plate tectonics in the Archean: Observations versus interpretations. Science China Earth Sciences. 2024;**67**(1):1-30

[35] Arienti G et al. Regional-scale 3D modelling in metamorphic belts: An implicit model-driven workflow applied in the Pennine Alps. Journal of Structural Geology. 2024;**180**. Article no.: 105045. DOI: 10.1016/j.jsg.2023.105045

[36] Frassi C et al. Popularizing structural geology: Exemplary structural Geosites from the Apuan Alps UNESCO global Geopark (northern Apennines, Italy). Land. 2022;**11**(8). Article no.: 1282. DOI: 10.3390/land11081282

[37] Reche J et al. A geological heritage itinerary across the Andes in the Isla Grande de Tierra del Fuego. In: Acevedo RD, editor. Geological Resources of Tierra del Fuego. Springer Geology. Cham: Springer; 2021. pp. 269-288. DOI: 10.1007/978-3-030-60683-1_14

[38] Moura P, da Glória Motta Garcia M, Brilha J. Guidelines for Management of Geoheritage: An approach in the Sertão central, Brazilian Northeastern semiarid. Geoheritage. 2021;**13**(2) Article no.: 42. DOI: 10.1007/s12371-021-00566-8

Chapter 2

An Evaluation of Garnet – Clinopyroxene Geothermometer

Harel Thomas and Haritabh Rana

Abstract

The garnet-clinopyroxene pair commonly found in upper amphibolite, granulite, and eclogite facies assemblage, as well as in garnet peridotites serves as a basic tool to estimate the equilibrium temperature for these metamorphic rocks. Several empirical and experimental calibrations for garnet-clinopyroxene thermometers have been proposed in the last four decades. Due to several calibrations for this pair, scholars often find difficulty in choosing the most optimum and valid thermometer. In the present study, eleven garnet-clinopyroxene thermometers formulated since 1972 have been evaluated to find the most valid thermometer checked on 89 sample data collated from the published global literature and processed through Gt-Cpx.Exe software. The authors used the relationship of LnKD versus the inverse of temperature and regression values. Out of the eleven geothermometer models, five models showing highest regression values with clustering of data at smaller ranges and less deviation for the collated data have been considered the best one: Raheim and Green (Contributions to Mineralogy and Petrology 48: 179–203, 1974); Mysen and Heier (Contributions to Mineralogy and Petrology 36: 73–94, 1972); Jun Lui (International Geology Review 40: 579–608, 1998); Ganguly and Saxena (Minerals Rocks 19: 1–291, 1987) and Ganguly (Geochimica et Cosmochimica Acta, 43: 1021–1029, 1979).

Keywords: exchange reaction, garnet, clinopyroxene, thermometry, high-grade metamorphism

1. Introduction

Since the advent of thermodynamics in petrological studies, geothermobarometry has played a vital role in deciphering metamorphic conditions and understanding the evolution of the crust. In the last fifty years, several geothermobarometers have been proposed for rocks ranging from greenschist to eclogite facies, such as garnet biotite and garnet cordierite thermometer by Thompson 1976, garnet hornblende thermometer by Ravna 2000, and many more.

Valid geothermobarometry is a fundamentally important tool in deciphering metamorphic conditions and understanding the evolution of the crust as it provides information about the pressure-temperature conditions at which the rocks have formed, serving as a window into the lower continental crust. To determine the metamorphic conditions of rocks from greenschist to eclogite facies, and at a range of

pressures, several geothermometers and geobarometers have been proposed in the last few decades that serve as pressure-temperature sensors helpful in decoding the chemical evolution of the rocks.

Several thermobarometric studies have been undertaken over the years, which led to the development of a range of thermometers and barometers, such as garnet-clinopyroxene thermometry [1, 2], garnet-orthopyroxene thermometry [3], garnet-biotite thermometry [4, 5], garnet-hornblende thermometry [6], garnet cordierite thermometry [7], and two pyroxene thermometry [8].

The study of garnet-clinopyroxene geothermometry has a long history, and we now have several versions of the geothermometer. As the assemblage of garnet-clinopyroxene occurs in an array of rock types ranging from eclogites to albite-epidote amphibolites and amphibolites to granulites to garnet peridotites, this potential underscores the need to carefully evaluate the accuracy and precision of the thermometer. The Fe-Mg substitution in the garnet-clinopyroxene system along with the effect of X_{Ca} garnet and X_{Na} clinopyroxene are not fully understood. Although few models have tried to understand the effect of these substitutions, still there has been less work done on the assessment of these thermometers. To recommend the best calibration for geologists, the authors have compared eleven garnet-clinopyroxene thermometer models proposed since 1972, the first equation proposed by Mysen and Heier [9]. Quantification of garnet-clinopyroxene Fe-Mg equilibrium is a widely applied thermometer for high-grade upper amphibolite, granulite, and eclogite facies assemblages, as well as garnet peridotite, where the distribution of the Fe^{+2} and Mg between coexisting garnet and clinopyroxene is expressed by the exchange reaction:

$$1/3Mg_3Al_2Si_3O_{12} + CaFeSi_2O_6 = 1/3Fe_3Al_2Si_3O_{12} + CaMgSi_2O_6 \quad (1)$$

$$\text{Pyrope} + \text{Hedenbergite} = \text{Almandine} + \text{Diopside} \quad (2)$$

The partitioning of Fe^{+2} and Mg, expressed by the distribution coefficient between coexisting garnet and clinopyroxene, has clearly shown that this distribution is a function of both physical conditions, as well as compositional variations of the phases involved [9–20]:

$$K_D = \frac{\left(Fe^{2+}/Mg\right)^{Gt}}{\left(Fe^{2+}/Mg\right)^{Cpx}} \quad (3)$$

A brief description of various models of garnet-clinopyroxene geothermometers considered for this comparative study is summarized as follows:

2. Mysen and Heier (1972)

Mysen and Heier [9], studied the Hariedland eclogites of Western Norway and justified K = f (T) as a basis for the genetic classification of eclogites. They used the equation proposed by Banno [21] to calculate the distribution coefficient $K_D^{Fe2+-Mg}$ for the calculation of temperature. Banno [21] also suggested that the effect of pressure and variable chemical composition on the distribution coefficient was found to be

negligible. The pressure range used for calculation is large enough (6–36 kbar) so that the effect of pressure on the distribution coefficient $K_D^{Fe2+-Mg}$ for the calculation of temperature is found to be negligible. Their formulation is:

$$T(K) = \frac{2475}{\ln K_D + 0.781} \tag{4}$$

3. Raheim and Green (1974)

Raheim and Green [15] conducted an experimental study of eclogites using (a) a mineral mix, (b) a glass of typical tholeiitic composition, and (c) a series of glasses of tholeiitic composition. They calculated the distribution coefficient keeping $Fe^{2+}$and Mg in consideration while assuming other variables Na/Ca and Ca/Al values constant. Also, the effect of Fe_2O_3 values was found to be negligible. They formulated the equation as:

$$T(K) = \frac{(3686 + 28.35 * P)}{(\ln K_D + 2.33)} \tag{5}$$

4. Ellis and Green (1979)

Ellis and Green [11] carried out an experimental study on a series of basaltic compositions and compositions within the simple system CaO-MgO-FeO-Al_2O_3-SiO_2 on the effect of Ca on garnet-clinopyroxene Fe-Mg exchange equilibrium in the range of 24–30 kb pressure and 750°-1300°C temperature. Their formulation is as follows:

$$T(K) = \frac{3104 * X_{Ca}^{Gt} + 3030 + 0.01086 * (P–1)}{\text{In } K_D + 1.9034} \tag{6}$$

X_{Ca}^{Gt} has been used as a parameter in the equation. The authors opined that the Ca effect is believed to be the nonideal mixing of Ca and Mg in garnet and clinopyroxene. The previous inconsistencies of temperature dependence on K_D are proposed to be reconciled and resolved in this model. To check the effect, the graph of $\ln K_D$ versus X_{Ca}^{Gt} has been plotted as shown in **Figure 1**, showing a very gentle positive slope and X_{Ca}^{Gt} values scattered for a range less than 0.3, which means as the value of $\ln K_D$ increases, X_{Ca}^{Gt} values increases very gently.

5. Ganguly (1979)

Ganguly [12] critically evaluated all the available thermodynamic mixing data of garnet and clinopyroxene proposed till 1979 and integrated these with the thermochemical and selected experimental data to express the Fe-Mg in distribution coefficient giving the equation as:

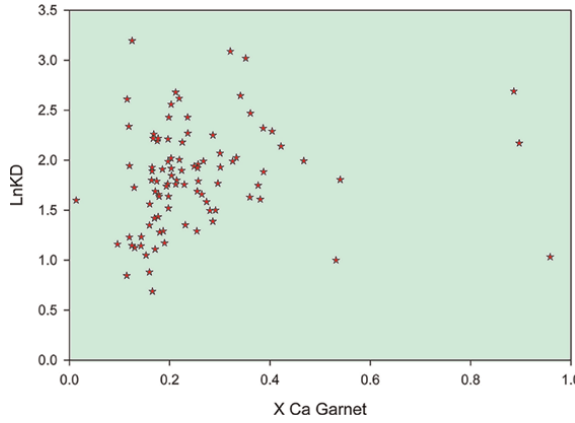

Figure 1.
Graph of lnK_D versus $X_{Ca}{}^{Gt}$.

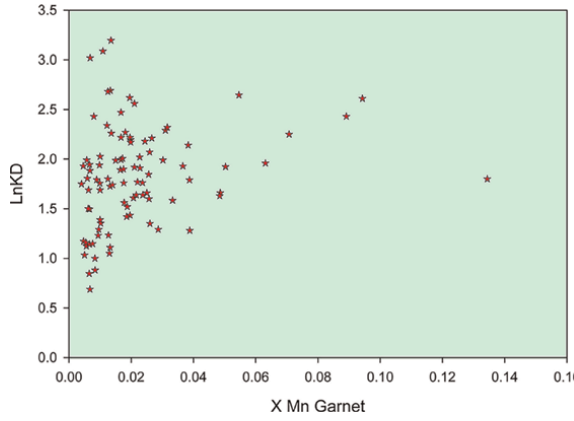

Figure 2.
Graph of lnK_D versus $X_{Mn}{}^{Gt}$.

$$T(K) = \frac{\left(4801 + 11.07^{*}P(kb) + 1586^{*}X_{Ca}{}^{Gt} + 1308^{*}X_{Mn}{}^{Gt}\right)}{In\ K_D + 1.9034} \qquad (7)$$

The application of the proposed model is said to be restricted to Na-poor bulk compositions due to a lack of sufficient data on the mixing properties of jadeite with hedenbergite and diopside. The error estimation of this model is said to be ±25°C. X_{Ca} and X_{Mn} of garnet have been used as a factor in the formulation. The graph of lnK_D versus $X_{Mn}{}^{Gt}$ has been plotted as shown in **Figure 2** where X_{Mn} values are clustered at a very low range less than 0.02. Both X_{Ca} (**Figure 1**) and X_{Mn} of garnet show the same behavior concerning lnK_D.

6. Wells (1979)

Wells [16] tried to explain the formation of granulite facies rocks in Southern West Greenland using thermometers calibrated against the result of phase equilibrium

experiments. Assuming that the departures from the ideal mixing in the pyroxene and garnet phases are mutually canceled out, Wells gave the following equation:

$$T(K) = \frac{((24440 + 0.06524^{*}(P-1))}{13.41 - 3^{*}R^{*}\text{In } K_D} \tag{8}$$

7. Dahl (1980)

Dahl [10] showed estimates of the analysis of thirteen mineral pairs, stating that the regressed parameters for Ca and Mn agree well with those calculated by Ganguly [12] and his formulation is as follows:

$$T(K) = \frac{170 + 0.01107^{*}(P\text{–}1) + 759.44^{*}\left(X_{Fe}{}^{Gt} - X_{Mg}{}^{Gt}\right) + 1414^{*}X_{Ca}{}^{Gt} + 1437^{*}X_{Mn}{}^{Gt}}{\text{In } K_D} \tag{9}$$

The graph of $\ln K_D$ versus $X_{Fe}{}^{Gt}$ shown in **Figure 3** shows a positive correlation with $\ln K_D$ as the values of $X_{Fe}{}^{Gt}$ increase with the increase in $\ln K_D$. The graph of $\ln K_D$ versus $X_{Mg}{}^{Gt}$, **Figure 4** shows a negative correlation with $\ln K_D$ as the values of $X_{Mg}{}^{Gt}$ increase with a decrease in $\ln K_D$.

8. Ganguly and Saxena (1987)

Ganguly and Saxena [13] modified the equation given by Ganguly [12], providing an updated calibration on composition and the Fe-Mg distribution between garnet and clinopyroxene with the modified equation as follows:

$$T(K) = \frac{4100 + 0.01107^{*}(P\text{–}1) + 1510^{*}\left(X_{Ca}{}^{Gt} + X_{Mn}{}^{Gt}\right)}{\text{In } K_D} \tag{10}$$

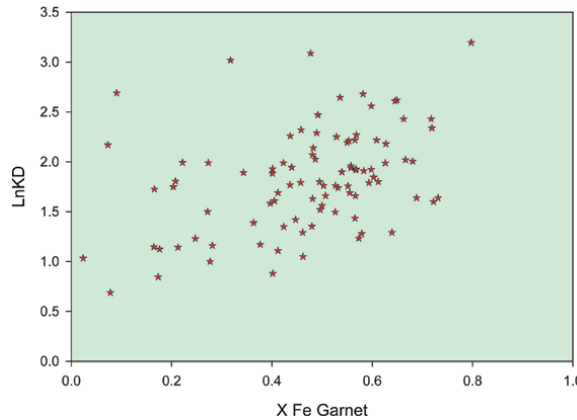

Figure 3.
Graph of $\ln K_D$ versus $X_{Fe}{}^{Gt}$.

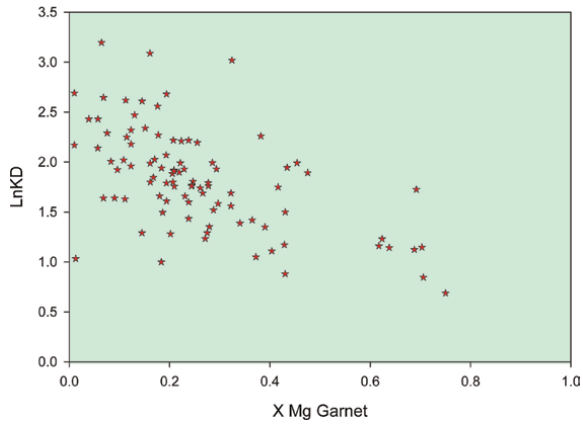

Figure 4.
Graph of lnK_D versus X_{Mg}^{Gt}.

9. Krogh (1988)

Krogh [14] reinterpreted the existing experimental data on the partitioning of Fe^{+2} and Mg between garnet and clinopyroxene [11, 15, 22] to construct a new expression including a curvilinear relationship between $\ln K_D$ and X_{Ca}^{GT} giving expression as:

$$T(K) = \frac{\left(\left(-6173^{*}\left(X_{Ca}{}^{Gt}\right)^{2} + 6731^{*}X_{Ca}{}^{Gt} + 1879 + 10^{*}P(kb)\right)\right.}{\text{In } K_D + 1.393} \tag{11}$$

The proposed model shows that the grossular content of garnet have the major compositional effect on Fe-Mg partitioning of garnet and clinopyroxene. This model is expected to give optimum results for X_{Ca} values ranging between 0.1 and 0.5.

10. Yang (1994)

Yang [18] carried out an experimental study of the compositional dependence of the garnet-clinopyroxene Fe^{+2}/Mg partition coefficient. The Mg number of garnet was found to have a significant effect on the K_D and his formulation is as follows:

$$T(K) = \frac{[1987.98 + (0.01766^{*}P) - (1629^{*}X_{Ca}{}^{*}X_{Ca}) + (3648.55^{*}X_{Ca}) - (6.59^{*}MgNo)]}{(\text{In } K_D + 1.076)} \tag{12}$$

11. Jun Lui (1998)

Jun Lui [19] gave a new formulation using new experimental data measured at 600 to 950°C, 0.8–3.0 GPa, and $f(O_2)$ defined by the fayalite-quartz-magnetite buffer in the basalt-H_2O system as:

$$T(K) = \frac{3820}{((1.828 + \text{In } K_D(1 + a(2.2 - P))} \quad (13)$$

The model is opined to be in excellent agreement with the low-temperature end amphibolite to high-temperature end granulites of crustal P-T conditions.

12. Krogh Ravna (2000)

Krogh Ravna [20] gave an updated calibration through multiple regression analysis on an extended dataset to refine the relationship between temperature, pressure, composition, and the Fe-Mg distribution between garnet and clinopyroxene. The formulation is as follows:

$$T(K) = \frac{\left(\begin{pmatrix} 1939.9 + 3270 * X_{Ca}{}^{Gt} - 1396\left(X_{Ca}{}^{Gt}\right)^2 + 3319 * X_{Mn}{}^{Gt} - 3535\left(X_{Mn}{}^{Gt}\right)^2 + 1105 * X_{Mg\#}{}^{Gt} - \\ 3561 * \left(X_{Mg\#}{}^{Gt}\right)^2 + 2324 * \left(X_{Mg\#}{}^{Gt}\right)^3 + 169.4 * P(GPa) \end{pmatrix}\right)}{(\text{In } K_D + 1.223)} \quad (14)$$

This calibration is said to be unaffected by the sodic variations of clinopyroxenes in the range of X_{Na}=0.051 giving optimum results for variegated rock types.

13. Valid garnet-clinopyroxene geothermometry in granulites

Granulites are typical rocks of the Earth's middle to lower crust formed under high-temperature conditions. They are found as xenoliths in basaltic volcanic rocks, mainly within continental rifts, but most granulites occur as complexes or terranes in orogenic settings that have suffered significant erosion and exhumation where we can access directly the deep crustal assemblages. Orogenic granulites display a wide compositional range [23] and are known from a variety of collisional belts such as Aldan Shield, Adirondack highlands, Southern granulite terrain, and Rajasthan, India, Ruby Range, Montana, USA, Antarctica, and many more that formed during different episodes, including the Archean, since granulites are very common here. Determination of bulk rock and mineral compositions, calculation of peak equilibration conditions, and dating of orogenic granulites are known to have important constraints on the thermal and chemical structure of the Earth's continental crust throughout Earth's history. Harley [23] showed that equilibration conditions deduced from orogenic granulites cover a wide range. In particular, pressures are highly variable, and the granulite field may be divided into low-pressure, medium-pressure, and a high-pressure facies [24]. Peak temperatures for many granulites scatter around 800°C [25], but an increasing number of ultra-high temperature granulite complexes (900–1100°C and 0.7–1.3 GPa) are being recognized [26, 27].

To test the validity and applicability of garnet-clinopyroxene thermometry, we have collated 89 samples from the literature all over the world (supplementary sheet attached). Samples were selected to fit the following criteria [3, 4]:

a. There is a clear description of textural equilibrium between garnet and clinopyroxene.

b. There are detailed and high-quality electron microprobe analyses of the minerals involved at least SiO_2, TiO_2, Al_2O_3, FeO, MnO, MgO, CaO, Na_2O, and K_2O, and the stoichiometry of the analyzed minerals was confirmed.

c. The core composition of garnet and rim composition of clinopyroxene have mostly been used. If there is growth zoning in garnet, only the rim composition was used, and accordingly, only the rim composition of matrix clinopyroxene has been used.

d. Data are used where elemental oxide totals for the minerals analyzed were 100±1.5%.

e. The effect of Fe_2O_3 on garnet and clinopyroxene has been considered negligible for the calculation of temperature.

14. Effect of Fe^{3+}, Na in clinopyroxene and Ca, Mn in garnet

While proposing several experimental and empirical calibrations of garnet-clinopyroxene thermometer, various assumptions have been made regarding Fe^{3+}, Na, and Ca content of pyroxenes, such as Raheim and Green [15] Na/Ca and Ca/Al content and [11] effect of Ca. In this contribution, the authors have considered quaternary parameters Fe^{2+}, Mg, Ca, and Mn of garnet and Fe^{2+}, Mg of clinopyroxene. Fe^{3+} content of garnet and clinopyroxene has been considered negligible. The collected samples are of granulitic terrain having high Fe, Mg content and low Mn content in garnet due to which the effect of Mn has been reduced profoundly. A very less amount of Na-Cpx is present in the collected samples, mostly falling in the range of 0–0.2. The 89 samples listed in the table (See supplementary data) fall in the mineral composition range: X_{Fe}= 0.06–0.61 (mostly between 0.2 and 0.4); X_{Mg} = 0.32–0.95 (mostly between 0.6 and 0.9) in clinopyroxene; X_{Fe} = 0.07–0.79 (mostly between 0.45 and 0.60); X_{Mg} = 0.009–0.70 (mostly between 0.1 and 0.3); X_{Mn} = 0.004–0.13 (mostly between 0.01 and 0.03) and X_{Ca} = 0.01–0.89 (mostly between 0.10 and 0.20) in garnet.

15. Results and discussion

The total of 89 pairs of data have been processed for the different models of garnet-clinopyroxene pair by the software Gt-Cpx.EXE [28, 29]. A comparison of the calculated $\ln K_D$ and 1/T for different geothermometric models has been undertaken. The plots of $\ln K_D$ vs 1/T are shown in **Figures 5–15**. The data selected in this way were used to check the temperature dependence of the distribution coefficient:

The Raheim and Green [15] **Figure 5** graph of $\ln K_D$ vs 1/T has been plotted as $\ln K_D$ = 1870/ T(°C) - 1.024 with R^2 = **0.995**.

Mysen and Heier [9] **Figure 6** $\ln K_D$ = 1165/ T (°C) + 0.068 with R^2 = **0.988**.

Jun Lui [19] **Figure 7**, as $\ln K_D$ = 1435/ T (°C) - 0.380 with R^2 =**0.988**.

Ganguly and Saxena [13] **Figure 8**, as lnKD = 2395 / T (°C) -1.145 with R^2 = **0.847.**

Ganguly [12] **Figure 9**, as $\ln K_D$ =2825/ T (°C) -1.551 with R^2 = **0.843.**

Krogh [20] **Figure 10**, as $\ln K_D$ = 1007/ T (°C) + 0.256 with R^2 = **0.601.**

Wells [16] **Figure 11**, as $\ln K_D$ = 1760 / T (°C) - 0.468 with R^2 = **0.582.**

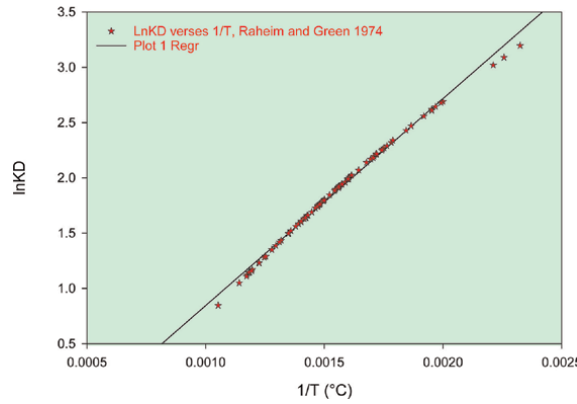

Figure 5.
Reciprocal relation of temperature (1/T) versus lnK_D for Raheim and Green [15] model.

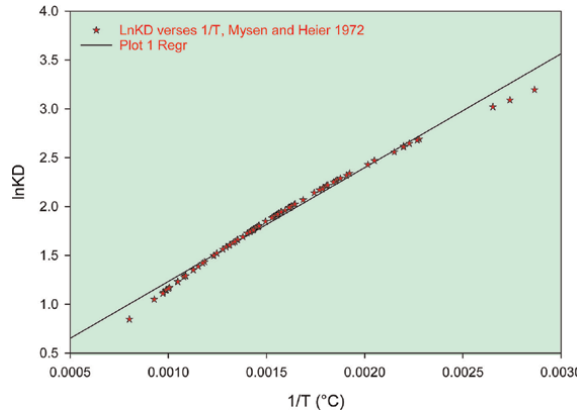

Figure 6.
Reciprocal relation of temperature (1/T) versus lnK_D for Mysen and Heier [9] model.

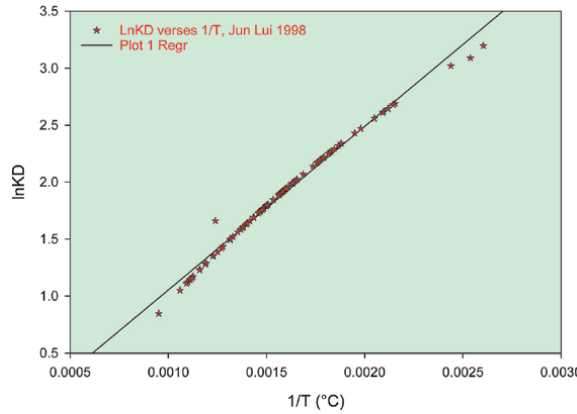

Figure 7.
Reciprocal relation of temperature (1/T) versus lnK_D for Jun Lui [19] model.

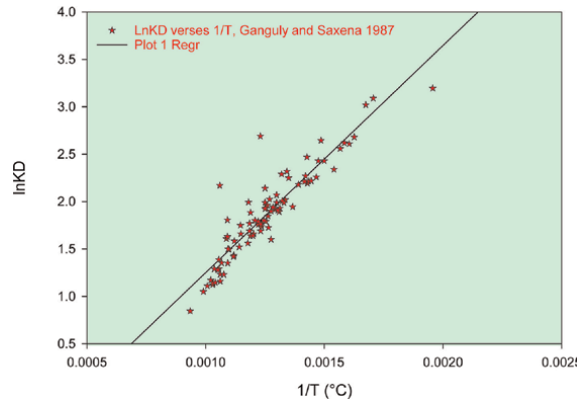

Figure 8.
Reciprocal relation of temperature (1/T) versus lnK_D for Ganguly and Saxena [13] model.

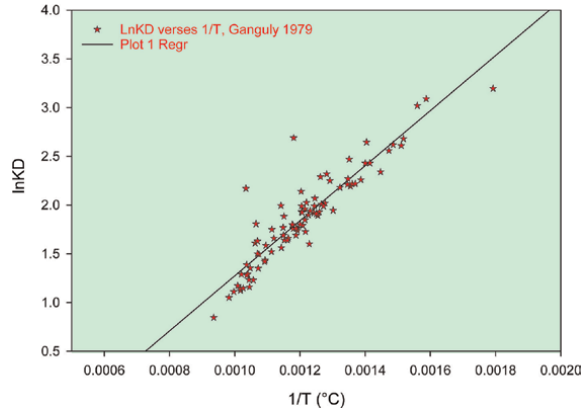

Figure 9.
Reciprocal relation of temperature (1/T) versus lnK_D for Ganguly [12] model.

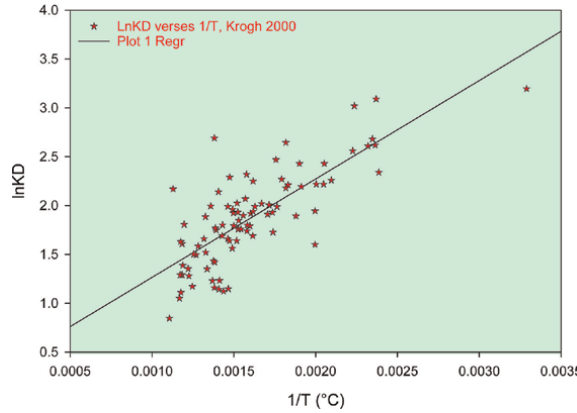

Figure 10.
Reciprocal relation of temperature (1/T) versus lnK_D for Krogh [20] model.

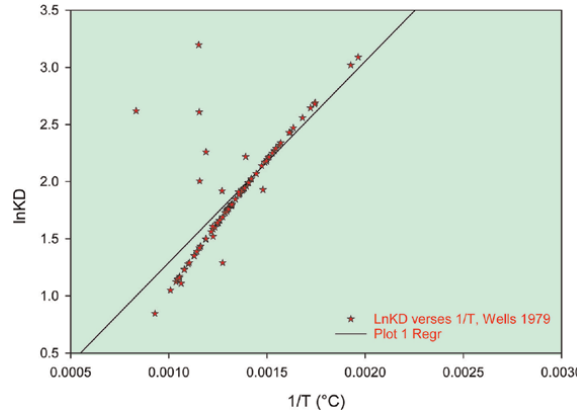

Figure 11.
Reciprocal relation of temperature (1/T) versus lnK_D for Wells [16] model.

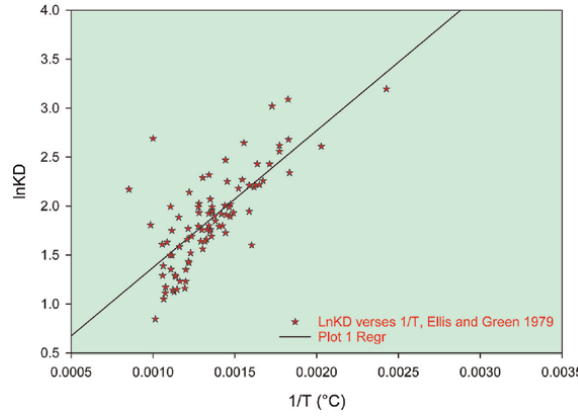

Figure 12.
Reciprocal relation of temperature (1/T) versus lnK_D for Ellis and Green [11] model.

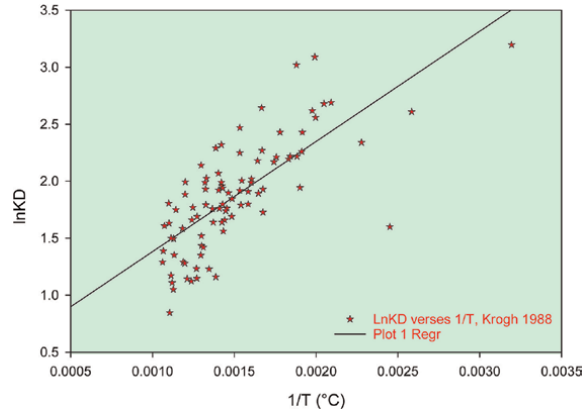

Figure 13.
Reciprocal relation of temperature (1/T) versus lnK_D for Krogh [14] model.

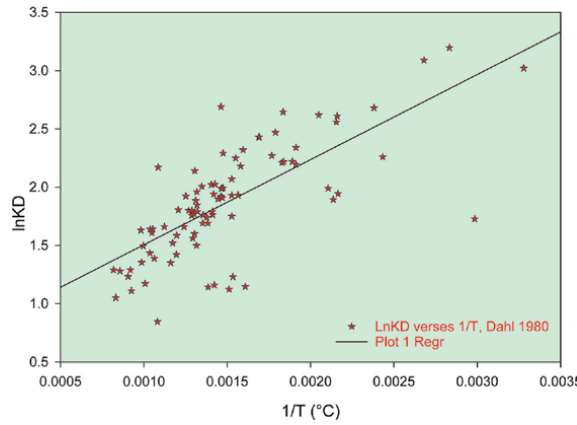

Figure 14.
Reciprocal relation of temperature (1/T) versus lnK_D for Dahl [10] model.

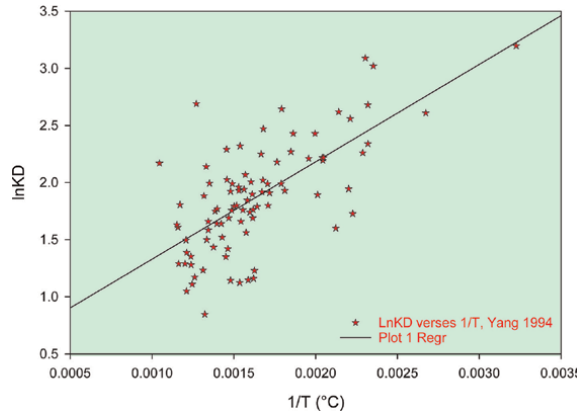

Figure 15.
Reciprocal relation of temperature (1/T) versus lnK_D for Yang [18] model.

Ellis and Green [11] **Figure 12**, as lnK_D =1397/ T (°C) –0.025with R^2 = **0.562**.
Krogh [14] **Figure 13**, as lnK_D = 966.7 / T (°C) +0.415 with R^2 = **0.546**.
Dahl [10] **Figure 14**, as lnK_D = 730.7 / T (°C) +0.774with R^2 = **0.525** and
Yang [18] **Figure 15**, as lnK_D = 852.7 / T (°C) + 0.476with R^2 = **0.458**.

From the very beginning, proper evaluation of metamorphic temperatures has been a matter of discussion. Various methods are applied for determining precise temperatures. Some researchers determine temperature by averaging the results from all applicable thermometers. Few also use consensus peak temperature in which a temperature is chosen where the spread in temperatures from each thermometer overlap. The averaging of results from different thermometers can be unjustified yielding an approximate estimation of temperature. Although, the use of consensus temperature can be found fissible for evaluation of temperature variation within a terrane. With the above considerations in mind, we have attempted to evaluate the accuracy of eleven models taking each separately and checking the regression and scattering of temperature values. In eleven models used despite the use of the compositional effect of X_{Fe}, X_{Mg}, $X_{Ca,}$ and X_{Mn} of garnet on lnK_D in various models, the

accuracy of models has not been resolved to a large extent. Raheim and Green [15], as well as Mysen and Heier [9], have given the best precision, followed by Jun Lui [19] which used an iteration method giving a confined range of temperature and less scattering. Ganguly [12] and Ganguly and Saxena [13] have used the compositional effect of X_{Ca} and X_{Mn} of garnet in their equation, although the scattering of temperature is a little more as compared to Raheim and Green [15], Mysen and Heier [9] and Jun Lui [19] leading to less regression values. The box plot in **Figure 16** shows the temperature range of the best five models. The model of Raheim and Green [15] has shown the clustering of temperature at a shorter range leading to the highest regression followed by Mysen and Heier [9] model giving the widest range of temperature as compared to other best models. Ganguly [12] and Ganguly and Saxena [13] models have yielded high-temperature values as compared to other best models, still clustering for a short range resulting in high regression values. The rest of the models have given a wide spread in the data leading to fewer regression values.

To observe the effect of X_{Fe} and X_{Mg} of clinopyroxene and X_{Fe}, X_{Mg}, $X_{Ca,}$ and X_{Mn} of garnet on $K_{D,}$ we have plotted the graphs between X_{Fe} and X_{Mg} of clinopyroxene vs K_D and X_{Fe}, X_{Mg}, $X_{Ca,}$and X_{Mn} of garnet on K_D (supplementary figures associated with this article can be obtained from the journal), respectively.

In the case of X_{Fe} and X_{Mg} of clinopyroxene, it is observed that X_{Fe}(CPX) is showing a horizontal trend as $X_{Fe}(CPX) = 2E{-}5/K_D + 0.275$ with $R^2 = 2E{-}07$, having a compositional range of 0.0692–0.6183 (mostly between 0.2 and 0.4) showing a scattering of values of X_{Fe}(CPX); while $X_{Mg}(CPX) = -0.00/K_D + 0.724$ with $R^2 = 6E{-}05$, is showing gentle negative slope having a compositional range of 0.324–0.9591 (mostly between 0.6 and 0.9) showing clustering of X_{Mg}(CPX) at higher range.

Despite the spread in the data of X_{Mg}(GT), it shows a negative slope as $X_{Mg}(GT) = -0.018/K_D + 0.39$ with $R^2 = 0.21$, having a compositional range of 0.0099–0.7058 (mostly between 0.10-0.30) shows clustering of data at intermediate range, inferred as to be a tendency for more magnesium bulk composition to yield lower K_D [2].

Based on the regression values and clustering of temperature ranges calculated for each model, it is evident that Raheim and Green [15], Mysen and Heier [9], Jun Lui [19], Ganguly and Saxena [13], and Ganguly [12] model show very good relation

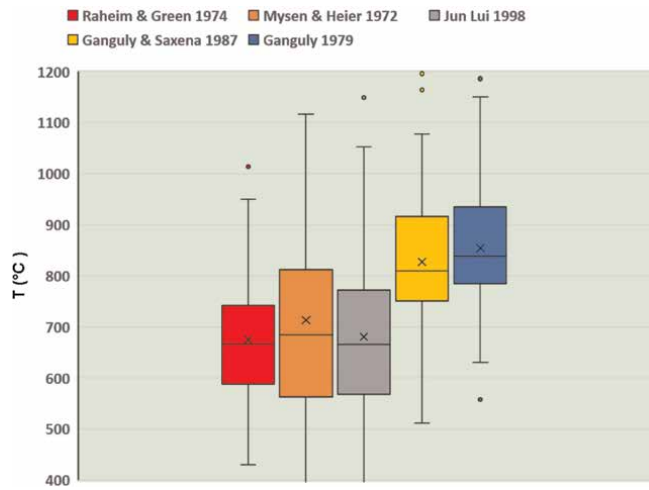

Figure 16.
Box plot showing the best five models with their calculated temperature range.

between $\ln K_D$ vs 1/T with the maximum number of points (values of temperature) providing best fit lines with high regression values and shorter range of temperature variation.

16. Conclusion

We emphasize that our testing of eleven versions of the GCPX thermometers to the empirical data collected from the literature for this comparative study applies only to rocks containing garnet and clinopyroxene whose compositions can be well described by $(Fe\text{-}Mg\text{-}Ca)_3Al_2Si_3O_{12}$ and $(Ca\text{-}Fe\text{-}Mg)Si_2O_6$, respectively. The result of this study may not apply to rocks of greatly different thermal regimes and/or mineral chemistry.

We conclude that the following five GCPX thermometers [9, 12, 13, 15, 19] are almost equally valid. These models show the highest regression values and maximum numbers of points (values of temperature) are providing the best fit lines **Figures 5–9**. Therefore, these models can be considered as the most appropriate ones to be used for the calculation of temperature. The other calibrations gave highly erratic results, and hence are not recommended.

However, Raheim and Green [15] are the best among them as the regression correlation coefficient value; R^2 is close to 1, which indicates that the maximum number of points defines the best fit line. Therefore, the temperature value obtained by Raheim and Green [15] model is more precise compared to the others.

Although it is always necessary to do further experimental work to refine the calibration of the GCPX thermometer using garnet and clinopyroxene with chemical compositions comparable to natural minerals, it is equally important to improve our knowledge of the various chemical interactions within minerals, such as garnet and clinopyroxene, so that we can improve the activity models for these minerals.

Acknowledgements

The authors thank the Head, Department of Applied Geology, Doctor Harisingh Gour Vishwavidyalaya, Sagar (M.P.), and the Department of Science and Technology, New Delhi, India for providing facilities as including PURSE- Phase-II for conducting present research work.

Supporting information

Additional supporting information may be found in the supporting information tab for this chapter: https://bit.ly/3tL7FKI

Supporting information description:

1. Table S1: Data of KD, lnKD, XFeCpx, XMgCpx, XFeGt, XMg Gt, XCaGt and XMnGt of different rocks samples by different authors

2. Table S2: Data of the Calculated Temperature (°C) of different rock samples by different authors.

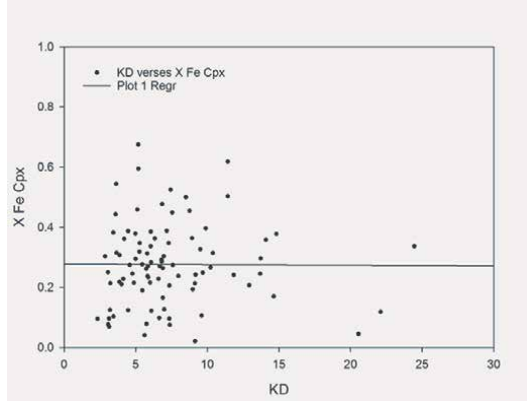

Figure S1a.
KD vs X_{Fe}^{Cpx}.

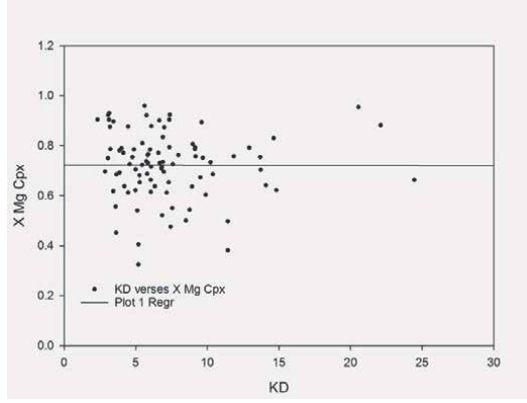

Figure S1b.
KD vs X_{Mg}^{Cpx}.

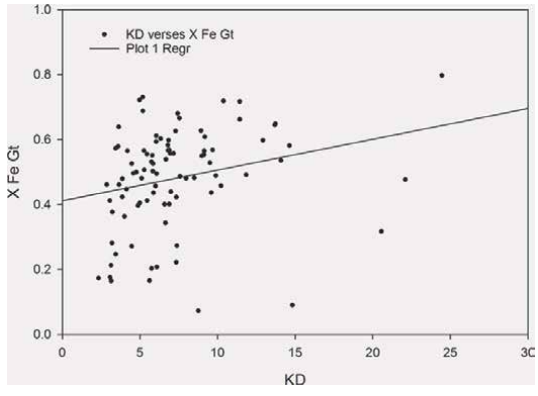

Figure S1c.
KD vs X_{Fe}^{Gt}.

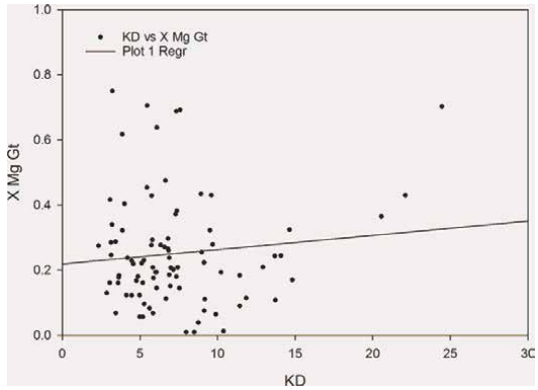

Figure S1d.
KD vs X_{Mg}^{Gt}.

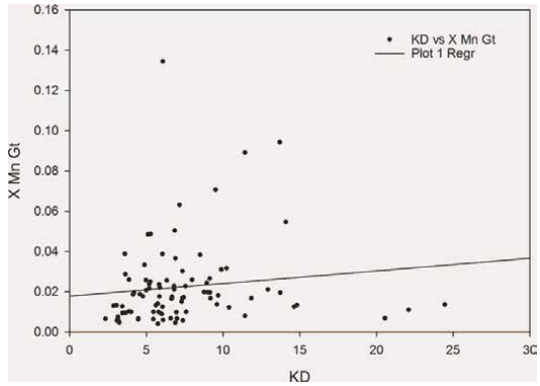

Figure S1e.
KD vs X_{Mn}^{Gt}.

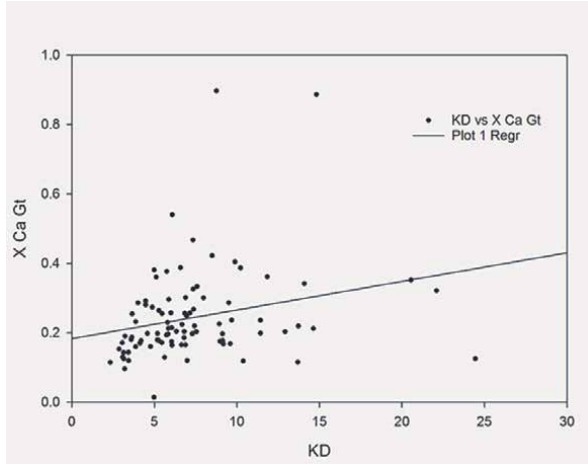

Figure S1f.
KD vs X_{Ca}^{Gt}.

3. Supplementary data:

    a. Figures S(1a-h): Graph of KD versus XFE, XMG, XCA, XMN of garnet and XFE, XMG of Clinopyroxene respectively.

    b. Appendix S1: Reference list of published journals whose data have been used.

Author details

Harel Thomas* and Haritabh Rana
Department of Applied Geology, School of Engineering and Technology, Doctor Harisingh Gour Vishwavidyalaya, Sagar, M.P., India

*Address all correspondence to: harelthomas@gmail.com

IntechOpen

References

[1] Fu B, Zheng YF, Li YL, Li SG. Applications of garnet–clinopyroxene geothermometers to eclogite assemblages. Acta Mineralogica Sinica. 1998;**18**:145-157

[2] Johnson CA, Bohlen SR, Essene EJ. An evaluation of garnet-clinopyroxene geothermometry in granulites. Contributions to Mineralogy and Petrology. 1983;**84**(2-3):191-198. DOI: 10.1007/BF00371285

[3] Thomas H, Rana H, Shahid M. Garnet—orthopyroxene (GOPX) geothermometer: A comparative study. Arabian Journal of Geosciences. 2018;**11**(24):771. DOI: 10.1007/s12517-018-4060-y

[4] Thomas H, Rana H. Valid garnet-biotite thermometer: A comparative study. Journal of the Nepal Geological Society. 2019;**58**:61-68. DOI: 10.3126/jngs.v58i0.24574

[5] Wu CM, Cheng BH. Valid garnet—biotite (GB) geothermometry and garnet—aluminum silicate—plagioclase—quartz (GASP) geobarometry in metapelitic rocks. Lithos. 2006;**89**(1-2):1-23. DOI: 10.1016/j.lithos.2005.09.002

[6] Thomas H, Rana H. Garnet-hornblende geothermometer: A comparative study. Journal of the Geological Society of India. 2020;**96**:591-596. DOI: 10.1007/s12594-020-1607-9

[7] Thomas H, Rana H, Anju M. Applicability of garnet—cordierite (GCRD) geothermometer. Journal of the Nepal Geological Society. 2020;**60**:147-161. DOI: 10.3126/jngs.v60i0.31271

[8] Thomas H, Shukla S, Rana H, Soni A, Bidolya J, Batri R, et al. Evaluation of two (opx-cpx) pyroxene geothermometer. Journal of the Nepal Geological Society. 2023;**66**:13-24. DOI: 10.3126/jngs.v66i01.57918

[9] Mysen BO, Heier KS. Petrogenesis of eclogites in high grade metamorphic gneisses, exemplified by the Hareidland eclogite, western Norway. Contributions to Mineralogy and Petrology. 1972;**36**(1):73-94. DOI: 10.1007/BF00372836

[10] Dahl PS. The thermal–compositional dependence of Fe2+ - Mg distributions between coexisting garnet and pyroxene: applications to geothermometry. American Mineralogist. 1980;**65**(9-10):852-866

[11] Ellis DJ, Green DH. An experimental study of the effect of Ca upon garnet-clinopyroxene Fe-Mg exchange equilibria. Contributions to Mineralogy and Petrology. 1979;**71**(1):13-22. DOI: 10.1007/BF00371878

[12] Ganguly J. Garnet and clinopyroxene solid solutions, and geothermometry based on Fe-Mg distribution coefficient. Geochimica et Cosmochimica Acta. 1979;**43**(7):1021-1029. DOI: 10.1016/0016-7037(79)90091-7

[13] Ganguly J, Saxena S. Mixtures and mineral reactions. Minerals and Rocks. 1987;**19**:1-291

[14] Krogh EJ. The garnet-clinopyroxene Fe-Mg geothermometer—a reinterpretation of existing experimental data. Contributions to Mineralogy and Petrology. 1988;**99**(1):44-48. DOI: 10.1007/BF00399364

[15] Råheim A, Green DH. Experimental determination of the temperature and pressure dependence of the Fe-Mg partition coefficient for coexisting garnet

and clinopyroxene. Contributions to Mineralogy and Petrology. 1974;**48**(3): 179-203. DOI: 10.1007/BF00383355

[16] Wells PRA. Chemical and thermal evolution of Archaean sialic crust, southern West Greenland. Journal of Petrol. 1979;**20**(2):187-226. DOI: 10.1093/petrology/20.2.187

[17] Pattison DRM, Newton RC. Reversed experimental calibration of the garnet-clinopyroxene Fe-Mg exchange thermometer. Contributions to Mineralogy and Petrology. 1989;**101**(1): 87-103. DOI: 10.1007/BF00387203

[18] Ai Y. A revision of the garnet-clinopyroxene Fe2+ - Mg exchange geothermometer. Contributions to Mineralogy and Petrology. 1994;**115**(4): 467-473. DOI: 10.1007/BF00320979

[19] Liu J. Assessment of the garnet-clinopyroxene thermometer. International Geology Review. 1998;**40** (7):579-608. DOI: 10.1080/ 00206819809465226

[20] Ravna K. The garnet–clinopyroxene Fe2+ - Mg geothermometer: an updated calibration. Journal of Metamorphic Geology. 2000;**18**(2):211-219. DOI: 10.1046/j.1525-1314.2000.00247.x

[21] Banno S. Classification of eclogites in terms of physical conditions of their origin. Physics of the Earth and Planetary Interiors. 1970;**3**:405-421. DOI: 10.1016/0031-9201(70)90083-X

[22] Mori T, Green DH. Laboratory duplication of phase equilibria observed in natural garnet lherzolites. The Journal of Geology. 1978;**86**(1):83-97. DOI: 10.1086/649657

[23] Harley SL. The origins of granulites: a metamorphic perspective. Geological Magazine. 1989;**126**(3):215-247. DOI: 10.1017/S0016756800022330

[24] Green DH, Ringwood AE. An experimental investigation of the gabbro to eclogite transformation and its petrological applications. Geochimica et Cosmochimica Acta. 1967;**31**(5):767-833. DOI: 10.1016/S0016-7037(67)80031-0

[25] Bohlen SR. Pressure-temperature-time paths and a tectonic model for the evolution of granulites. The Journal of Geology. 1987;**95**(5):617-632. DOI: 10.1086/629159

[26] Hokada T. Feldspar thermometry in ultrahigh-temperature metamorphic rocks: Evidence of crustal metamorphism attaining~ 1100 C in the Archean Napier Complex, East Antarctica. American Mineralogist. 2001;**86**(7-8):932-938. DOI: 10.2138/am-2001-0718

[27] Klemd R, Bröcker M. Fluid influence on mineral reactions in ultrahigh-pressure granulites: a case study in the Śnieżnik Mts.(West Sudetes, Poland). Contributions to Mineralogy and Petrology. 1999;**136**(4):358-373. DOI: 10.1007/s004100050544

[28] Thomas H. MPET4: A Computer program for coexisting garnet-clinopyroxene-plagioclase-quartz geothermobarometry. Journal of the Nepal Geological Society. 1998;**18**:409-415. DOI: 10.3126/jngs.v18i0.32275

[29] Thomas H, Paudel LP. Geothermobarometer based on coexisting garnet—Orthopyroxene—Plagioclase—Quartz equilibria. Journal of the Nepal Geological Society. 2016;**51**: 1-9. DOI: 10.3126/jngs.v51i0.24083

Chapter 3

Metamorphism, Metasomatism and Conditions of Formation of Industrial Minerals of the Sillimanite Group of the Fennoscandian Shield

Vladimir Shchiptsov

Abstract

The group of sillimanite minerals includes kyanite, sillimanite and andalusite, modifications. It is shown that high-alumina complexes are widespread throughout the Fennoscandian Shield, but the sources (protoliths) are sedimentary-volcanogenic formations of the preceding stages. Three metamorphogenic types of high-alumina formations have been identified: the Keivian (Archean), the Svekofennian (Paleoproterozoic) and the Southwestern Gneissian (Mesoproterozoic). The connection with tectono-metamorphic cycles has been established. The Keivian metamorphogenic type is characterised by the formation of high-alumina complexes under conditions of high pressures and average temperatures of amphibolite and less frequently granulite facies of metamorphism. The main industrial mineral is kyanite. The second metamorphogenic type (Svecofennian) is associated with the Svecofennian Province. The manifested metamorphism corresponds to a metamorphic series of low and medium pressures and medium and high temperatures. The main industrial mineral is andalusite. Two areas are distinguished: southeastern and northwestern. The third metamorphogenic type (Southwestern Gneissian) characterised by a wider range of PT conditions of metamorphism, which is reflected in the formation of industrial minerals of the sillimanite group (sillimanite and kyanite). Polycyclic metasomatosis of the acid-leaching stage plays the main role in the formation of deposits of the sillimanite group of minerals.

Keywords: metamorphism, metasomatism, acid leaching, palaeogeodynamics, sillimanite group of minerals, Neoarchean, paleoproterozoic, mesoproterozoic, Fennoscandian shield

1. Introduction

The main criterion for distinguishing high-alumina rocks from other formations is the chemical composition: $Al_2O_3 > K2O + Na_2O$ or $2Al/2 (K + Na) + Ca > 1$, i.e., chemically, these rocks are supersaturated with aluminium [1, 2]. The most important

factors in the formation of the sillimanite group of minerals are temperature (T) and pressure (P), redox conditions of the environment (Eh), depending on the content of free oxygen, chemical potentials of carbon dioxide, sulphur, fluor and some other elements affecting the acidity-alkalinity (pH) of the mineral formation environment. Under these conditions, depending on thermodynamic conditions, other minerals supersaturated with alumina relative to alkali and calcium were formed – corundum, spinel, garnets of the pyralspite group, cordierite and sapphirine. In addition, in high-alumina rocks, there are "neutral" minerals with respect to alumina content – quartz, hypersthene, mica, magnetite and sulphides.

The group of sillimanite minerals includes kyanite, sillimanite and andalusite, modifications of the same composition of matter but with characteristics of crystal structures. The Precambrian is mainly formed by areas with metamorphic high-alumina rocks. Andalusite occurs in low and medium-pressure metamorphic rocks (e.g., large deposits are known in South Africa, India and Australia). Sillimanite is characteristic of metamorphic rocks of low and medium pressures and medium and high temperatures (e.g., deposits are known in India, South Africa, the USA and Australia). Kyanite is found in metamorphic rocks of medium and high pressures and medium temperatures (for example, deposits are known in the USA, India, Russia and Brasilia). High-alumina complexes are productive for forming deposits of sillimanite-group minerals in them. Deposits of natural metamorphogenic deposits and quartz+(kyanite+sillimanite+andalusite) associations are formed, forming significant concentrations of the mineral sillimanite group in the stage of acid leaching during postmagmatic metasomatosis.

This article gives an overview of areas with high-alumina complexes of the Fennoscandian Shield. Three metamorphogenic types of high-alumina formations have been identified: the Keivian (Archean), the Svekofennian (Palaeoproterozoic) and the Southwestern Gneissian (Mesoproterozoic) with the location of deposits and occurrences of industrial minerals of the sillimanite group on the territory of Norway, Finland, Sweden and the Karelian-Kola region of Russia. Deposits of the sillimanite group of minerals of the metamorphogenic series are objects of practical importance for use in creating various industrial materials.

All minerals of the sillimanite group are characterised by the empirical formula Al_2SiO_5 and have the composition: Al_2O_3 – 63.1%, SiO_2 – 36.9%, but with characteristic features of crystal structures – coordination number 6 (for kyanite) $Al_2(SiO_4)O$, 4 (for sillimanite) $Al(AlSiO_5)$ and 5 (for andalusite) $AlAl(SiO_4)O$ [3, 4]. All modifications are industrial but differ among themselves in the conditions of formation.

The equilibria of Al_2SiO_5 polymorpth (andalusite, kyanite and sillimanite) with a triple point at P = 3.73 kbar and T = 506°C were calculated by using the thermodynamic dataset compiled by [5, 6]. These stable fields of andalusite, kyanite and sillimanite are used to determine the pressure boundaries between the And-Sil (high thermal T/P gradient) and Ky-Sil (low thermal T/P gradient) metamorphic facies series [7].

In the world practice, sillimanite-group minerals are formed in high-alumina metamorphic rocks under favourable conditions of metamorphism, accumulations of which are of industrial interest as sources of valuable mineral raw materials – kyanite, sillimanite and andalusite. The conditions of metamorphism and metasomatosis play the most important role in the formation of sillimanite-group deposits [4, 8–10]. Minerals of the sillimanite group, which are characterised by high melting point and are acid-resistant, do not soften when heated.

One of the essential properties of the sillimanite group is transition to mullite. Unlike other sillimanite-group minerals, kyanite passes into mullite at lower temperatures, but its volume increases more considerably. The most important application field of mullite is the refractory industry. Mullite consists of connected crystals that resist temperatures of up to 1800°C [9].

The United States is prevalent as to kyanite. Significant resources of andalusite are known from China, France, Peru and South Africa. Kyanite resources have also been identified in Brazil, India and Russia. India is the leading producer of sillimanite [11] (**Table 1**).

2. High-alumina complexes of the Fennoscandian shield

The formation of high-alumina complexes is associated with Precambrian polycyclic processes under conditions of amphibolite and granulite facies metamorphism from low to high-pressure and medium-high-temperature series with superposition of later metasomatic transformations of acid-leaching facies, which caused the formation of deposits and occurrences of sillimanite group on the Fennoscandian Shield.

High-alumina rocks on the Fennoscandian Shield include deep metamorphosed complexes supersaturated with alumina relative to alkali and calcium. The pre-metamorphic nature is determined by primary sedimentary-volcanogenic deposits, among which, in Precambrian strata, high-alumina rocks have undergone polymetamorphic transformations, which is typical for all shields of the world [10]. The main deposits of kyanite, sillimanite and andalusite ores in the Precambrian (USA, India, Brazil, South Africa and Russia) were formed in the productive rocks for sillimanite-group minerals [11, 12].

The most important factors of mineral formation include temperature (T) and pressure (P), redox conditions of the medium (Eh) depending on the content of free oxygen, chemical potentials of carbon dioxide, sulphur, fluor and other elements affecting the acidity-alkalinity (pH) of the mineral formation medium [4, 13]. The connection of conditions with thermal regimes, and hence with geodynamic conditions of metamorphism and magmatism, has been established [10]. The most important factors of mineral formation include temperature (T) and pressure (P), redox conditions of the medium (Eh) depending on the content of free oxygen, chemical potentials of carbon dioxide, sulphur, fluor and other elements affecting the

Country	2021	2022
United States (kyanite)	105,000	100,000
France (andalusite)	65,000	65,000
India (kyanite and sillimanite)	15,000	15,000
Peru (andalusite)	42,000	42,000
South Africa (andalusite)	170,000	160,000
The review is based on the generalised analysis of own and literature data.		

Table 1.
Kyanite and related minerals: World production (metric tonnes) [12].

acidity-alkalinity (pH) of the mineral formation medium. The connection of conditions of metasomatic petrogenesis with thermal regimes, and hence with geodynamic conditions of metamorphism and magmatism, has been established [14].

Analytical data on the Fennoscandian Shield, in the author's opinion, high-alumina complexes are represented by three metamorphogenic types – Keivian, Svecofennian and southwestern gneiss, associated with polycyclic evolution of belts (**Figure 1**). High-alumina formations of the Fennoscandinavian Shield belong to the Neoarchean and Proterozoic with overlapping acid stage metasomatism, which was the main reason for the formation of sillimanite-group deposits. Occurrences of high-alumina formations in Scandinavian Caledonides are noted in Norway.

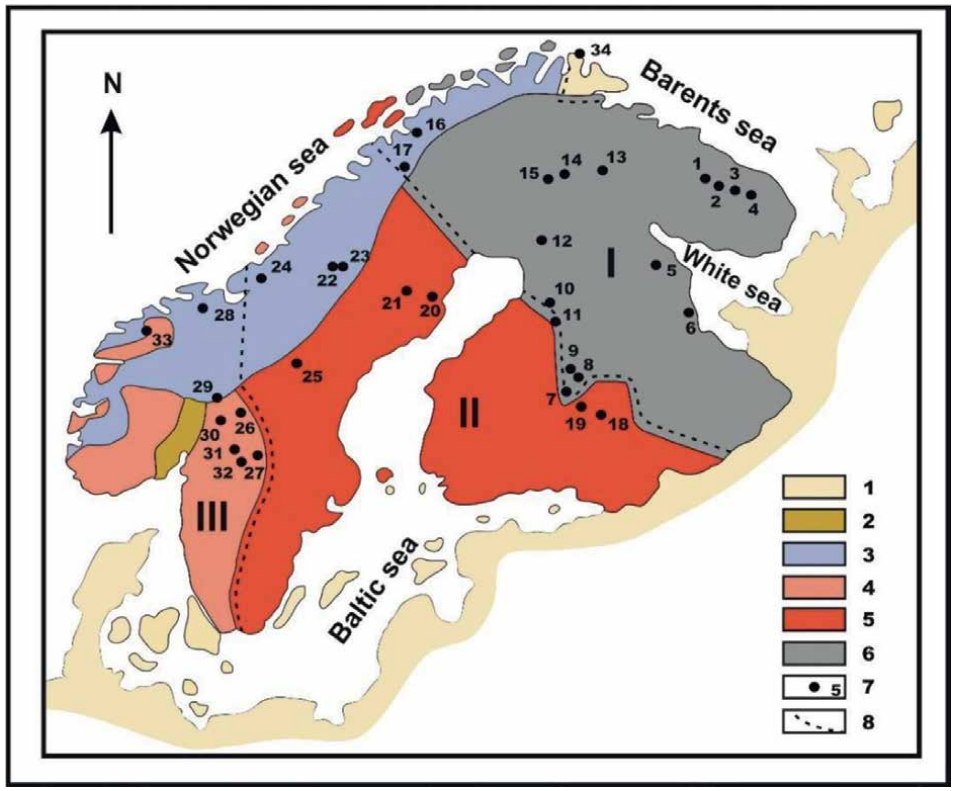

Figure 1.
Distribution of deposits and occurrences of industrial minerals of the sillimanite group in pelitic rock metamorphism on the Fennoscandian Shield. Compiler V. Shchiptsov. 1 – Phanerozoic <550 Ma; 2 – Oslo rift, 250–300 Ma; 3 – Scandinavian Caledonides, 490–390 Ma; 4 – Southwestern gneiss province (900–1700 Ma), including the Transcandinavian magmatic belt (650–1800 Ma); 5 – Svecofenian Province, 1800–2000 Ma; 6 – Archean and Paleo-Mesoproterozoic rock complexes (1600–3400 Ma) – Norbotten, Karelian, Belomorian; Kola Provinces and Lapland-Kola zone; 7 – deposits and occurrences of sillimanite group; 8 – development boundaries of high-alumina formations of I, II and III metamorphogenic types. Note: simplified geological map based on [15]. Deposits and occurrences of sillimanite group 1 – Keivskoe; 2 – Vorgelurta, Tavurta, Tyapsh-Manyuk; 3 – Chervyrta, Bolshoi Rov, Vostochnaya Shyyryrta, Kirpyrta, Yagelyrta, Bezimyannaya, Shyyryrta; 4 – Kayvurta, Nyssi, Manyuk; 5 – Khizovaara; 6 – Terbeostrov; 7 – Hokkalampi; 8 – Hirvivaara; 9 – Koli; 10 – Kivisuo; 11 – Tetrilampi; 12– Leteensuo; 13– Hallavaara; 14 – Mutsoiva; 15 – Mantuvaara; 16 – Skjomen; 17 – Nasafjellet; 18 – Vakhvayarvi; 19 – Rantakylä; 20 – Boliden; 21 – Säter; 22 – Øyungen, 23 Tverrådalen; 24 – Fongen-Hyllingen; 25 – Åreskutan; 26 – Hålsjöberg; 27 – Hökensås; 28 – Romsdal; 29 – Solø; 30 – Odal; 31 – Sumadalen; Sormbrua, Gullsteinberget, Knøsberget, Kjeksberget; 32 Bample; 33 – Lesjaverk; 34 – Dønnesfjord.

The Keivian type was formed due to palaeogeodynamic processes in the Archean (**Figure 1** – Area I). This type is associated with the formation of mainly large deposits of kyanite in conditions of kyanite type of high-baric metamorphism and accompanying metasomatism at later stages. This area is characterised by deeper erosion. The Archean protoliths of the host gneisses were formed by erosion and redeposition of Neoarchean rocks. The widespread occurrences in this zone of high-temperature subfacies – kyanite-biotite-muscovite and garnet-kyanite-biotite-orthoclase, corresponding to the conditions of temperature (on average) 600°C and pressure 7.5–8 kbar, is characteristic. Kyanite and staurolite–kyanite schists and gneisses are potential sources of kyanite.

In the western part of area I, high-alumina pelitic complexes are metamorphosed under conditions of moderately baric kyanite-sillimanite type of metamorphism. The formation of deposits and occurrences of kyanite, partly sillimanite and andalusite (the latter, we can assume, as a result of superimposed metamorphism of the sillimanite-andalusite type) in the western part of the Karelian Province in the Neoarchean greenstone belts is associated with them.

The metamorphogenic high-alumina type is distinguished for area II (**Figure 1**). This type is widespread in the southeastern part of the Svecofennian Province and in Sweden in the Skelefteo County area, including the neighbouring Counties, as well as in relict remains noted in the Scandinavian Caledonides. Paleoproterozoic metamorphic transformations of high-alumina rocks were manifested with different intensities repeatedly under conditions of low-baric metamorphism in the range of 650–730°C, 3.8–5 kbar and 460–500°C, 3–4 kbar [16, 17]. There is no mineral paragenesis of progressive metamorphism in the Svecofennian Province containing kyanite, which is an important distinguishing feature. Advanced stage metamorphism was manifested in relatively low-temperature transformations corresponding to andalusite-muscovite subfacies. The pattern of mineral alteration of the metapelites is evidence of falling temperature and increasing water and alkali potential. The conditions correspond to the stability of andalusite; sillimanite is formed much less frequently.

The third metamorphogenic type is the southwestern gneissic type (Province III, **Figure 1**). An important feature of this type is the presence in the Southwestern Gneiss Province of polygenic and polychrome high-alumina formations (900–1700 Ma), also formations related to high-alumina rocks of the Caledonian orogeny (490–390 Ma). Several bodies of rare kyanite-bearing quartz rocks with aluminium phosphates are formed on the border of the Svekonorwegian Province and the Svekofennian Province.

3. Deposits and occurrences of industrial minerals of the sillimanite group on the Fennoscandian shield

The main factors causing the occurrence of alumina deposits and occurrences include, along with the concentration of the sillimanite mineral group, the multistage transformation of their transformation, accompanied by the concentration of the useful component, its separation in the appropriate mineral form with certain physical properties, crystal size, purity of the crystal lattice, etc. [18].

The mode of the leading endogenous processes, and hence the associated metasomatism, changed in a regular way [19, 20]. Three natural types of ores of the

sillimanite mineral group were distinguished: metamorphogenic, metamorphogenic-metasomatic and metasomatic.

3.1 Features of deposits and occurrences of the Keivian type (Archean)

Kyanite-bearing gneisses of the Neoarchean Keivian Formation are represented by kyanite, quartz-kyanite and staurolite–kyanite gneisses [1]. Crystalline high-alumina gneisses represent a unique accumulation of alumina from scientific and practical points of view. The Greater Keivy is the world's largest surface area Kyanite Province. On about 2000 km^2, 90% of explored reserves of high-quality kyanite ores are easily enriched [10, 21, 22]. The main deposits and large occurrences are shown in **Figure 1**, namely Vorgelurta, Tavurta, Tyapsh-Manyuk, Chervyrta, Bolshoi Rov, Vostochnaya Shyyryrta, Kirpyrta, Yagelyrta, Bezimyannaya, Shyyryrta, Kayvurta, Nyssi, Manyuk. The gneisses contain, on average, 35% of kyanite. In addition, the rock-forming minerals are quartz, muscovite, biotite, plagioclase and staurolite. Garnet, chlorite, graphite zircon, etc., are present in varying quantities in the host complexes. In some parts, there are accumulations of andalusite and sillimanite. The last accumulations of sillimanite are marked in **Figure 1** (point 1).

Three types of kyanite ores are distinguished by textural and structural features [23]. The ore types are: (1) fibrous-needle ores, among which fine-prismatic, parallel-fibrous, sheaf-like fibrous and radial-beam varieties are distinguished; (2) paramorphic – coarsely paramorphic with kyanite crystals up to 12 × 3 cm and finely paramorphic; (3) concretionary radial-structural with kyanite nodules up to 10–15 cm across.

The main crystallographic shapes of kyanite in the ore are acicular (**Figures 2** and **3**) and columnar (**Figure 4**). Acicular or fibrous-acicular kyanite makes up 61.9% of the deposits and columnar or paramorphic kyanite 35.7%. Kyanite crystal morphology is largely responsible for the morphology of aggregates (**Figure 4**) and ore washability.

An important feature of high-alumina kyanite gneisses of the Keivian ore field is their carbon saturation, which affects the colour of kyanite. Most researchers accept the primary sedimentary biogenic origin of carbon [23].

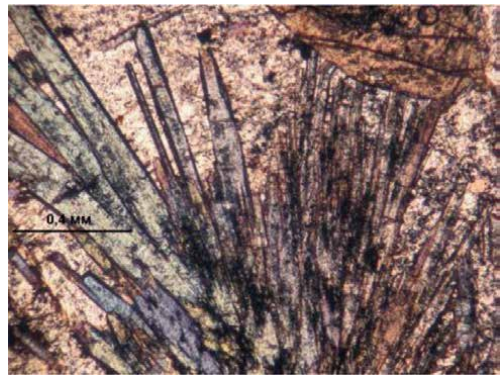

Figure 2.
The most common form of needle-like crystals in the kyanite schists Keivy [18].

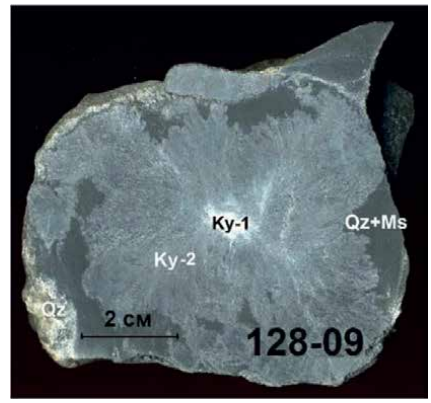

Figure 3.
Typical unit – concretion of needle-like crystals of kyanite [18].

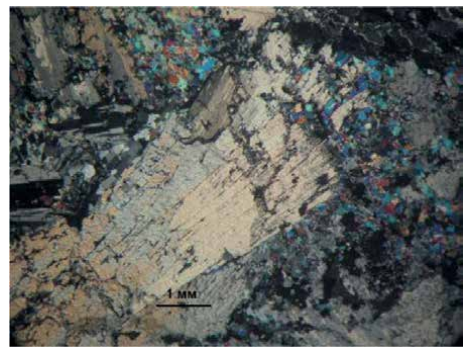

Figure 4.
The second major form of crystals of kyanite – columnar [18].

The content of rare metals and REE in concentrates of kyanite, muscovite, graphite and quartz show that muscovite and graphite are enriched with La, Ce and Nd, high contents of zirconium were identified in muscovite [24].

Formation bodies of amphibolites are widely developed among the crystalline gneisses of the Keivian group.

The Khizovaara structure is a relict part of the North Karelian greenstone belt; in its northern part, kyanite ores formed, forming the Khizovaara kyanite field (**Figure 5**).

The metaandesites underwent successive endogenous and exogenous reworking, the source of alumina accumulation. Two horizons of high-alumina gneisses have been identified [25]. The first horizon is represented by metaandesites, metamorphism of which is manifested in conditions of garnet-kyanite-biotite-orthoclase subfacies with the transition to staurolite-jedrite-kyanite and garnet-kyanite-biotite-muscovite subfacies of the kyanite-sillimanite facies series according to V.A.Glebovitsky [13].

The second horizon consists of rocks of the graywacke series, in which the signs of chemical weathering crust have been established [25, 26]. The source of high-alumina minerals is aluminosiliceous sediments, a significant part of which may represent poorly sorted siliciclastic material of underlying rocks of the dacite-andesite formation.

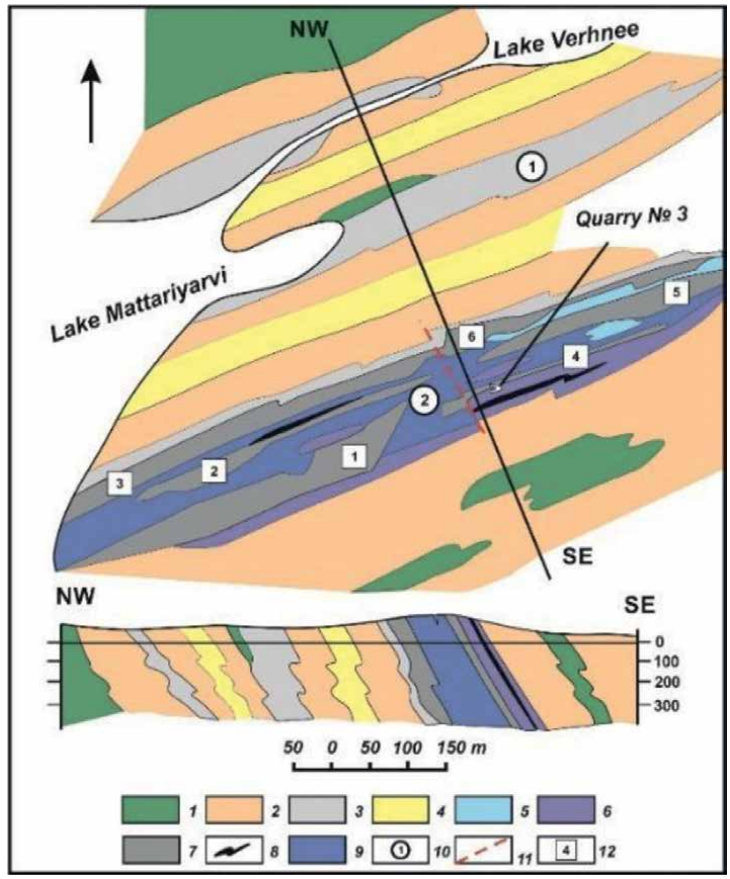

Figure 5.
Geological scheme of the kyanite ore deposit Yuzhnaya Lens of the Khizovaara ore field. Compiler V. Shchiptsov. 1 – amphibolites; 2 – amphibole-biotite schists; 3 – kyanite-biotite gneisses (high-alumina horizon I); 4 – mica schists; 5 – kyanite-feldspar quartzites; 6 – amphibole-kyanite-staurolite metasomatic rocks; 7 –kyanite quartzites (high-alumina horizon II); 8 – graphite-kyanite quartzites; 9 – muscovitised kyanite quartzites; 10 – Severnaya Lens (1); Yuzhnaya Lens (2); 11 – faulting; 12 –number of ore body.

The genesis of kyanite ores of the Khizovaara ore field depends entirely on the specificity and degree of manifestation of regional metamorphism and metasomatism. A favourable environment is characterised by an alumina content of at least 20% Al_2O_3 in the natural rock. Acidic and basic metasomatites are developed in metamorphic rocks at average temperatures of 450–600°C and pressures of 5–8 kbar [27–30]. Kyanite ore formation is shown in the example of the Yuzhnaya Lens deposit, which is geochemically characterised as an area of acid-leaching facies (**Figure 6**). The formation of primary metamorphogenic kyanite ores occurred before the acid-leaching phase and is detached by a significant time interval. Acid metasomatites of the Yuzhnaya Lens deposit were formed under conditions of medium temperatures and elevated pressures with high activity of volatiles, which leads to stability of other minerals, for example, pyrite (**Figure 7**). Three types of natural kyanite ores are localised in the Khizovaara ore field – metamorphic, metamorphogenic-metasomatic and metasomatic. The metamorphogenic-metasomatic type occupies an intermediate position when mineral aggregates are formed by an incomplete metasomatic mechanism, partially preserving the features of metamorphic rocks.

Figure 6.
Southeast side of the pilot pit No. 4. Photo by V. Shchiptsov.

Figure 7.
Pyrite veining in kyanite quartzites (open pit No. 4). Photo by Shchiptsov.

The main deposits of the Khizovaara ore field are the Yuznaya Lens, Severnaya Lens and Vostochnaya Lens deposits. In **Figure 5** the Yuzhnaya Lens deposit is labelled by number 2, and the Severnaya Lens deposit – by number 1.

The Yuzhnaya Lens deposit consists of six deposits. Two types of kyanite ore are identified in the main deposit No. 4 (**Figure 5**) [26, 28]. The first type is ores with needle kyanite. The needles are mostly less than 1 mm in size and grey in colour with a steel tint, but fine-needle kyanite with a delicate blue colour up to 10 cm in size has also been noted (**Figure 8a**). This type contains pyrite up to 15%, which is explained by high activity of volatiles in conditions of quite mobile behaviour of iron (**Figure 7**). The second type is the ores with radial-radial kyanite and massive texture (**Figure 8b**). They make up only 9%. The negative point is the relatively high content of TiO_2 associated with finely dispersed rutile. The results of U–Pb dating on zircons in the zones of submeridional folding and the associated stage of metasomatic kyanite formation gave the age of 1800 ± 7 Ma [31].

Morphological parameters and compositions of the two deposits are given in **Table 2**.

Valence and coordination unsaturated aluminium atoms are present in kyanite grains, the arrangement of which for kyanite of three varieties differs by different degree of ordering. The highest-frequency part of the spectrum is close to light grey

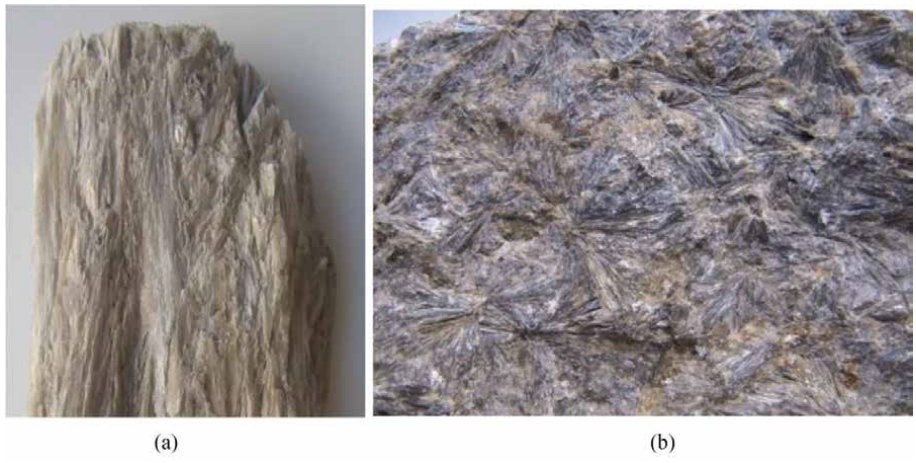

Figure 8.
Morphological types of kyanite ores of the deposit Yuzhnaya Lense. a – elongate thinly-acicular kyanite aggregate (needle thickness 0.5–1.00 mm); b – radial-beam (beam size 0.5–1.00 cm in length). Photo by V. Shchiptsov.

Deposit		Yuzhnaya Lens	Severnaya Lens
Number of deposits (ore bodies)		6	1
Deposit parameters, m	From – to m)	40–100	500
	Average thickness	55	
Length, m		950	500
Mineral composition of ore		Two types of ores: the first type – quartz 70–85%, kyanite 10–25% muscovite 0. 5–1%, plagioclase, biotite, amphibole, graphite, talc; pyrite 0–15%, pyrrhotite, magnetite; rutile, apatite, titanite, garnet, turmaline; the second type – quartz 50–60%, kyanite 10–40%; pyrite 0–10%, muscovite, feldspar, graphite, pyrrhotite, arsenopyrite, rutile	Kyanite 18–25%, quartz, feldspar, garnet, biotite, muscovite, staurolite, sulphides
Chemical composition of ore (average)		SiO_2 54.26;TiO_2 0.74; Al_2O_3 32.30; Fe_2O_3 7.33; FeO 0.14; MnO 0.01; MgO 0.10; CaO 0.42; Na_2O 0.15; K_2O 0.16; Loi 4.34; S 5.66	SiO_2 69.90; TiO_2 0.57; Al_2O_3 20.36; Fe_2O_3 4.16; FeO 0.43 MnO 0.01; MgO 0.31; CaO 0.63; Na_2O 0.47; K_2O 0.14; Loi 2.53; S 2.62

Note: **Figure 3** *shows the Yuzhnaya Lens deposit under 2, the Severnaya Lens deposit under 1.*

Table 2.
Characteristics of the main deposits of kyanite ores of the Khizovaara ore field.

and dark grey kyanites; blue kyanite has a significant difference in the silicate part of the IR spectrum, is structured and has a perfect packing [30].

Highly aluminous complexes are present in the composition of the Chupa paragneissic complex. The formation of structural and textural features and mineral composition of the pseudostratified complex in the modern sense. This complex by composition and rock ratio corresponds to tectonic breccia [32]. It is in the conditions of polycyclic high-baric metamorphism of the kyanite type [13, 33] that

high-alumina metamorphogenic formations were formed in a favourable environment. Their areas in the White Sea Province are quite widespread, but they have no economic importance due to the low kyanite content in these formations. Only small deposits of kyanite ores in metamorphites of the Belomorian mobile belt are noted, and the temperature decrease from garnet-kyanite to kyanite-muscovite subfacies is recorded [34].

In the northwestern area of distribution of high-alumina rocks of the Keivian type in the active tectonic zone of the Karelian Province, deposits and occurrences of kyanite and less frequently andalusite ores have been identified, shown in **Figure 1** (Hokkalampi, Hirvivaara, Koli, Kivisuo, Tetrilampi, Leteensuo, Hallavaara, Mutsoiva, Mantovaara) [35, 36]. A distinctive feature is that metamorphic rocks are products of transformation or solid-phase recrystallisation of existing Archean protoliths metamorphosed at the lowest temperatures of the kyanite facies.

The Hokkalampi, Hirvivaara and Koli deposits are associated with sericite-quartz schists and quartzites with a more uniform mineral composition (**Figure 9**). The main minerals are quartz, sericite, kyanite and andalusite; minor minerals are pyrophyllite, tourmaline, chlorite and sometimes dumortierite. The kyanite content ranges from 4 to 25% [37]. **Figure 9** shows a band of small occurrences of kyanite ores in schists and quartzites along the shore of Lake Pielinen [37].

The Hallavaara occurrence represents kyanite formations resulting from intense chemical weathering processes at the turn of 2.2 Ga and subsequent metamorphism

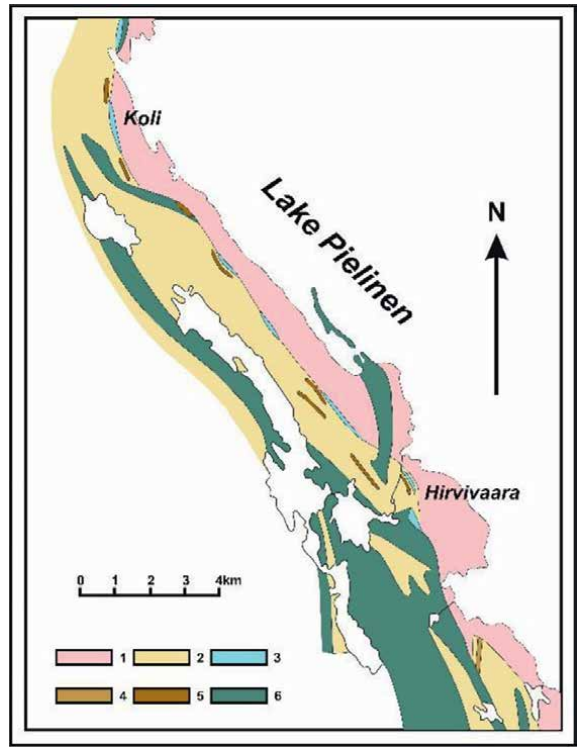

Figure 9.
Geological scheme of the Koli – Hirvivaara area (Finland). Compiled by V. Shchiptsov on the General Geological Map of Koli-Hirvivaara district [37]. 1 – gneiss-granites; 2 – micaceous quartzites; 3 – kyanite quartzites; 4 – staurolite schists; 5 – conglomerates; 6 – intrusive rocks of basic composition.

of buried kaolin clays. Between 1973 and 1981, Partek Corp. mined andalusite-bearing mica schist at Mantovaara [35].

In eastern Norway, small deposits of kyanite ores (Skjomen and Nasafjellet) have been identified in Archean protoliths in the Scandinavian Caledonides [38, 39].

3.2 Features of deposits and occurrences of the Svecofennian type (Paleoproterozoic)

The Svekofennian Province covers an area of 800 × 800 km in Finland and Sweden. In the east, the province borders with the Karelian Province, in the northeast with the Norrbotten Province, and in the west with the Scandinavian Caledonides and the South Scandinavian province [40]. In this area, deposits and occurrences associated with high-alumina complexes are noted in the southeastern and northwestern parts of the Svekofennian Province (Svekofennian type II, **Figure 1**).

The andalusite formation occurs in layered and thinly rhythmically layered quartz-biotite and phyllite schists with staurolite, andalusite and garnet [41]. Under low-pressure conditions, andalusite ore accumulations are formed in the upper parts of rhythms that previously included a large amount of clayey material in a favourable zone of amphibolite metamorphism under successive facies change – biotite, garnet (epidote-amphibolite facies), staurolite-andalusite, sillimanite-muscovite, sillimanite-potassium feldspar with subzones of biotite-sillimanite and cordierite-garnet (amphibolite facies) and hypersthene (granulite facies) zones [42, 43].

For example, in the Rantasalmi area, it was found that polymorphic alteration occurs under conditions very close to those under which the decomposition of muscovite into potassium feldspar and sillimanite occurs at a temperature of 645°C and pressure of 3.4 kb.

The metapelites contain sub-latitudinal bands of high-alumina rocks, which were the source for the formation, under favourable conditions, of promising lenticular deposits, most of which were subjected to acid leaching associated with Svecofennian activation at the turn of 1.9–1.8 Ga.

Pseudomorphs filled with muscovite and sillimanite, interpreted as melted staurolite porphyroblasts, occur in this area. Such a process is described for an area northwest of town Kitee, which hosts deposits of andalusite schist, labelled 18 and 19 in **Figure 1**. Andalusite and staurolite ores are formed in a sub-latitudinal band of high-alumina rocks in the southeastern part of the Svecofennian Province [17, 44].

Figure 10 shows a schematic map of metamorphism, where areas with high-alumina rocks of polycyclic formation are highlighted. In the northeastern part of the figure, number 4 shows a band of andalusite-staurolite-mica schists in a generalised format; it is here that the occurrences of staurolite schists shown in **Figure 1** (points 18 and 19) are located. 1 (points 18 and 19), in the southwest direction the thickness of sillimanite-staurolite gneisses, passing to garnet-cordierite-sillimanite-feldspar-biotite gneisses, is traced, and in the southwest, the metamorphic thickness is represented by cordierite gneisses. The granitoid and gneiss-granite complexes are in fact satellites of the Central Finland granitoid complex (age 1890–1870 Ma [40]).

The Andalusitovy occurrence, located 4 km west of the Kharlu settlement, is a cluster of grey andalusite ores. The andalusite ores of metamorphogenic type morphologically represent a ridge of high-alumina schists extending in the NW direction (**Figure 11**). Formed xenomorphic and with prismatic outlines, andalusite in association with staurolite is not paragenetic. Early cross-bedded staurolite is replaced by andalusite.

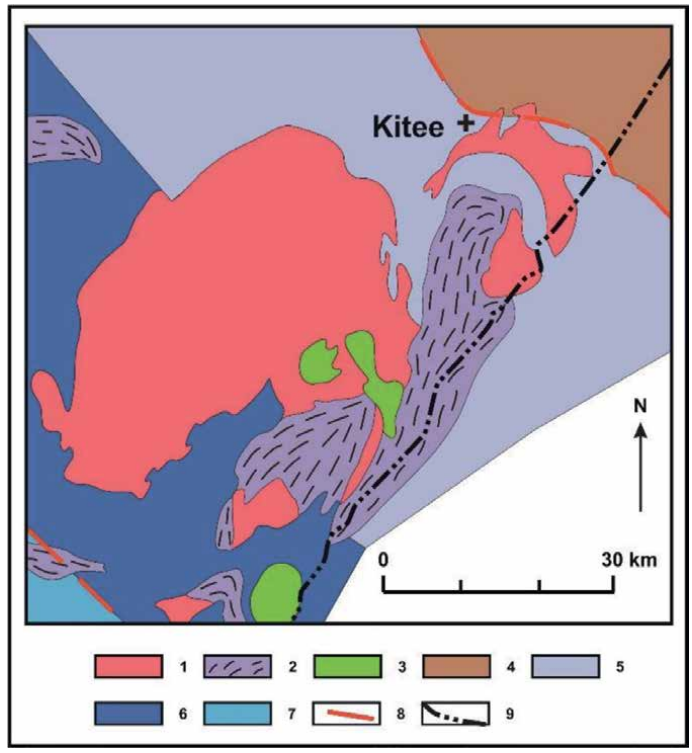

Figure 10.
Schematic metamorphic map of the southeastern part of Svecofennian Province (compiled by V. Shchiptsov on the basis of the map of metamorphism [44]). 1 – granitoids; 2 – gneiss-granite; 3 – gabbro, 4 – andalusite-staurolite-micaceous schists, 5 – sillimanite-staurolite gneiss; 6 – garnet- cordierite- sillimanite-K-feldspar- biotite gneiss, 7 – cordierite gneiss; 8 – fault or shear zone, 9 – the state border between Russia and Finland.

Figure 11.
Garnet-staurolite-andalusite schists (Andalusite section, northern Ladoga). Photo by V. Shchiptsov.

The band of alumina schists, stretched in the sublatitudinal direction, experienced metamorphism of andalusite-sillimanite type, according to V.A. Glebovitsky [13].

Figure 12.
Andalusite-sericite quartzites at the large Säter occurrence (Sweden). Photo by V. Shchiptsov.

Promising andalusite occurrences, formed because of the active metamorphism of Proterozoic supracrustal rocks, were discovered in the Skellefteo Ore Field area, northern Sweden (**Figure 1**, point 20). Composition: sericite-quartz and muscovite-sericite schist contain 30–40% andalusite.

To the west (Kristineberg area), there are also several andalusite occurrences known from literature sources [45], among which Säter (**Figure 1**, point 21; **Figure 12**) is currently among the most promising [46]. Most of the fine-grained andalusite occurs as brownish or pinkish grains in sericite quartzite. While sericite quartzite is coarser-grained and weakly banded, andalusite is also coarser-grained. The andalusite content is estimated to be up to 30–40 volume % at UV light and up to 27 weight % by regulatory calculations. Andalusite is formed by metasomatosis in association with muscovite. Quartz vein formations complete the process.

The shown occurrences of sillimanite-group minerals (**Figure 1**, point 25 Åreskutan) is related to the Seve nappe complex of caledonite and is not related to the Svekofennian type. Sillimanite and kyanite belong to the accessory group of minerals according to the latest materials [47].

In andalusite schists containing up to 30–35% of andalusite in the rock (**Figure 12**), two varieties of metasomatic andalusite associations are recorded in the Svekofennian and southwestern provinces: andalusite-quartz and muscovite-andalusite-quartz. The metasomatic columns are as follows (**Table 3**):

St+Bt+Pl+Qtz±Gr
Bt+Pl+Qtz
Pl+Qtz
And+Qtz
Qtz
St+Bt+Pl±Gr+Ms+Qtz
Bt±Pl+Ms±And+Qtz
Ms+And+Qtz
Qtz

Note: St – staurolite; And – andalusite; Sil – sillimanite; Qtz – quartz; Bt – biotite; Ms – muscovite; Grt – garnet; Pl – plagioclase.

Table 3.
Metasomatic columns.

3.3 Features of deposits and occurrences of the Southwestern Gneissian type (Mesoproterozoic)

The third metamorphogenic type belongs to the southwestern part of the Fennoscandian Shield (type III, **Figure 1**).

The specificity of the type consists in the fact that in this territory, promising objects for andalusites, kyanites and sillimanites associated with Mesoproterozoic high-alumina complexes of the Gothian (1.5–1.27 Ga) and Svekonorwegian (1.1–0.92 Ga) tectonic-metamorphic cycles have been identified [48].

So far, geological exploration has been carried out to evaluate deposits of predominantly kyanite mica schist and some kyanite quartzites.

Until 1993, the Swedish company Svenska Kyanite AB had mined the Hålsjöberg deposit, but as it failed to compete with American producers, mining was terminated and the company ceased to operate.

Here, alumina-phosphate mineralisation is widespread in the kyanite high-baric complex (**Figure 1** – 26 – Hålsjöberg; 27 – Hökensås), which is of great scientific interest. Only a few areas with widespread aluminophosphate mineralisation have been studied worldwide. Among the known ones is the Swedish kyanite complex. This group was formed in a high-baric environment (kyanite-muscovite schist subface) and is represented by muscovite-kyanite and kyanite-andalusite schists [49, 50]. The genetic model proposed by Wise and Loh [51], according to which kyanite and early phosphates were formed as a result of the impact of hydrothermal solutions on high-alumina rocks, is accepted.

Some authors [52, 53], based on chemical data and field observations, assumed that granitoids represent the protolith. Others argue because of field observations in favour of a sedimentary origin [54, 55]. The answer to this question, as the Master's thesis [56] suggests, is still open. Although D. Larsson [53] has presented convincing empirical evidence in favour of a granitoid origin of the protolith, controversy exists, primarily due to field observations of distinctly sedimentary in appearance structures.

Currently, the most common hypothesis is that of a two-stage evolution of leaching in an epithermal volcanic environment, followed by metamorphism of the amphibolite facies. Although this hypothesis seems rather complicated in some respects, it allows explaining the structure of sedimentary rocks found in kyanite-bearing rocks.

Sillimanite occurrences are most widely distributed in the Mesoproterozoic gneisses of Southern Norway, which underwent medium- and high-gradient metamorphism. Sillimanite-bearing metasedimentary rocks interbedded with felsitic gneisses of the Mesoproterozoic volcanic origin of the Telemark Supergroup (1.0–1.5 Ga) in the Bumble-Modum sector and neighbouring areas. The Bamble sector consists mainly of supracrustal gneisses (including metapelites and metasemipelites), quartzites and amphibolites, penetrated by gabbroic to granitic intrusions. Sillimanite occurrences have so far been found only in pelitic strata of the Bumble-Modum sector (**Figure 1**, point 32) [57, 58], which are like the strata hosting sillimanite deposits of Bushmanland (South Africa). They contain sillimanite-cordierite rocks in the Bumble area [57] and small bodies of massive sillimanite rocks found in mica gneisses, Modum area [59]. Of course, these bodies are too small to attract industrial attention, but they may serve as indicators of a suitable environment for the deposition of the necessary aluminium protoliths.

Aluminium, silicon and oxygen form bonds with each other in large amounts. In this respect, the three Al_2SiO_5 polymorphs (andalusite, kyanite and sillimanite) represent the equilibria caused by changing RT conditions during related or unrelated

tectonic-metamorphic events. The equilibria of Al_2SiO_5 polymorpth (andalusite, kyanite and sillimanite) with triple points are of great interest when considering high-alumina rocks. Recently, rocks containing three subdimensions have been discovered and described in Norway [60]. The presence of three minerals in the Lesjaverk deposit (**Figure 1**, point 33) is a rare occurrence in nature. There are six possible crystallisation sequences established in 17 deposits studied in the world.

Polymorphic rocks with three Al_2SiO_5 from the Lesjaverk deposit were described by D. Whitney and W. Samuelson [61]. They interpreted the sequence as andalusite → kyanite → sillimanite. In strata with early andalusite, the formation of andalusite is generally not associated with later Barrovian metamorphism that formed kyanite-sillimanite under moderate P–T conditions. This object has important petrological significance in evaluating occurrences of sillimanite-group minerals of the Southwestern Gneiss Metamorphogenic Type III.

It is noteworthy that Norwegian kyanite quartzites from Gullsteinberget, Knøsberget, Kjeksberget, Sormbrua, containing 15–30% kyanite, are in the Southwestern Gneiss Province (high-alumina formation of III metamorphogenic type). These occurrences are labelled in **Figure 1** with a generalised point under No. 31. **Figure 13** shows a generalised scheme of one of the kyanite quartzite occurrences studied by geologists of the Geological Survey of Norway. In addition to kyanite, quartz was studied in similar metasomatites. It was found that fine-grained quartz, which forms 70 to 85 vol.% of these rocks, generally contains less than 50 μg g^{-1} (total sum) of the structurally incorporated trace elements B, Li, Al, Ge, Ti, Fe, Mn, K and P. Such analytical results allow us to define this quartz as high-purity quartz (HPQ) for use as raw material for special applications in high-technology industries [39, 62]. These rocks can be considered as potential resources of kyanite and high-purity quartz, which occur in Proterozoic supracrustal rock units.

The advantages of Norwegian kyanite quartzites have been shown by A Müller et al. [62].

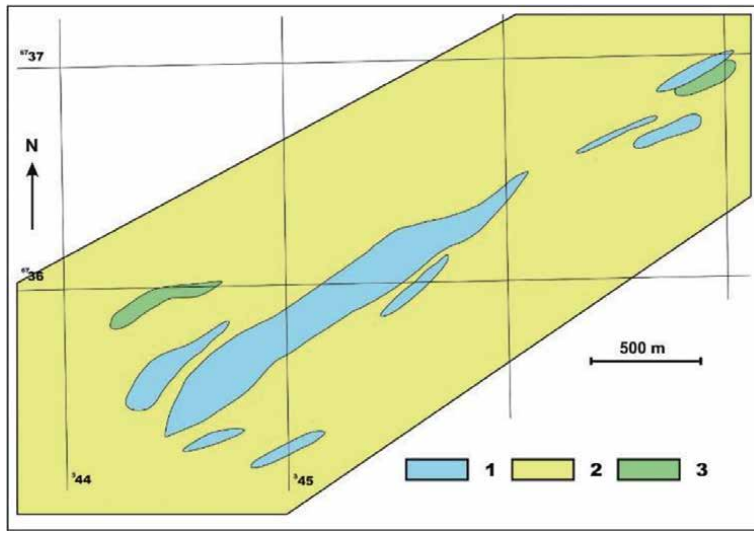

Figure 13.
Simplified scheme of the geological structure of the Gullsteinberget kyanite quartzite deposit (Norway). Compiler V. Shchiptsov. 1 – kyanite quartzites; 2 – biotite gneisses; 3 – amphibolites.

4. Discussion

The Fennoscandinavian Shield is represented by the largest Precambrian bedrock in Europe, covering more than a million km^2 throughout Norway, Sweden, Finland and the Karelian-Kola region in Russia [40]. In Sweden and Norway, partly Precambrian crystalline rocks are overlain by the Scandinavian Caledonides, and in the Kola Peninsula, certain areas are occupied by outcrops of Palaeozoic alkaline massifs (Khibiny, Lovozero, Kovdor and others) and in Norway by the Oslo rift complex. The most important events are associated with the evolution of 2800–2700 Ma, 2000–1800 Ma and 1500–1270 Ma.

In those times, continental crust was segregated from the Earth's mantle in three multiphase orogenies. The resultant Archean, Paleoproterozoic and Mezoproterozoic crust divided into some areas with characteristic litologic traits [40].

As a result of these events, the areas of distribution of high-alumina strata, which are present in all Precambrian structures – Southwestern Gneiss Province (900–1700 Ma), including the Transcandinavian magmatic belt (650–1800 Ma); Svecofennian Province, 1800–2000 Ma; Archean and Paleo-Mesoproterozoic rock complexes (1600–3400 Ma) – Norbotten, Karelian, Belomorian; Kola Provinces and Lapland-Kola zone – were isolated (**Figure 1**).

High-alumina rocks metamorphosed in amphibolite and granulite facies of metamorphism created a favourable environment for forming deposits of the sillimanite group of minerals.

The equilibrium of Al2SiO5 polymorpth (andalusite, kyanite and sillimanite) with triple point allows its use in characterising the fields of high-alumina strata and identifying three metamorphogenic types of high-alumina rocks determined by PT-parameters of metamorphism [5, 6]. The first type is the Keivian, the second is the Svecofennian, and the third is the Southwestern Gneissian type (Mesoproterozoic). Deposits and occurrences of kyanite, andalusite and sillimanite are associated with these types. Deposits and occurrences of kyanite were formed in metamorphic rocks of medium and high pressures and medium temperatures. Deposits and occurrences of andalusite are formed in metamorphic rocks of low and medium pressures and low and medium temperatures. Sillimanite is characteristic of metamorphic rocks of low and medium pressures and medium and high temperatures.

In a certain way, we can conclude that for the first type, the main industrial mineral is kyanite, the second type – andalusite, the third type – sillimanite and andalusite. As emphasised above, postmagmatic metasomatosis (acid leaching) played a major role in the formation of deposits and occurrences of the sillimanite group of minerals, especially characteristic of the Keivian type [29, 30].

5. Conclusion

Summarising the materials on high-alumina complexes of the Fennoscandinavian Shield, we can conclude that three types in this territory formed polycyclic and under various geodynamic conditions. Great importance is attached to the manifestation of processes related to acid leaching. The list of literature sources reflects the depth and versatility of the research conducted on the Fennoscandian Shield.

Thus, these mineral assemblages are important both from geological sense and economic geology. In the world economy, industrial minerals of the sillimanite group

(andalusite, sillimanite and kyanite) are mined from Precambrian shield rocks. The Fennoscandian Shield is no exception. The Keivsky type with world-class kyanite reserves evidences this. Magmatogenic formations have low contents of sillimanite-group minerals, e.g. pegmatites. Magmatogenic minerals of the sillimanite group belong in practice to the class of gemstones, and samples of these minerals can be found in many mineralogical museums of the world.

The Kola Peninsula has large reserves of kyanite ores in the Keiv Province (kyanite as a non-traditional metallic raw material) Khizovaara kyanite ore field (kyanite as an industrial mineral for multi-purpose use).

In Sweden, there are still prospects for the development of the Hålsjöberg and Hökensås kyanite deposits. Significant andalusite occurrences exist in the Shellefteå area of Boliden, Mångfallberget and Säter, Nyborg.

Norway is a promising area for discovering large deposits of kyanite and sillimanite.

Finland market research on the global andalusite, kyanite and sillimanite trade is carried out. The end of 2022 report shows the trend of Finland's participation in the global andalusite, kyanite and sillimanite market and estimates the country's foreign trade in andalusite, kyanite and sillimanite during 2011–2021 [63]. It can be concluded that an in-depth analysis of the prospects of the country's foreign trade in andalusite, kyanite and sillimanite has been carried out, and a forecast of the development of the andalusite, kyanite and sillimanite market until 2026 has been given.

Funding

This research was funded by state assignment to the Institute of Geology Karelian Research Centre, RAS, with theme N10220404400124-6-1.5.5.

Conflicts of interest

The author declares no conflict of interest.

Author details

Vladimir Shchiptsov[1,2]

1 Institute of Geology Karelian Research Centre RAS, Russia

2 Petrozavodsk State University, Petrozavodsk, Russia

*Address all correspondence to: vv.shchiptsov@gmail.com

IntechOpen

References

[1] Bel'kov IV. Kyanite Schists of the Keivyu Formation. Moscow: Leningrad; 1963. p. 136 (Russian)

[2] Kulish EA. High Alumina Metamorphic Rocks of the Lower Archean of the Aldan Shield and their Lithology. Khabarovsk: V. A. Solov'ev; 1973. p. 368 (Russian)

[3] Kerrick DM. The Al_2SiO_5 polymorphs. Mineral Society of America, Reviews in Mineralogy. 1990;**22**:406

[4] Haldar S. Introduction to Mineralogy and Petrology. 2nd ed. Elsevier; 2020. p. 429

[5] Berman RG. Thermobarometry using multiequilibrium calculations: A new technique with petrologic applications. Canadian Mineals. 1991;**38**:833-855

[6] Pattison DM. Instability of Al_2SiO_5 "triple-point" assemblages in muscovite+biotite+quartz-bearing metapelites, with implications. American Minerals. 2001;**86**:1414-1424

[7] Bushmin SA, Glebovitsky VA. Scheme of mineral facies of metamorphic rocks and its application to the Fennoscandian shield with representative sites of orogenic gold mineralization. Transactions of KarRC RAS. 2016;**2**:3-27. DOI: 10.17076/geo265

[8] Harben PW, Bates RL. Industrial Minerals Geology and World Deposits. London: Industrial Minerals Division Metal Bulletin Plc; 1990. p. 312

[9] Harben PW. The Industrial Mineral Handy Book—A Guide to Markets, Specifications and Prices. Worcester Park: Industrial Mineral Information; 2002. p. 412

[10] Ogorodnikov VN, Koroteev VA, Voitekhovsky YL, Shchiptsov VV, et al. Kyanite ores of Russia. In: Koroteev VA, editor. Institute of Geology and Geochemistry. Ural: Branch of the Russian Academy of Sciences; 2012. p. 334 (Russian)

[11] Hatfield AK. Kyanite and related minerals. USGS: Annual report. U.S. Department of the Interior U.S. Geological Survey; 2021. pp. 411-419

[12] Mineral Commodity Summaries 2023. U.S. Geological Survey, Reston, Virginia: Manuscript approved for publication. 2023. Available from: https://www.kriittisetmateriaalit.fi/wp-content/uploads/2023/02

[13] Glebovitsky VA. Problems of Evolution of Metamorphic Processes in Mobile Areas. Leningrad: Nauka; 1973. p. 127 (Russian)

[14] Rundkvist DV, Bushmin SA, Glebovitsky VA, Mikhailov DA, Rudnik VA. Basics of typification of Precambrian metasomatites. In: Precambrian Metasomatites and Their Ore Content. Moscow; 1989. pp. 5-15 (Russian)

[15] Koistinen T, Stephens MB, Bogatchev V, Nordgulen Ø, Wennerström M, Korhonen J. Geological Map of the Fennoscandian Shield, Scale 1:2 000 000. Geological Surveys of Finland, Norway and Sweden and the North-West Department of Natural Resources of Russia. Espoo, Finland: Geological Survey of Finland; 2001

[16] Baltybaev SK, Levchenkov OA, Levsky LK. The Svekofennian Belt of Fennoscandia: Spatial and Temporal Correlation of Early Proterozoic

Endogenous Processes. Saint-Petersburg: Nauka; 2009. p. 328 (Russian)

[17] Sharov NV, editor. Ladoga Proterozoic Structure (Geology, Deep Structure and Mineralogy). Petrozavodsk: KarKC RAS; 2020. p. 435 (Russian)

[18] Koroteev VA, Ogorodnikov VN, Voitekhovsky YL, Shchiptsov VV, et al. Non-bauxite aluminium raw materials of Russia. In: Koroteev VA, editor. Institute of Geology and Geochemistry. Ural: RAS; 2011. p. 228 (Russian)

[19] Glebovitsky VA. Scheme of mineral facies and thermodynamic regime oetamorphism. In: Thermodynamic Regime of Metamorphism. Leningrad; 1976. pp. 105-119 (Russian)

[20] Bushmin SA, Glebovitsky VA. Scheme of mineral facies of metamorphic rocks. Notes of RMO. 2008;**CXXXIV**(2):1-13 (Russian)

[21] Bel'kov IV. Kyanite Deposits in Mineral Deposits of the Kola Peninsula. Leningrad: Nauka; 1981. pp. 163-177 (Russian)

[22] Korovkin VA, Turyleva LV, Rudenko DG, et al. . In: Yakobson KE, editor. Subsoil of the North-West of the Russian Federation. Saint-Petersburg: Kartogr. fka VSEGEI; 2003. p. 500 (Russian)

[23] Neradovskiy YN, Voitekhovskiy YL. Atlas of Structures and Textures of Crystalline Shales of Bolshikh Keyvy. Apatity: K & M Publishing House; 2013. p. 116 (Russian)

[24] Voytekhovskiy YL, Neradovskii YN, Grishin NN. Rare metals and earths in kyanite shales of Bolshiye Keivy, Kola Peninsula. In: Proceeding of All-Russian Conf. Rare Metals: Mineral-Raw Material Base, Development, Production, Consumption. Moscow: IMGRE. pp. 43-44 (Russian)

[25] Grodnitsky LL, editor. Khizovaarskoe Kyanite Field. Petrozavodsk: KarRC RAS; 1988. p. 104 (Russian)

[26] Shchiptsov VV, Bubnova TP, Zavertkin AS, et al. Kyanite ores of the Khizovaara ore field (North Karelia). Trudy KarRC RAS. 2020;**6**:75-96. (Russian). DOI: 10.17076/them1252

[27] Glebovistky VA, Bushmin SA. In: Sokolov YM, editor. Postmigmatites metasomatism. Leningrad: Nauka; 1983. p. 216 (Russian)

[28] Ogorodnikov VN, Koroteev VA, Voitehovsky YL, Shchiptsov VV, et al. Morphogenetic types and technology of enrichment of kyanite ores. In: Koroteev VA, editor. Institute of Geology and Geochemistry. Ural: RAS; 2013. p. 310 (Russian)

[29] Bushmin SA. Facies, facies series of metasomasotites and ore specialization of metamorphic belts. In: Precambrian Metasomatites and their Ore Content. Moscow; 1989. pp. 46-64 (Russian). DOI: 10.1134/S1075701508080011

[30] Bushmin SA. Metasomatites of the Khizovara deposit (North Karelia). Izvestia AS USSR. 1978;7:127-138 (Russian)

[31] Sergeev SA, Lobach-Zhuchenko SB. Age of fuchsite metasomatites of izovaara (North Karelia) by U-Pb dating of single zircon grains. Reports of the Russian Academy of Sciences. 1993;**333**(1):73-75 (Russian)

[32] Volodichev OI, Korol NE, Kuzenko TI, Sibilev OS. Metamorphism of Early Precambrian complexes in the eastern part of the Fennoscandian hield.

In: Geology of Karelia from the Archean to the Present Day. Petrozavodsk: KarRC RAS; 2011. pp. 49-55 (Russian)

[33] Volodichev OI. In: Glebovistky VA, editor. Metamorphism of Disthene Gneisses (on the Example of theWhite Sea Complex). Leningrad: Nauka; 1975. p. 170

[34] Volodichev OI. In: Glebovistky VA, editor. White Sea Complex of Karelia. Leningrad; 1990. p. 248 (Russian)

[35] Marmo J. Alumiiniilikaatit.//Suomen teollisuusmineraalit ja teollisuuskivet. Toim. I.Haapala. Helsinki: Yliopistopaino; 1988. pp. 85-92

[36] Lehtinen MJ. Industrial minerals and rocks. In: Mineral Deposits of Finland. Amsterdam: Elsevier; 2015. pp. 685-706. DOI: 10.1016/b.978-0-12-410438-9.00026-1

[37] Aurola E. Kyaniitti ja pyrofylliitti esiintymät Poh. 1959; 287-333. 10.1080/00206819909465144

[38] Ihlen PM. Utilisation of sillimanite minerals, their geology, and potential occurrences in Norway – An overview. Norges Geologiske Undersøkelse Bulletin. 2000;**436**:113-128

[39] Müller A, Ihlen P, Wanvik JE, Flem B. High-purity quartz mineralisation in kyanite quartzites, Norway. Mineralium Deposita. 2007;**42**(5):523-535. DOI: 10.1007/s00126-007-0124-8

[40] Lehtinen M, Nurmi PA, Rämö OT, editors. Precambrian geology of Finland key to the evolution of the Fennoscandian Shield. Amsterdam: Elsevier B.V.; 2005. 736 p

[41] Velikoslavinsky DA. A Comparative Characteristic of Regional Metamorphism Is Moderate and Low. Leningrad: Nauka; 1972. p. 192 (Russian)

[42] Nagaitsev YV. Petrology Metamorphic Rocks of Ladoga and Belomorsky Complex. Leningrad: Nauka; 1974. p. 180 (Russian)

[43] Sokolov VA, editor. Geology of Karelia. Leningrad: Nauka; 1987. p. 231 (Russian)

[44] Korsman K, Korja T, Pajunen M, et al. The GGT/SVEKA transect: Structure and evolution of the continental crust in the Paleoproterozoic Svecofennian Orogen Finland. International Geology Review. 1999;**41**:287-333. DOI: 10.1080/00206819909465144

[45] Edelman N. Stratigraphy and Metamorphism in the Kristineberg Area. Stockholm: Sveriges Geologiska Undersökning; 1967. p. 45

[46] Einarsson U, Theolit T. Andalusitprojektet I Sater. Prap 92 017. Stockholm: SGU (Swedish); 1992

[47] Li B, Massonne HJ, Zhang J. Evolution of a gneiss in the Seve nappe complex of Central Sweden. Hints at an early Caledonian, medium-pressure metamorphism. Lithos. 2020;**2020**:376-377

[48] Eilu P, editor. Mineral Deposits and Metallogeny of Fennoscandia. Finland: Geological Survey of Finland; 2012. p. 401

[49] Ek R. Nysten, P.E. Phosphate mineralogy of the Hålsjöberg and Hökensås kyanite deposits. Geologiska Föreningens I Stockholm, 1990, 112(1). p. 9-18. 10.1080/11035899009453156

[50] Lundegårdh H. The Östmark formation and neighbouring rocks in the Proterozoic of Värmland, western Sweden. Geologiska Föreningen i Stockholm

Förhandlingar. 1980;**2**:137-140. DOI: 10.1080/11035898009450891

[51] Wise WS, Loh SE. Equilibria and origin of minerals in the system Al_2O_3-$AlPO_4$-H_2O. American Mineralogist 1976, N 61. 409-413.

[52] Bergström L. An occurrence of kyanite in a pegmatite in Western Sweden. In: Geologiska Föreningens i Stockgolm Förhandlingar. Vol. 82. Issue 2. 1960. pp. 270-272. DOI: 10.1080/11035896009449197

[53] Rodhe A, Andréasson P-G. Protoliths of the kyanite deposits at Hökensås. Protogine Zone of southern Sweden In: Geologiska Föreningen i Stockholm Förhandlingar. 1992;**114**(2):193-194. DOI: 10.1080/11035899209453884

[54] Larsson D. Transition of granite to quartz-kyanite rock at Hålsjöberg, southern Sweden: Consequence of acid leaching and later metamorphism. In: Geologiska Föreningen i Stockholm Förhandlingar. 2001;**123**(4):237-246. DOI: 10.1080/11035890101234237

[55] Andréasson PG, Dallmeyer RD. Origin and tectonic significance of high-alumina deposits along the Protogine Zone, southern Sweden. Journal of Metamorphic Geology. 2001;**N13**:461-474. DOI: 10.1111/j.1525-1314.1995.tb00234

[56] Sjoqvist A. Protolith of kyanite-bearing, quartz-rich rock in Hålsjöberg, western Sweden. Master Thesis, Degree Project in Geology hp. Stockholm: Stockholm University; 2017. 47 p

[57] Morton RD, Batey R, O'Nions RK. Geological investigations in the Bamble Sector of the Fennoscandian Shield South Norway 1. The Geology of Eastern Bamble. Norges geologiske undersøkelse. 1970;**263**:1-72

[58] Starmer IC. The major tectonics of the Bamble series between Søndeledfjord and Kilsfjord (Aust-Agder and Telemark). Norges Geologiske Undersøkelse. 1978;**338**(1978):37-58

[59] Andersen T, Grorud H-F. Age and lead isotope systematics of uranium-enriched cobalt mineralization in the Modum complex, South Norway: Implications for Precambrian crustal evolution in the SW part of the Baltic Shield. Precambrian Research. 1998;**91**(3-4):419-432. DOI: 10.1016/50301 9268/50301-9268(98)00061-8

[60] Taagvold H. Lesjaverk: Funnsted for de tre polymorfe mineralene kyanitt, andalusitt og sillimanitt. Stein. 2016;**43**(1):2-14 (Norwegian)

[61] Whitney DL, Samuelson WJ. Crystallization sequences of coexisting andalusite, kyanite, and sillimanite, and a report on a new locality: Lesjaverk, Norway. European Journal of Mineralogy. 2019;**31**(4):731-737. DOI: 10.1127/ejm/2019/0031-2873

[62] Müller A, Wanvik J, Kronzle A. Norwegian kyanite quartzites – potential resources of high purity quartz? In: NGU, Project no.: 270400. 2005. p. 70

[63] Finland Trade of Andalusite. Kyanite and Sillimanite: Import, export, market prospects. BAC Trade Research Reports & Analysis. 2022;**2022**:25

Chapter 4

Sol Hamed Ophiolitic Complex, Southern Eastern Desert, Egypt: Petrological, Economic Potentiality and Structural Implications

Tarek Sedki, Haroun A. Mohamed, Shehata Ali and Rafat Zaki

Abstract

The Sol Hamed (SH) area is a part of the Arabian-Nubian Shield (ANS) ophiolites occurred within Onib-Sol Hamed suture zone in the southern Eastern Desert (SED) of Egypt. The ophiolitic assemblages in this area are represented by serpentinite, metagabbro and arc assemblages represented by metavolcanics. They later intruded by gabbroes and granites. Geochemically, the compatible trace elements enrichment in SH serpentinites indicate derivation from a depleted mantle peridotite source. They show affinity to the typical metamorphic peridotites. The Cr and TiO_2 contents indicate supra-subduction zone (SSZ) environment. Their Al_2O_3/SiO_2 and MgO/SiO_2 ratios support the SSZ affinity and are similar to ANS peridotites with fore-arc setting. Structurally, the area represents four deformational events can be well-known in the Neoproterozoic rocks (D_1, D_2, D_3 and D_4); There is major three fault sets affected the area. Magnesite in SH serpentinites are cryptocrystalline. It is occurring as snow-white veins and stock-works. These characteristics are typical of Kraubath type magnesite deposits. Gold is confined to malachite-bearing quartz veins, smoky quartz veins and alteration zones. Malachite-bearing quartz veins trending NW-SE cut through gabbroic rocks. The barren quartz veins are vertical with E-W directions. Alteration zones with NW-SE trend and vertical dip intrude metagabbros and metavolcanics.

Keywords: ophiolites, supra-subduction zone, serpentinites, magnesite, mineralization, gold deposits

1. Introduction

The Arabian–Nubian Shield (ANS) crustal growth occurred during the Neoproterozoic Era [1]. The ANS represents a combination of well-preserved tectono-stratigraphic terrains characterized by well-defined suture zones which are marked by ophiolite assemblages [2–4]. During mid-Neoproterozoic, Juvenile arc terrains formation around Mozambique Ocean margins and collision occurred producing the ANS [3, 5, 6]. In late Neoproterozoic (~630 Ma), arc accretion

terminated once East and West Gondwana fragments collision occurred closing the Mozambique Ocean and generating the East African–Antarctic Orogen [7, 8]. Therefore, ANS suture zones are classified to older arc–arc suture zones which separated ~700–870 Ma arc terrains and younger arc–continent suture zones formed at ~630 Ma [2, 9–12]. It is generally accepted that most of the ANS ophiolites were generated in supra-subduction zone (SSZ) environment [13–18]. They formed due to seafloor spreading above active subduction zones. Several tectonic scenarios were attributed for the ANS ophiolites formation: (1) NMORB setting (i.e., fragments of normal oceanic crust [19]: (2) remnants of back-arc basins (e.g., [9, 20, 21]); or (3) fore-arc setting due to seafloor spreading during initiation of subduction process [4, 13–15, 17, 22]. Various ophiolite complexes may possibly be generated in diverse SSZ tectonic settings. In order to contribute to resolve this existed debate, we introduce new geochemical data on Sol Hamed serpentinites in the southern Eastern Desert to better constraint their tectonic setting. The Egyptian Precambrian belt which is the NE part of the ANS is consisted of an Upper Proterozoic assemblage of volcano-sedimentary succession, scattered over thrusting mafic-ultramafic rocks (i.e., ophiolite complex) and intruded by syn- to late-tectonic granitoids and mafic–ultramafic intrusions. Later, Precambrian peralkaline granites and Tertiary alkaline ring complex intrude the country rocks of the area. The Sol Hamed ophiolitic complex is a part of Allaqi-Heiani-Onib-Sol Hamed-Yanbu arc–arc suture (**Figure 1**; [23, 24] which represent one of the two longest and most complete Neoproterozoic ophiolite suture in the Arabian Nubian Shield [25].

2. Materials and methods

2.1 Field study

For this purpose, field trip was carried out during the period of 20–27 April 2019 by using the Landsat image and the available geologic maps (scale 1:50000) were used. About 15 rock samples were collected representing the exposed serpentinites in the mapped area (**Figure 2**). Thin sections were prepared for each sample.

2.2 Laboratory work

For this purpose, petrographic investigation of 15 thin sections and 4 polished sections were prepared. The petrographical study was achieved using MEIJI ML 9000 Polarizing Microscope equiped with automatic photo micrographic attachement ToupCam Digital Camera XCAM1080PHA. Chemical analyses of 10 samples were carried out at the Central Laboratories of the Geological Survey of Egypt. The selected samples represent the best aerial coverage of the examined area. Before bulk rock chemical analyses were carried out, the samples were cleaned and grinded in an electric agate mill, homogenized, dried on the oven for 60 min at 105 degree then mix with 50% from wax polyvinyl meta-acylate additives. Determination of the chemical composition of both major and some trace elements was performed by using a Philips X-ray fluorescene technique model PW/2404, with Rh radiation tube and eight analyzing crystals. Crystal (LIF-200) was used for estimating Ca, Fe, K, Ti and Mn, while crystal (TIAP, PX-1) was used for estimating Mg and Na. Crystal (Ge) was used for estimating P and Crystal (PET) was used for estimating Si and Al.

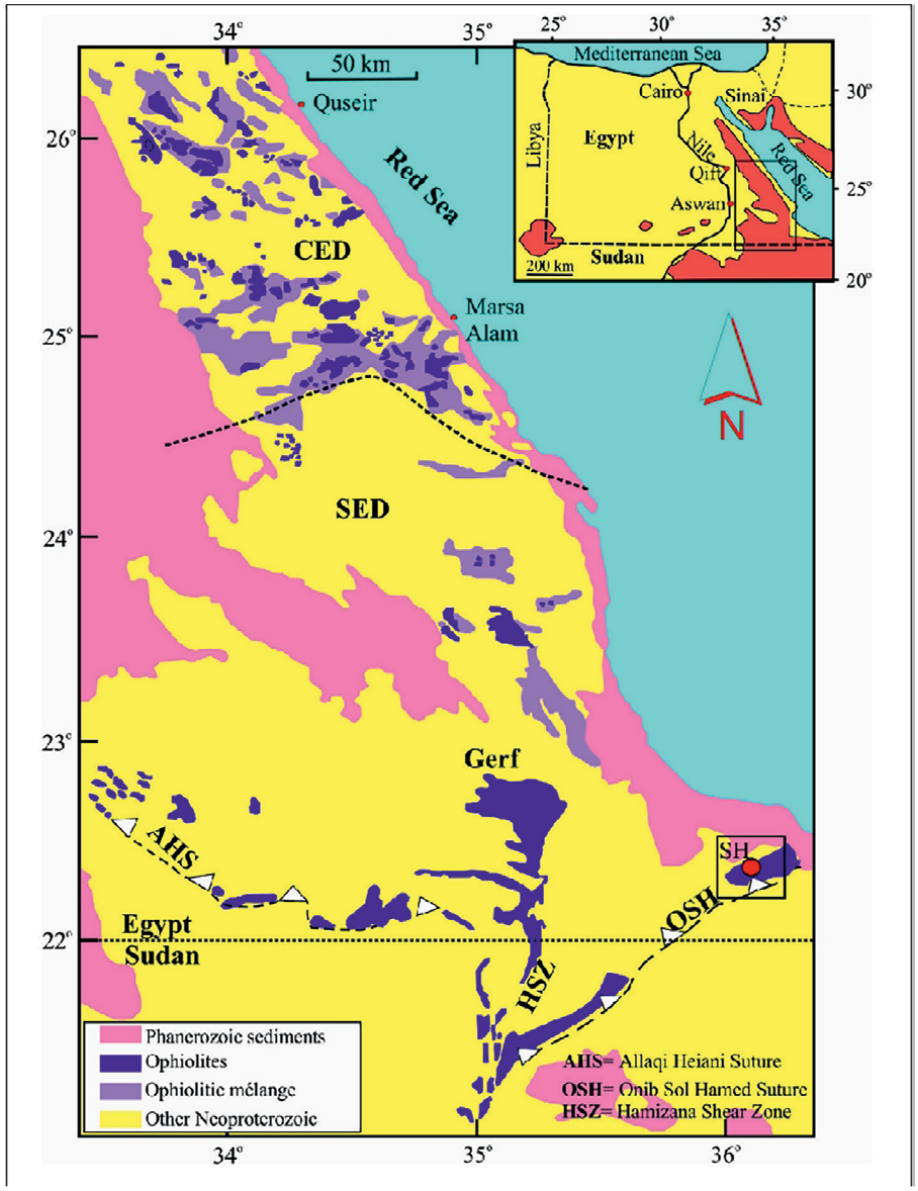

Figure 1.
Map showing the distribution of ophiolites in the central Eastern Desert (CED) and southern Eastern Desert (SED) of Egypt (Modified from [23]). The location of Sol Hamed (SH) ophiolites is also indicated. The inset map shows the general map of Egypt.

The concentration of the analyzed elements was determined by using software Super-Q with accuracy 99.5% and confidence limite 95.6%. Ten samples of these rocks were also analyzed to determine their REE contents using the simultaneous inductively coupled plasma emission spectrometer (720 ICP-OES, Agilent Technologies), with accuracy 96%. Nine samples from SH magnesites were analyzed for major elements by the same technique of XRF mentioned above. All analytical results are given in **Tables 1** and **2**.

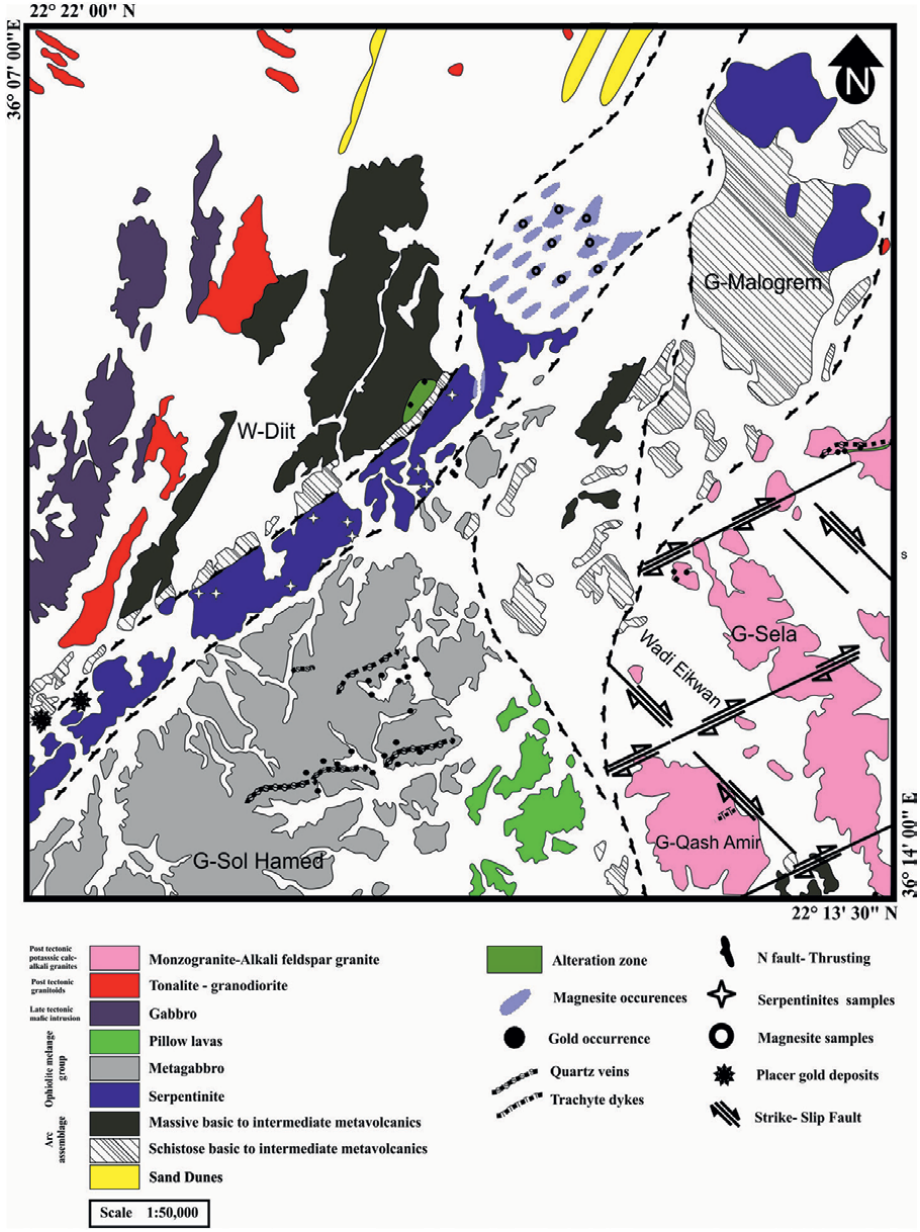

Figure 2.
Geological map of SH (after EMRA, 1995, [26]).

3. Geologic setting

Sol Hamed area located in north of Gabal Elba in the southern Eastern Desert. Its rock units consist of mainly ophiolitic assemblage and arc-related metavolcanics and granitoids.

Ophiolite complex contains three NE-SW trending sub-vertical lithological zones, ultramafic in the NW side, gabbros in the middle and pillow lava in SE (**Figure 2**).

Sample no	1	2	3	4	5	6	7	8	9	10
Major oxides (wt. %)										
SiO_2	45.699	46.286	45.709	45.539	45.957	45.654	44.360	44.050	44.857	47.617
TiO_2	0.057	0.056	0.011	0.058	0.012	0.023	0.023	0.023	0.035	0.012
Al_2O_3	0.550	0.993	0.491	0.465	0.046	0.231	1.015	0.915	0.346	0.115
$Fe_2O_3^T$	7.788	8.365	7.771	9.294	9.099	9.799	9.249	9.954	8.660	6.924
MnO	0.103	0.089	0.114	0.081	0.092	0.173	0.056	0.034	0.104	0.104
MgO	45.470	43.832	45.709	44.261	44.575	44.063	44.778	44.863	45.226	45.182
CaO	0.218	0.134	0.171	0.290	0.196	0.058	0.203	0.160	0.750	0.046
Na_2O	0.103	0.190	0.011	0.012	0.012	0.000	0.282	0.000	0.012	0.000
K_2O	0.011	0.056	0.011	0.000	0.012	0.000	0.034	0.000	0.012	0.000
Total	100	100	100	100	100	100	100	100	100	100
LOI	12.690	10.340	12.490	13.920	13.180	13.260	11.340	12.600	13.280	13.350
SiO_2/MgO	1.005	1.056	1.000	1.029	1.031	1.036	0.991	0.982	0.992	1.054
Al_2O_3/SiO_2	0.012	0.021	0.011	0.010	0.001	0.005	0.023	0.021	0.008	0.002
MgO/SiO_2	0.995	0.947	1.000	0.972	0.970	0.965	1.009	1.018	1.008	0.949
Mg#	92.077	91.247	92.131	90.450	90.692	89.940	90.592	89.961	91.220	92.855
Trace elements (ppm)										
V	40.200	29.500	27.400	37.200	26.100	22.160	40.200	14.010	34.100	19.500
Cr	2655.400	2701.100	2706.600	2656.800	2688.800	2580.200	2701.200	2654.100	2708.600	2425.900
Ni	2377.100	1800.300	2056.300	2057.300	2070.100	1840.200	1816.200	2055.400	1657.200	1999.100
Cu	63.100	15.100	24.100	50.530	43.210	53.210	54.210	8.290	47.310	33.510
Zn	56.900	13.460	24.900	23.070	35.100	17.900	34.800	17.200	11.890	23.050

Sample no	1	2	3	4	5	6	7	8	9	10
Co	166.500	121.400	120.500	162.300	165.200	152.400	154.200	152.400	117.200	136.100
Ga	1.560	1.050	0.900	1.300	1.200	1.110	1.200	1.400	1.330	1.340
Rb	0.330	0.350	0.500	0.400	0.450	0.500	0.450	0.350	0.300	0.280
Sr	55.020	46.150	47.900	62.100	60.100	72.110	50.100	88.990	48.080	48.100
Zr	120.000	118.000	127.000	119.000	121.000	120.000	123.000	122.000	121.000	118.000
Nb	0.100	0.090	0.085	0.100	0.100	0.100	0.090	0.080	0.090	0.100
Ba	35.600	15.100	25.000	15.120	19.800	17.110	16.430	45.040	20.000	29.500
La	0.100	0.100	0.100	0.100	0.100	0.100	0.100	0.100	0.100	0.100
Ta	0.085	0.085	0.085	0.085	0.085	0.085	0.085	0.085	0.085	0.085
Pb	4.800	13.140	16.100	15.100	16.900	19.900	17.100	4.660	24.050	14.700
Th	0.200	0.200	0.200	0.200	0.200	0.200	0.200	0.200	0.200	0.200
Tl	0.037	0.038	0.040	0.300	0.260	0.040	0.038	0.040	0.300	0.280
Li	10.100	5.000	7.000	6.120	5.500	8.200	8.980	9.900	1.710	7.150
Hf	0.020	0.020	0.020	0.020	0.020	0.020	0.020	0.020	0.020	0.020
Cs	0.850	0.750	0.090	0.090	0.088	0.090	0.080	0.680	0.070	0.060
Sn	0.085	0.085	0.085	0.085	0.085	0.085	0.085	0.085	0.085	0.085
Bi	0.010	0.030	0.025	0.020	0.010	0.020	0.030	0.030	0.025	0.020
Cd	2.100	2.100	3.200	3.400	2.150	2.500	3.500	3.400	3.450	2.900
In	0.010	0.010	0.010	0.010	0.010	0.010	0.010	0.010	0.010	0.010
W	0.090	0.090	0.090	0.090	0.090	0.090	0.090	0.090	0.090	0.090
Mo	0.010	0.010	0.010	0.010	0.010	0.010	0.010	0.010	0.010	0.010
Re	0.003	0.003	0.003	0.003	0.003	0.003	0.003	0.003	0.003	0.003
Sb	1.830	2.400	3.110	1.140	3.150	2.700	3.100	3.100	1.980	2.330

Sample no	1	2	3	4	5	6	7	8	9	10
As	4.210	5.330	3.700	5.700	5.300	4.800	4.500	5.210	4.910	3.800
Ag	185.000	190.000	195.000	191.000	187.000	170.000	193.000	192.000	190.000	194.000
S	0.040	0.040	0.040	0.040	0.040	0.040	0.040	0.040	0.040	0.040
Se	0.300	0.500	0.400	0.300	0.700	0.230	0.300	0.400	0.700	0.500
Be	0.850	0.700	0.900	0.850	0.900	0.900	0.800	0.700	0.700	0.800
Te	5.500	5.400	5.500	5.500	4.110	4.800	5.700	4.300	4.980	5.120
Rb	1.810	1.000	1.200	1.700	1.450	1.700	0.330	0.800	0.200	1.300
Sc	4.100	4.010	3.800	3.550	4.200	3.700	3.940	4.010	4.300	3.900
U	0.090	0.090	0.090	0.090	0.090	0.090	0.090	0.090	0.090	0.090
Rare earth elements (ppm)										
Y	0.080	0.080	0.080	0.080	0.080	0.080	0.080	0.080	0.080	0.080
Ce	0.250	0.249	0.248	0.250	0.250	0.250	0.250	0.250	0.250	0.250
Dy	0.079	0.082	0.080	0.080	0.080	0.080	0.080	0.080	0.080	0.080
Eu	0.078	0.080	0.080	0.080	0.080	0.080	0.080	0.080	0.080	0.080
Er	0.078	0.084	0.080	0.080	0.080	0.080	0.080	0.080	0.080	0.080
Gd	0.081	0.077	0.080	0.080	0.080	0.080	0.080	0.080	0.080	0.080
Ho	0.083	0.078	0.080	0.080	0.080	0.080	0.080	0.080	0.080	0.080
Nd	0.100	0.100	0.100	0.100	0.100	0.100	0.100	0.100	0.100	0.100
Pr	0.100	0.120	0.100	0.100	0.100	0.100	0.100	0.100	0.100	0.100
Sm	0.083	0.079	0.082	0.083	0.078	0.078	0.079	0.084	0.083	0.078
Tm	0.077	0.081	0.080	0.080	0.080	0.080	0.080	0.080	0.080	0.080
Tb	0.080	0.079	0.080	0.080	0.080	0.080	0.080	0.080	0.080	0.080

Sample no	1	2	3	4	5	6	7	8	9	10
Yb	0.083	0.077	0.080	0.080	0.080	0.080	0.080	0.080	0.080	0.080
Lu	0.082	0.076	0.080	0.080	0.080	0.080	0.080	0.080	0.080	0.080
ΣREE	1.334	1.342	1.330	1.333	1.328	1.328	1.329	1.334	1.333	1.328
La/Yb	1.325	1.429	1.538	1.688	1.310	1.205	1.358	1.410	1.447	1.266
Gd/Yb	0.976	1.000	1.000	1.000	1.000	1.000	1.000	1.000	1.000	1.000
La/Sm	1.205	1.266	1.220	1.205	1.282	1.282	1.266	1.190	1.205	1.282

Table 1.
Major, trace and rare earth elements of the studied rocks.

	1	2	3	4	5	6	7	8	9
SiO_2	0.70	0.68	0.40	1.30	0.23	0.30	0.90	0.30	0.30
TiO_2	0.00	0.00	0.00	0.00	0.00	0.00	0.00	0.00	0.00
Al_2O_3	0.10	0.10	0.10	0.10	0.10	0.10	0.10	0.10	0.10
Fe_2O_3	0.04	0.05	0.10	0.32	0.03	0.06	0.05	0.05	0.06
Fe	0.03	0.03	0.07	0.22	0.02	0.04	0.03	0.04	0.04
MnO	0.00	0.00	0.00	0.00	0.00	0.00	0.00	0.00	0.00
Mn	0.00	0.00	0.00	0.00	0.00	0.00	0.00	0.00	0.00
MgO	42.70	42.30	42.60	41.10	45.50	43.00	45.10	43.40	41.10
CaO	5.80	5.18	5.50	5.18	1.60	5.30	2.60	4.18	5.30
Na_2O	0.40	0.15	0.18	0.15	0.50	0.01	0.01	0.15	0.01
K_2O	0.00	0.01	0.00	0.00	0.00	0.00	0.00	0.00	0.00
P2O5	0.02	0.02	0.02	0.02	0.02	0.07	0.02	0.02	0.02
LOI	49.10	49.30	50.10	49.00	49.30	50.30	49.50	50.50	51.01
Total	98.89	97.82	99.07	97.40	97.30	99.19	98.31	98.74	97.94

Table 2.
Magnesite chemical analysis.

This belt signifies the north-eastern outlet of the Hamizana Shear Zone (**Figure 1**). The ophiolitic ultramafics include both sheared and massive varieties. Serpentinites show low to medium relief. They cropped out in the central and eastern parts. Furthermore, they are transformed along NE-SW trending shear zones to talc, talc- and quartz-carbonates, and magnesite particularly in the eastern parts. Most quartz carbonates present in the area sideways the contact between serpentinites and metavolcanics. Magnesites fill the cracks and fissures creating stock-work within the serpentinite (**Figure 3a**).

The massive ultramafic complex comprises serpentinized dunite, peridotite and pyroxenite. The serpentinized dunite swarm few chromite pods [27]. The complex is net-veined with white-blue gray magnesite filling the fractures due to hydrothermal alteration. Serpentinite is geologically bounded in NW and SE by schistose basic to intermediate metavolcanics and ophiolitic metagabbro, correspondingly.

Metagabbros occur as large masses of low to medium relief. They are serene in the southern part of the study area, separated by basic dykes (**Figure 3b**) and quartz veins. They current SE of the serpentinites with a perfect tectonic contact trending NE–SW and dip to NW (**Figure 2**). They are locally layered, sheared and warped as flaser structure (**Figure 3d**). They are cut by acidic dykes of apogranite (synonym of Albitized granite) (**Figure 3e**) and metagabbro-diorite dykes forming parallel and nearly vertical NE-SW trending dykes (**Figure 3b**). They are also intruded by post-tectonic granitoids (i.e., tonalite and monzogranite) at SE of Gabal Sol Hamed (**Figure 3f**).

Basaltic pillow lavas situated NW to W of Gabal Qash Amer and related with the volcaniclastics. The original pillow customs are easily familiar and dip to the SW. They have gone through constrain deformation designated by the lineated and stretched pillow volcanics.

Figure 3.
Field photographs show a) the stock-work in magnesite bearing serpentinites, b) Bas basic dyke cutting the ophiolitic gabbro, c) Brecciated quartz-vein, d) Flaser structure of metagabbro, e) acidic dykes of apogranite and f) post-tectonic granitoids intruded within metagabbro.

The arc assemblages comprise basic to intermediate metavolcanics and their pyroclastic rock varieties. The acidic metavolcanics display schistose structure with main direction of 50o and dip 60o SE. The meta-rhyolites showing at the northeastern and western part of the area, wounding by quartz veins and enclosed by sand dune particularly in the north central part. The massive basic to intermediate metavolcanics produce out at the northern part. In the western side of Wadi Diit, a small belt of massive and schistose metavolcanics is observed (**Figure 2**). These rocks are slightly foliated and comprise thin beds of fine laminated volcaniclastics and tuffs. There are also lapilli tuffs with plagioclase and quartz clasts of lapilli size. Gradational connection

with gabbroic rocks existing south of the volcanic rocks. North of this volcanic belt, there is a sharp intrusive contact with tonalite rocks.

The arc granitoids with low to medium relief crop out at the NW part of the area and are characterized by presence of dioritic xenoliths.

Granitic rocks befall in Qash Amer and El Sela area. Qash Amer muscovite granites signify the highest peak in the area. They are categorized by fractures, exfoliation, and weathering boulders. The El Sela younger granites take place as high-relief remote and dispersed granitic masses vacating the southern East part of the mapped area (**Figure 2**). They are characterized by cavernous weathering and exfoliation. They interrupt younger metavolcanics and are occupied by different types of trachytic dikes and quartz. These granites show joints and fractures that are occupied by iron oxide containing radioactive minerals.

Numerous basic and acidic dykes separated the area. Acidic dykes are detailed in Wadi Diit, where they cut tonalite and metavolcanics. Generally, they are trending either NE-SW or N-S. They include rhyolite, apogranite and dacite. Basic dykes are abundant and trend mainly either NE-SW or NW-SE. They changed through all the rock units described above particularly tonalite, metavolcanics and ophiolitic gabbro (**Figure 3b**). They comprise andesite and dolerite (**Figure 3b**) with N-S trend.

The veins can be subdivided into three main types, quartz, and ankerite and pegmatite veins. The studied area is rich in quartz veins with different thickness trending mainly N-S and NE-SW particularly in the metavolcanics. It is white color and sometimes rich with iron oxides and copper minerals. Other types of quartz are brecciated, cemented by iron oxides (**Figure 3c**). Sometimes, smoky quartz detailed especially in the gabbroic rocks. Quartz veins cut through all the rock units. The veins are brecciated, stained red with iron oxides and may comprise pyrite crystals (**Figure 3c**). Many quartz veins are supplementary with hydrothermal alteration zones in the metavolcanic rocks. Ankerite veins befall as big veins at junction of Wadi Diit with Wadi Badbari. They changed the schistose metavolcanics, trending either NE–SW or E-W with a vertical dip.

4. Petrography

4.1 Serpentinites

Serpentinites recorded in SH. They are fine-grained and light green to dark green in color and essentially consist of serpentine minerals (>80%) together with variable amounts of carbonates, magnetite (**Figure 4a**), and brucite as well as chromian spinel. In few samples, talc is observed and Olivine is completely altered to serpentine and opaques along its irregular fractures. Clinopyroxenes are partially and/or completely altered to tremolite and chlorite. The rocks exhibit pseudomorphic (**Figure 4b**) and interpenetrating textures. Antigorite is the main serpentine mineral together with lesser chrysotile and Lizardite Antigorite occurs as large plates and fibrous and scaly aggregates (**Figure 4b**). Chrysotile occurs as fibrous veinlets that commonly transformed into carbonate and traversing the antigorite matrix (**Figure 4a**). In some parts, bastite texture is associated with schiller structure where magnetite defines cleavage planes of the original orthopyroxene (**Figure 4a**). Chromian spinel in the serpentinites occurs as both subhedral to euhedral crystals (**Figure 4a**) and irregular grains, while in the sheared varieties spinel is mostly brecciated. Carbonates occur as sparse crystals, patches, and fine aggregates.

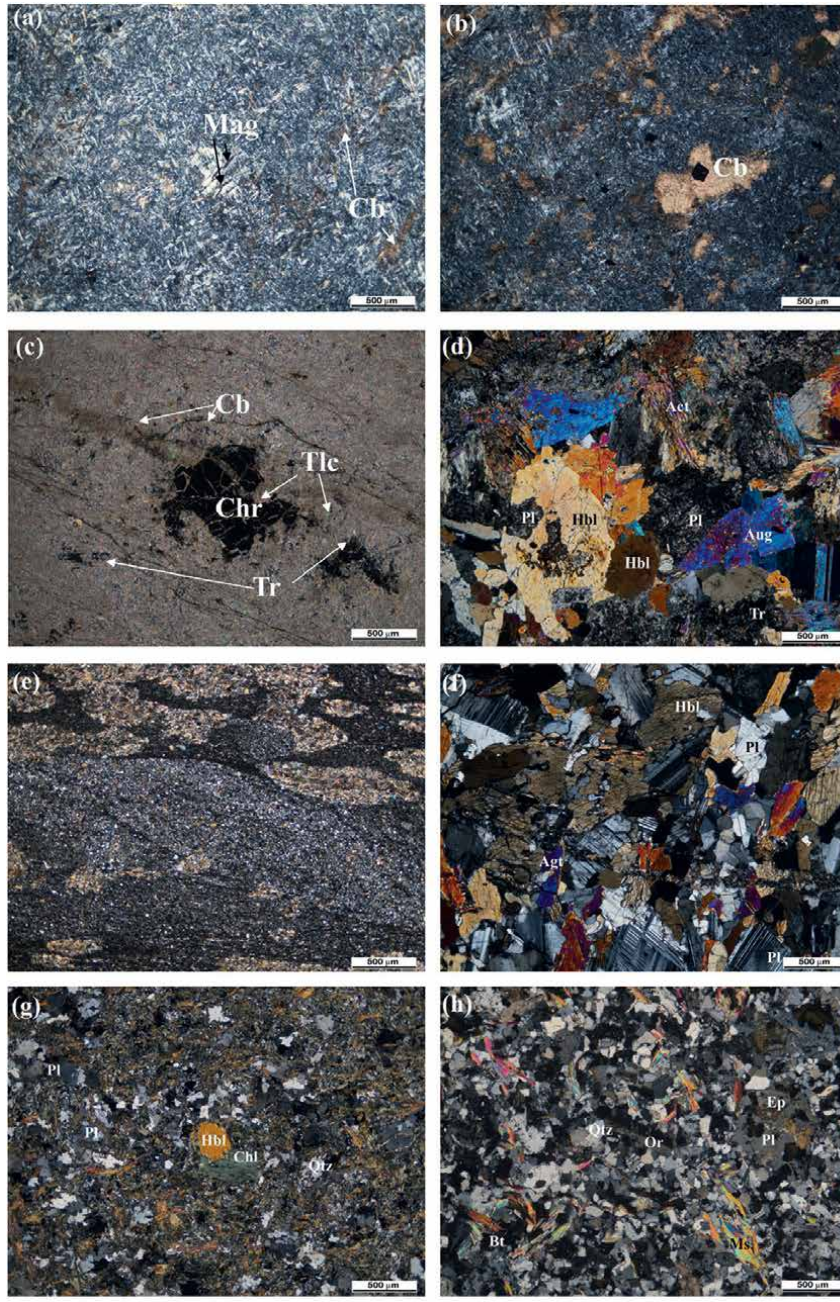

Figure 4.
Photomicrograph showing a) Serpentinites with fine-grained and light green to dark green in color and consist of serpentine minerals organized with variable amounts of carbonates, magnetite, b) Pseudomorphic and interpenetrating textures of serpentinites, carbonates as an alteration product of serpentine minerals, c) Tremolite-talc rocks composed of tremolite and talc together with olivine and orthopyroxene relics, d) Metagabbro with fine crystals of plagioclase and is variably altered to tremolite, actinolite and chlorite. The secondary amphibole are highly abundant and mainly represented by actinolite commonly pale green and moderately pleochroic, often simply twinned and occurs as fibrous prisms and tablets. Augite occurs as irregular shreds and remnants within the pseudomorphic amphibole, e) Andestic and basaltic composition of metatuffs, f) Crystals of plagioclase and Hornblende in metagabbro-diorite, g) Plagioclase and Hornblende in diorite and h) Plagioclase, K-feldspars, quartz, muscovite, biotite in syn-tectonic granite

4.2 Carbonate serpentinite

Carbonate serpentinites are composed of serpentine minerals and carbonates as the main components. Carbonates occur as an alteration product of serpentine minerals (**Figure 4b**) whereas; opaques represent the main accessories. Carbonate samples are mostly stained with iron oxides, whereas some appear as veinlets corroding rock.

4.3 Tremolite-talc rocks

Tremolite-talc rocks are composed of tremolite and talc together with olivine and orthopyroxene relics (**Figure 4c**). Accessory minerals are represented by carbonates and opaques. Talc and tremolite are formed as alteration products of olivine and orthopyroxene. Tremolite forms fibro-lamellar sheaves piercing talc, orthopyroxene and olivine.

4.4 Ophiolitic Metagabbros

These metagabbros are massive, holocrystalline, medium to fine-grained with a grayish-green to dark green color. They show ophitic to sub-ophitic textures, and mainly consists of plagioclase (60–50%) and amphibole (40–30%), together with rare fresh relics of clinopyroxene. The secondary minerals are chlorite, zoisite, clinozoisite, epidote, sericite and calcite, while the accessories are sphene, apatite and opaque minerals.

Plagioclase crystals are euhedral to subhedral and many exhibit albite twinning. Variable alteration of plagioclase to epidote, zoisite and clinozoisite, as well as sericite, is observed. Zoning of plagioclase occurs, but is generally uncommon. Primary magmatic hornblende is less abundant and when observed it occurs as prismatic and bladed aggregates that poikilitically encloses fine crystals of plagioclase (**Figure 4d**) and is variably altered to tremolite, actinolite and chlorite. The secondary amphibole is highly abundant and mainly represented by actinolite commonly pale green and moderately pleochroic, often simply twinned and occurs as fibrous prisms and tablets (**Figure 4d**). Augite occurs as irregular shreds and remnants within the pseudomorphic amphibole (**Figure 4d**). Chlorite is present as flakey and fibrous aggregates and is closely associated with amphibole, epidote and calcite. Epidote occurs as anhedral granular aggregates replacing plagioclase and amphibole. Accessory minerals such as apatite occurs as fine laths embedded in plagioclase and amphibole.

4.5 The metavolcanoclastic rocks (meta-tuffs)

The meta-tuffs are encountered in the western part of the mapped area but with restricted extension. They are massive, fine-grained, bedded, laminated and sometimes associated with thin bands of brownish opaque minerals. Microscopically, they are composed essentially of metamorphosed ash and lapilli tuffs, containing mineral and rock fragments. The mineral fragments are represented by plagioclase and quartz, whereas the rock fragments are andesitic and rarely basaltic in composition (**Figure 4e**).

4.6 Metagabbro-diorite

Microscopically, these rocks consist mainly of plagioclase, amphibole together with subordinate amounts of pyroxene and opaques. Few samples contain very small

amounts of quartz. Opaques, sphene and apatite are the accessories, while calcite, actinolite, chlorite and epidote represent the secondary products. Ophitic and sub-ophitic textures are common, whereas the porphyritic texture is rarely observed. Plagioclase ranges in composition from labradorite to oligoclase and generally occurs as subhedral to anhedral crystals, partly saussuritized. Amphiboles are represented by less abundant primary, prismatic crystals of brownish green color and politically enclosing minute crystals of plagioclase (**Figure 4f**). Secondary hornblende is predominating and form pseudomorphs after pyroxene. It commonly occurs as pale green subhedral crystals sometimes enclosing small crystals of plagioclase. Pyroxene occurs as relics of altered greenish blue crystals. It is commonly an augite altered to secondary hornblende as indicated by the presence of the original pyroxene in the core mantled by secondary hornblende (**Figure 4f**).

4.7 Diorite

Mineralogically the diorites are composed mainly of plagioclase and hornblende (**Figure 4g**). Locally, chlorite partially replaces hornblende and quartz is a minor constituent. Hypidiomorphic texture is characteristic, Apatite, zircon and Fe oxides are common accessories.

4.8 Syn-tectonic granite

These rocks are represented by micro-granite. It is medium-grained and shows granular to granular porphyritic in texture. It is made up of plagioclase, K-feldspars, quartz, muscovite, biotite (**Figure 4h**), accessory minerals (zircon, opaque minerals), and secondary minerals (chlorite, sericite and calcite). Plagioclase constitutes about 40% of the granite. Crystals are anhedral and equant, and albite twinning is ubiquitous. Plagioclase crystals are usually un-zoned. Potassium feldspar constitutes up to 20% of the rock. It occurs as small irregular crystals, often totally or partially enclosed by plagioclase; in some instances, plagioclase with myrmekitic intergrowths appears to invade the adjacent orthoclase. Quartz constitutes about 30% or the granite. It occurs as medium-sized, anhedral crystals, sometimes with sutured margins, and also as small, drop-like inclusions in either feldspar. It generally has undulous extinction. Muscovite constitutes up to 10% of the rock. It occurs as euhedral isolated laths, sometimes with small rounded quartz inclusions, and sometimes occurs as ragged intergrowths with quartz. Occasional ragged crystals of biotite occur, which may be partially replaced by chlorite. Calcite occurs as fine interlocked crystals commonly form micro-bands or filling the polygonal spaces among the plagioclase laths.

5. Results

Major oxides recalculated on an anhydrous basis and plotted volatile-free to reduce the variable element dilution effects resulting from serpentinization process. The studied serpentinites have relatively higher loss of ignition (LOI) values (10.34–13.92 wt. %). The MgO content is hardly affected by serpentinization process and its elevated values in SH serpentinites (MgO = 43.83–45.71 wt. %) reflect highly depleted mantle source [28, 29]. Their high Mg# (89.94–92.85) are like modern oceanic peridotites [30] indicating a limited mobility of Mg and Fe. Their very low

Na_2O (0.00–0.28 wt. %) and K_2O (0.00–0.06 wt. %) contents are comparable to those from the Eastern Desert supporting this study [13, 15]. The serpentinization processes possibly increased the LOI contents without significant modification of the major element composition [31]. The Ca–metasomatism is a common issue in Egyptian serpentinites [32], however the very low CaO contents (0.05–0.75 wt.%) in the serpentinites indicates restricted effect of carbonate metasomatism. So, we suggest that the protolith major element compositions must have been preserved during the hydration processes and that the geochemistry of the studied serpentinites display mostly the original nature.

SH serpentinites display affinity to the typical metamorphic peridotites on the AFM diagram [33]; **Figure 5a**. The bulk-rock Al_2O_3 content is relatively unaffected by serpentinization and therefore retains its original primary signature [30]. The studied serpentinites have Al_2O_3 contents (0.05–1.02 wt. %) comparable to oceanic and active margin peridotites and fore-arc and Pan-African serpentinites **Figure 5b**; [13, 15, 18, 34, 35]. Like other Eastern Desert ultramafites, the SH serpentinites have SiO_2/MgO ratios and Al_2O_3 contents analogous to ophiolitic peridotite [13, 15, 17, 19, 36, 37] **Figure 5c**. The serpentinites the nature of peridotitic komatiite by using of Jensen's cation plot after [38], **Figure 5d**. The Al_2O_3 and CaO depletion is typical of fore-arc peridotites, **Figure 6a**;[39] and characterizes ED ophiolitic ultramafites [15, 17, 19, 37]. In terms of Al_2O_3/SiO_2 and MgO/SiO_2

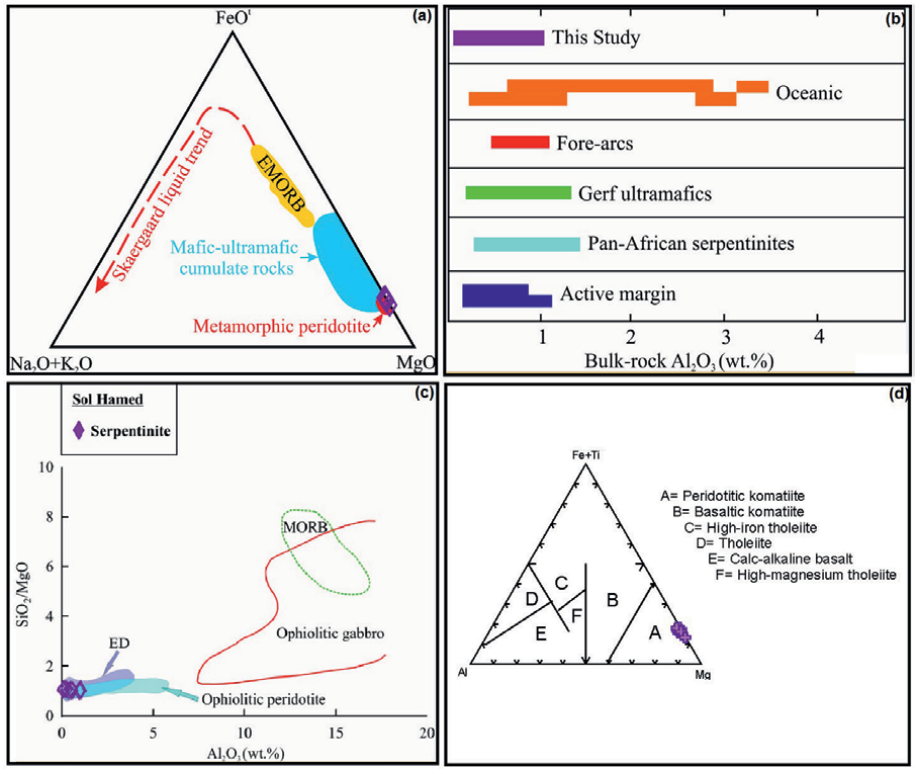

Figure 5.
a) AFM diagram for SH serpentinites after [33], b) Bulk-rock Al_2O_3 (wt. %) contents of SH compared with those from other tectonic settings from [34] and the Pan-African serpentinites [18, 35], c) SiO_2/MgO ratios vs. Al_2O_3 diagram. Ophiolitic peridotite, ophiolitic gabbro and MORB are from [36]. Data from Eastern Desert (ED) are shown for comparison [13, 15, 17, 19, 37] and d) Jensen's cation plot after [38].

ratios, they are like Arabian–Nubian shield and fore-arc peridotites (**Figure 6b**; [13, 15, 29, 44, 46], low value of Al_2O_3/SiO_2 (fore-arc field), suggesting that these rocks were derived from a mantle source with high degrees of partial melting. The studied serpentinites have enriched compatible trace elements (Cr = 2426–2709 ppm, Ni = 1657–2377 ppm and Co = 117–167 ppm) suggesting derivation from a depleted mantle peridotite source.

The SH mantle rocks are highly depleted in incompatible trace elements relative to the primitive mantle (**Figure 6c**). They are variably depleted in Nb consistent with SSZ geochemical characteristics [47] similar to abyssal and fore-arc peridotites [45, 48]. Moreover, the positive Pb-anomaly on spider diagrams resembles abyssal and fore-arc peridotites [45, 48] (**Figure 6c**). This specific positive Pb-anomaly may proposes a protolith origin or reflects the result of fluid percolation during serpentinization processes [49, 50]. The serpentinites has low concentrations HFSE such as Nb, Hf, Ta, Ce, U and Th, comparatively high concentration of LILE such as Ba and Sr. Subduction zone trace element signatures are clear due to the enrichment of LILE (Sr and Ba) over HFSE (Nb, Ti, Y, Ce, U and HF) and negative Ta anomaly [22]. The REE diagram displays HREE enrichment and LREE depletion. The Av.ΣREE contents of serpentinites is 1.33 ppm.

Chondrite normalized REE patterns show very low fractionated patterns (La/Yb) = (1.398). The LREE of the studied ultramafic show a low degree of fractionation (La/Sm = 1.24). The degree of fractionation of HREE is also low (Gd/Yb = 0.998), (**Figure 6d**).

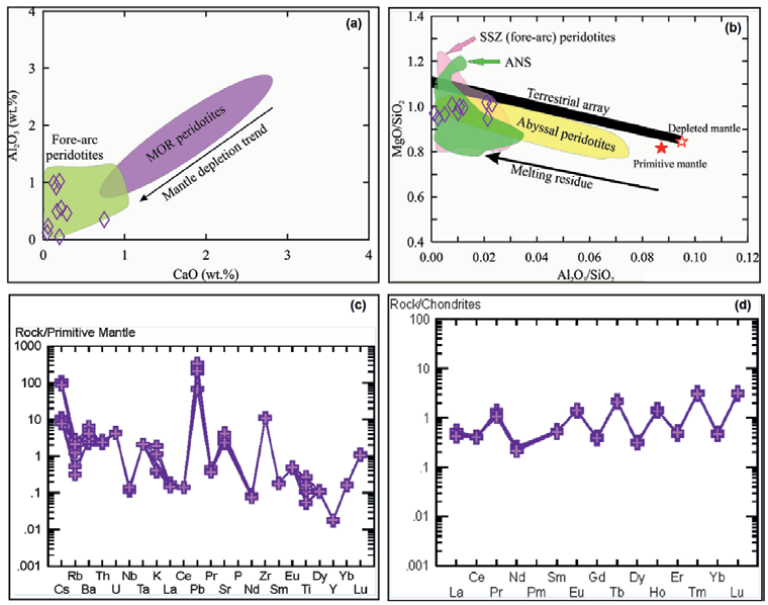

Figure 6.
a) CaO vs. Al_2O_3 diagram showing SH serpentinites compared with fore-arc and MOR peridotites after [39], b) MgO/SiO_2 vs. Al_2O_3/SiO_2 diagram. Primitive and depleted mantle values are after [40] and [41], respectively. The "terrestrial array" represents the bulk silicate Earth evolution [42, 43]. Abyssal and fore-arc peridotite fields are after [29, 44, 45]. ANS ophiolitic peridotite field is after [13, 46], c) Primitive mantle-normalized trace element patterns, and d) Chondrite-normalized REE patterns for the SH mantle section. Normalizing values are after [40].

DOI: http://dx.doi.org/10.5772/intechopen.1003957

6. Discussion

Metamorphism ranging from low-grade greenschist to medium-grade amphibolite facies usually influenced the ophiolitic ultramafites of the Egyptian ED forming serpentinite and/or mixtures of serpentine, talc, chlorite, carbonates and magnetite e.g., [13, 15, 51–53]. The time and source of carbonate metasomatism that commonly affected the Egyptian ultramafites still debated. [32] adopted mixing between mantle-derived CO_2-rich fluids and remobilized sedimentary carbonate. [54] suggested pure CO_2-bearing mantle source based on stable isotopes (i.e., O, C). Moreover, CO_2 input from mantle and metamorphic-degassing was proposed to explain the origin of the magnesite veins in serpentinites from the ED e.g., [55, 56]. Even with changes occurred during serpentinization in the mineral compositions of peridotites, geochemical data of serpentinites suggest negligible modification of major elements (except for Ca) at the hand-specimen scale e.g., [31, 50, 57]. Therefore, the low CaO contents (0.05–0.75 wt. %) in the serpentinites indicate restricted effect of Ca–metasomatism. The CaO contents are not correlated with LOI further confirming this implication. Moreover, the trace element compositions (except U and Sr) are not significantly modified during serpentinization e.g., [45, 50, 58]. Accordingly, the major and trace element data reflect the primary signature of the serpentinites protolith in subduction zones [50, 59, 60]. LOI reach up to 10.34–13.92 wt. %, which supports the role of hydrothermal alteration. In the MgO-$Fe_2O_3^T$-Al_2O_3 ternary diagram of [61], all samples plot in the metamorphic metasomatic field (**Figure 7a**). The MgO/SiO_2 and Al_2O_3/SiO_2 ratios of serpentinites agree with SSZ peridotites from fore-arc setting, **Figure 6b**; [29, 44]. In the Hf-Th-Nb diagram [63] used to regulate the tectonic character of ultramafic rocks, all samples plot in the destructive field of plate margins (**Figure 7b**). Generally, the Al_2O_3 and CaO depletion characterizes fore-arc peridotites (**Figure 6a**) [30, 39]. The Cr vs. TiO_2 diagram also supports the SSZ setting for the SH serpentinites, **Figure 7c**; [64].

The studied rocks show low Al_2O_3 content reflecting depleted upper mantle source [30]. Their high Mg#, Cr and Ni are consistent with a depleted mantle peridotite source [15, 69]. The MgO/SiO_2 and Al_2O_3/SiO_2 ratios (**Figure 6b**) accord with peridotites generated from subduction-related magma source. It is supporting by using Zr vs. Nb binary diagram [65], all samples plot in the depleted mantle sources (**Figure 7d**). Comparing SH ophiolites with other ophiolites such as, Troodos in Cyprus, [67], Gerf ophiolite in South Eastern Desert [15] and Wadi Ghadir ophiolites in Central Eastern Desert [22]. Using the criteria in [64], we conclude that the chemical signature, the crystallization arrangement and mantle residue of SH ophiolites are similar to supra-subduction zone ophiolites formed in fore-arc basins based on the Ti–V variation diagram [66], (**Figure 7e**).

Numerous geochemical studies demonstrated restricted mobility of major elements during serpentinization and protolith primary signature were retained e.g. [50, 57, 70]. The SH serpentinites have low CaO contents comparable to ophiolitic peridotites [36]. Moreover, their low Al_2O_3/SiO_2 ratios (mostly <0.03) are similar to fore-arc mantle wedge serpentinites suggesting that their protoliths had experienced partial melting before serpentinization which has no effect on this ratio e.g., [50, 58, 71]. Also, their low MgO/SiO_2 ratios (< 1.1) resemble serpentinised lherzolites and harzburgite [50]. They have low TiO_2 contents (0.01–0.06 wt. %) compared to depleted mantle composition but like subduction zone serpentinites [41, 50]. Their major element data consistent with harzburgitic source (**Figure 7f**).

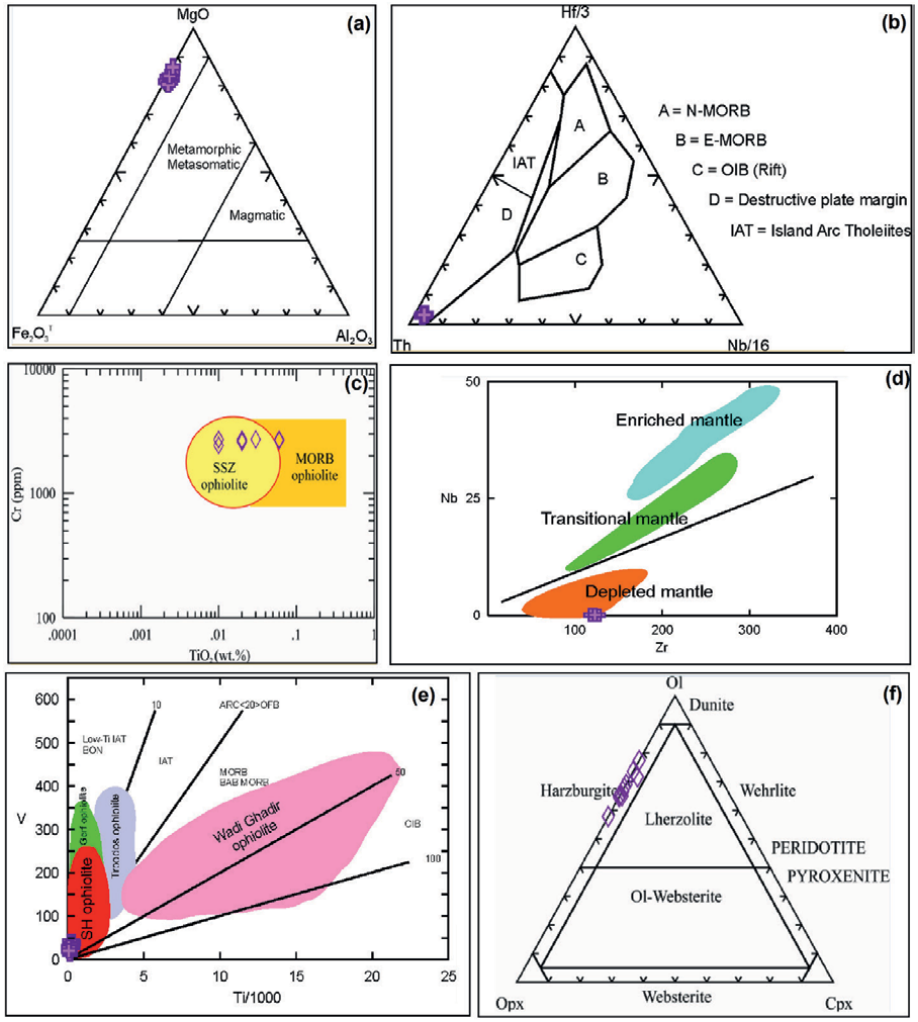

Figure 7.
a) MgO-$Fe_2O_3^T$-Al_2O_3 ternary diagram for the ultramafic rocks. Zone after [61] and lines after [62], b) Hf/3-Th-Nb/16 ternary diagram of [63], c) Cr vs. TiO_2 plot to discriminate SSZ and MORB ophiolites after [64], d) Zr vs. Nb diagram after [65], e) Ti–V discrimination diagram [66], where Sol Hamed (SH) ophiolites (Red) compare with forearc/arc ophiolites, Troodos (blue) ophiolite from [67], Gerf (Green) ophiolite from [15] and Wadi Ghadir ophiolites (Pink) from [22] and f) Ol–Cpx–Opx diagram [68].

7. Structural setting

7.1 Deformation history

The structure of the SH area is complex, and partially agreed [27], the area situated in a supra-structural position between three major Pan-African terranes (SE Desert, Gabgaba, and Gebeit terranes). Four deformational events can be distinguished in the Neoproterozoic rocks [72–75];

- **D1** event: E–W thrust faults and related E–W (F1) folds which considered as early stages of collision of Gerf and Gabgaba arc terranes.

- **D2** event: NW–SE thrust faults and related NW–SE (F2) folds were formed, characterized by local high-P, low-T metamorphism and reflected as late stages of collision of Gerf and Gabgaba arc terranes. The mineralization in this stage is described as remobilization of Cu–Ni–Pt sulfides in ultramafic rocks, alteration talc/serpentinites and listwaenites; Talc carbonate, gold-bearing quartz veins.

- **D3** event: conjugate NNW-trending sinistral and NNE-trending dextral transpression, as well as N–trending tight folds (F3). NW–SE shear zones and open folds, crenulation cleavage, SC fabrics, sigmoidal foliation patterns that defined in late- to post-tectonic granitoids. This stage characterized by local contact metamorphism. The mineralization in this stage is styled as kaolinitized alteration zones along D3, shear zones; ferregination and silicification of copper sulfide zones and gold–quartz veins. Shortening connected to collision of east and west Gondwana; tectonic escape toward oceanic free face to N along WNW striking Najd faults.

- **D4** event: E–W dextral strike-slip and dip-slip normal faults striking NNW–SSE to N–S and E–W may be related to Red Sea rifting. This stage characterized by dike swarms along faults. The mineralization in this stage is styled as disseminated secondary uranium and anomalous secondary concentrations of Pb, Zr, Y, Nb, Ta, in late dikes.

7.2 Faults and structural analysis

The SH complex is characterized by flat-lying and steeply dipping ductile shear zones trending ENE and associated thrust sheets (**Figures 2** and **8a**). The strike-slip shear zones which surround the SH to the N and S show tectonic transport to the ENE where SH mass movement in this direction generated over thrusts of the SH on the volcanic–sedimentary succession. The ENE tectonic direction transport is inferred from moderately-plunging WSW-directed mineral lineation, rodding, minor fold axes and from long axes of the deformed pillows. Shears and thrust planes are characterized by either siliceous mylonites or talc iron rich schists and ankerite-carbonates.

There are three major faults on the investigated area (**Figure 8b**).

- The first is NE-SW trending faults and is mainly present in the volcanic-sedimentary assemblage and Gabal SH.

- The second is E-W faulting affects all the basement rocks and disturbs the NE-SW trending faults.

- The third is N-S faults are probably related to some stages of the Red Sea rifting, and affected all the rock units including sandstone and Quaternary marine sediments of the Red Sea coast.

The direction of the shear zone on the investigated area has NE, the principal stress access has WNW to EW (**Figure 8a**). The associated structural features are signified by:

- NNE–SSW normal faults,

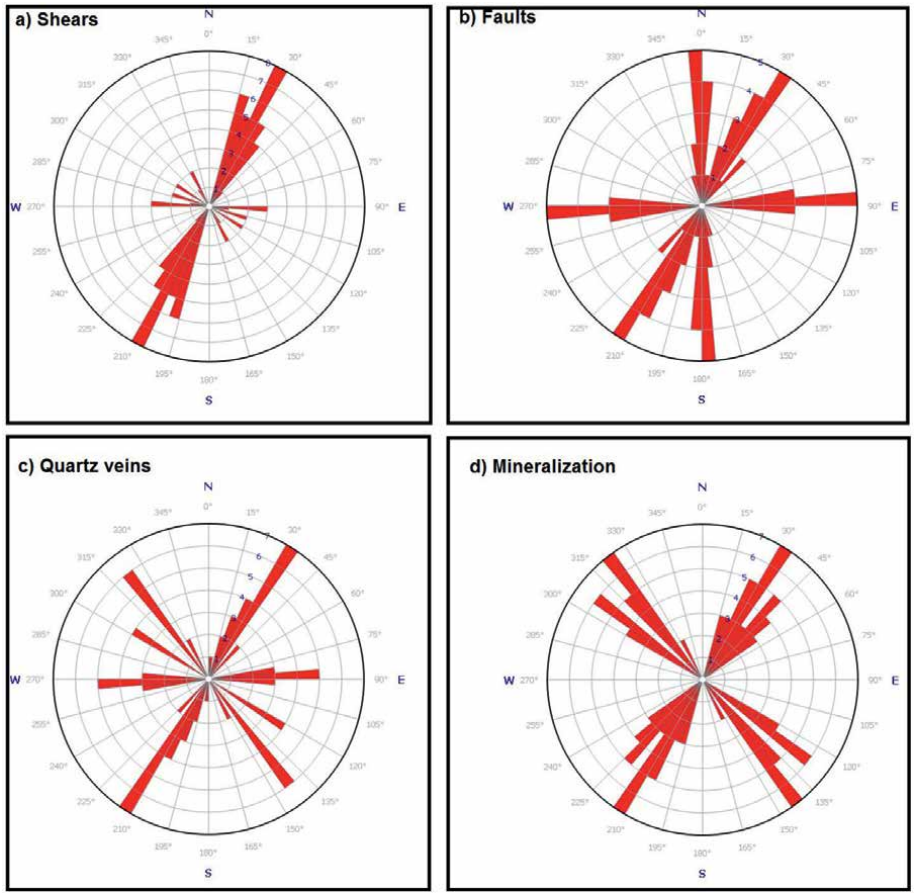

Figure 8.
Structural analysis of Sol Hamed area.

- NW-SE reverse faults,
- NE–SW, NW-SE, WNW-ESE, NNE–SSW and EW quartz veins (**Figure 8c**).

The mineralized structures (**Figure 8d**), are represented by

- Quartz veins have mainly NE–SW and NNW–SSE trends
- Faults have mainly NE–SW trends
- Breccia and alteration have mainly NW-SE trend

El Sela shear zone is separated by two main faults in the direction of ENE–WSW and NNW–SSE (**Figure 2**). The earlier trend associated with the major shear zone is injected by quartz veins. This shear zone is dissected into three parts by two strike slip faults trending NNW–SSE. Field observations indicate that the granites are affected by different stages of alteration, mainly at El Sela shear zone. These granites are invaded by ENE–WSW quartz veins. These veins caused hydrothermal alteration

associated with radioactive mineralization in the fine-grained granites. Secondary uranium mineralization is observed as canary-yellow thin layers deposited along small cracks and micro-fractures.

7.3 Kinematic indicators

Various kinematic indicators are used to fix the sense of movement with the common settled in the brittle-ductile system. The most common kinematic indicators on the SH area are mylonites (**Figure 9a**) and quartz fish (**Figure 9b**) shows dextral sense of movement. Mylonites take place in extraordinary strain zones (mylonite zones) and are understood as exhumed ductile shear zones. The sense of replacement on a shear zone is usually expected to lie subparallel to striations, stretching and mineral lineations.

8. Ore mineralogy

The opaque mineral content in the studied rock types from 2–6% of the rock volume. They are represented by sulphides, magnetite, hematite and gold.

Sulphides minerals are mainly represented by arsenopyrite, pentlandite, pyrrhotite and pyrite. Minor crystals of chalcopyrite and bornite are observed in few samples. Arsenopyrite occurs as subhedral to euhedral rhombic crystals either independent or associated with pyrrhotite (**Figure 10a**). It shows white color and displays strong anisotropism of blue color. Pentlandite occurs either as homogeneous or zoned grains (**Figure 10b**). Pyrrhotite forms irregular grains with bluish shade and moderate reflectance and sometimes replaced by light creamy to yellow isotropic pentlandite (**Figure 10a**). Pyrite occurs as subhedral to euhedral crystals either replaced by magnetite (**Figure 10c**). The replacement of pyrite by magnetite indicates oxidizing conditions.

Magnetite appears as anhedral crystals with peripheral granules of pyrite. Magnetite forms well-formed euhedral crystals of light gray color and moderate reflectance (**Figure 10c**). Hematite exhibits whiter color and cherry red internal

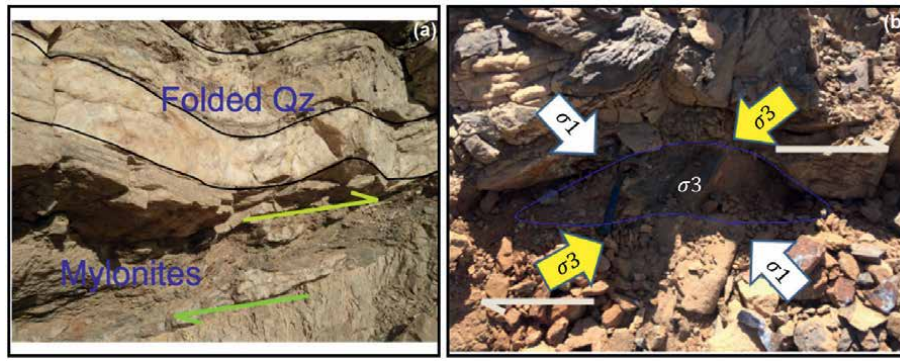

Figure 9.
a) Mylonite derived from a narrow shear zone transecting a weakly deformed granodiorite. b) Quartz fish from a quartzite mylonite shows dextral sense of movement. Quartz in the matrix is dynamically recrystallized and developed an oblique foliation.

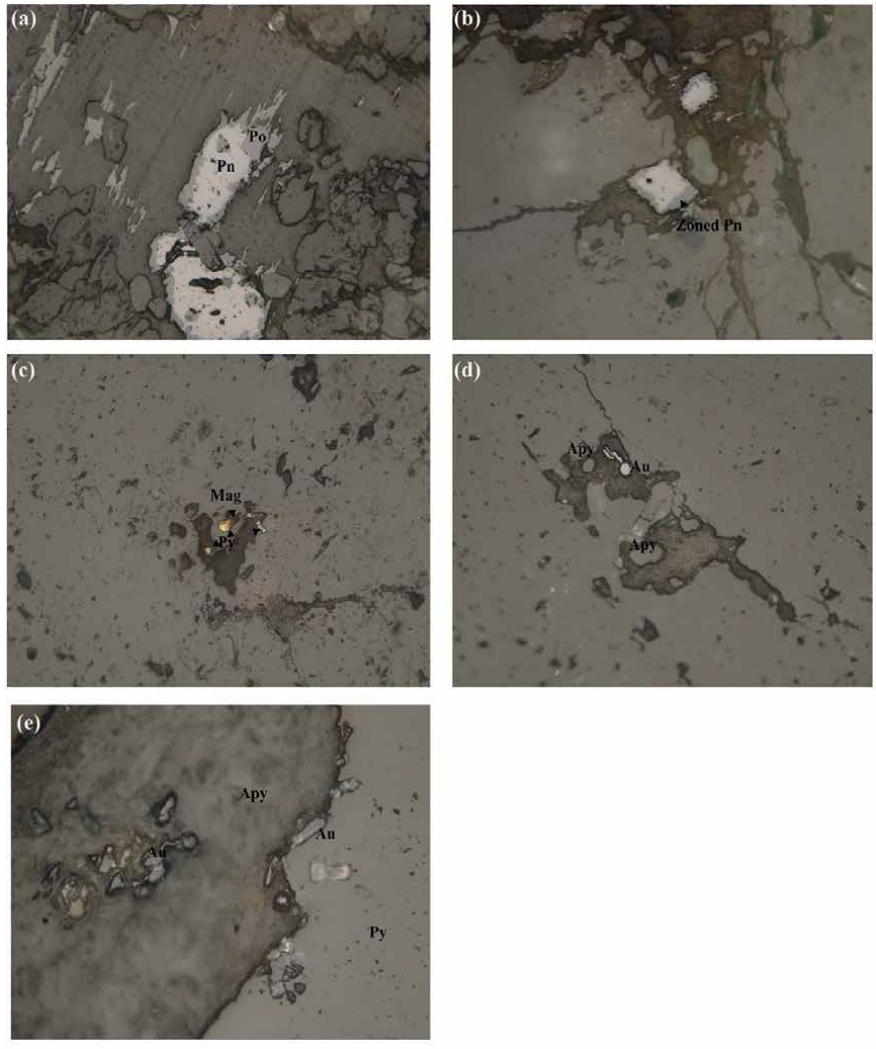

Figure 10.
Photomicrograph showing a) Pyrrhotite forms irregular grains with bluish shade and moderate reflectance and sometimes replaced by light creamy to yellow isotropic pentlandite, b) Pentlandite occurs either as homogeneous or zoned grains, c) Magnetite forms well-formed euhedral crystals, d) Gold as inclusions in arsenopyrite crystals and e) Pyrite-arsenopyrite contacts and The gold grains range in color from yellow to creamy yellowish color and with occur as sub-rounded grains or as straight-edged grains.

reflection. It shows isotropism in minor parts, which reveals its alteration from previous existing magnetite.

Gold is only recorded in highly altered quartz veins associated with the granitic masses. It occurs as disseminated grains that have bright yellow color with greenish tint. These grains occur as inclusions in arsenopyrite crystals (**Figure 10d**) and at pyrite-arsenopyrite contacts (**Figure 10e**). The gold grains range in color from yellow to creamy yellowish color and with occur as sub-rounded grains or as straight-edged grains (**Figure 10d** and **e**).

9. Economic potentiality

9.1 Magnesite mineralization

Economically, the important magnesite deposits occur in two types: the Venarch and Kraubath type [76]. The Venarch type deposits have the world's largest reserves [76]. They form strata-bound lensoid bodies of coarsely crystalline spar-magnesite hosted by marine sediments. Genetically, they are associated with shallow marine water of chloride-type evaporites. Kraubath type deposits are cryptocrystalline magnesite [76] and less common than spar-magnesites. However, they are important because of their high-quality magnesite product. These deposits comprise stock-works and veins of white magnesite formed in ultramafic country rocks. The origin of Kraubath magnesite type deposits favor hypogene-hydrothermal formation [76].

Magnesite deposits of SH serpentinites are cryptocrystalline formed by hydrothermal solution effects on the serpentinite host rocks and occur in three forms. The first is represented by white patches consisting of vertical veins and horizontal sheets. The second is found as veinlets represented by stock-work shape, characterized by nodules clusters and exposed as pockets within the serpentinites. The third is widespread in Wadi Diit NE of Gabal SH and is intercalated with surficial deposits. It is found as veinlets with stock-work shape and has low grade magnesite ore. These features are consistent with Kraubath type deposits (**Figure 11**).

The magnesite pockets exposed at the NE ends of SH serpentinites and along NNE trending shear zone (**Figure 2**). The magnesium source in magnesite is likely the magnesium-rich minerals (e.g., serpentine, olivine) occurred within ultramafics. Serpentinite appears to be the host for over 90% of all known magnesite veins worldwide.

The chemical data of magnesite ore is recalculated and presented in **Table 2**. The collected samples contain average (wt. %) 42.98 MgO, 0.57 SiO_2, 0.09 Fe_2O_3, 4.5 CaO, and 0.023 P_2O_5. They show depletion in some incompatible major elements (i.e., Ca, Al and Na) relative to the average primitive composition of upper mantle [77]. Possibly some of this CaO might has been lost during serpentinization [78] and shows strongly negative correlation with MgO (Pearson correlation factor = −0.864) in **Table 3**. Iron also shows loss during serpentinization.

9.2 Gold deposits

Ophiolitic serpentinites surrounded the metavolcano-sedimentary assemblage are the likely sources for gold mineralization in the vein-type gold deposits which invaded the island-arc volcanic and volcaniclastic rocks and/or the granitic rocks [79, 80].

The vein-type mineralization occurred in the sheared ophiolitic serpentinites (**Figure 12a**) associated with the Pan-African Orogeny. Linear zones of serpentinites display abundant alterations along thrusts and shear zones with the development of talc, talc-carbonate and reddish-brown quartz-carbonate rock (i.e., listwaenite) (**Figure 12b**). Listwaenite is commonly mineralized with gold [81, 82]. Malachite-bearing quartz veins with NW-SE direction cut through gabbroic rocks and show mylonitic structure, pinch and swell phenomenon. They are extremely fractured containing considerable content of malachite and disseminated sulfide minerals (**Figure 12c** and **f**). Mineralized smoky quartz veins with NE-SW direction and

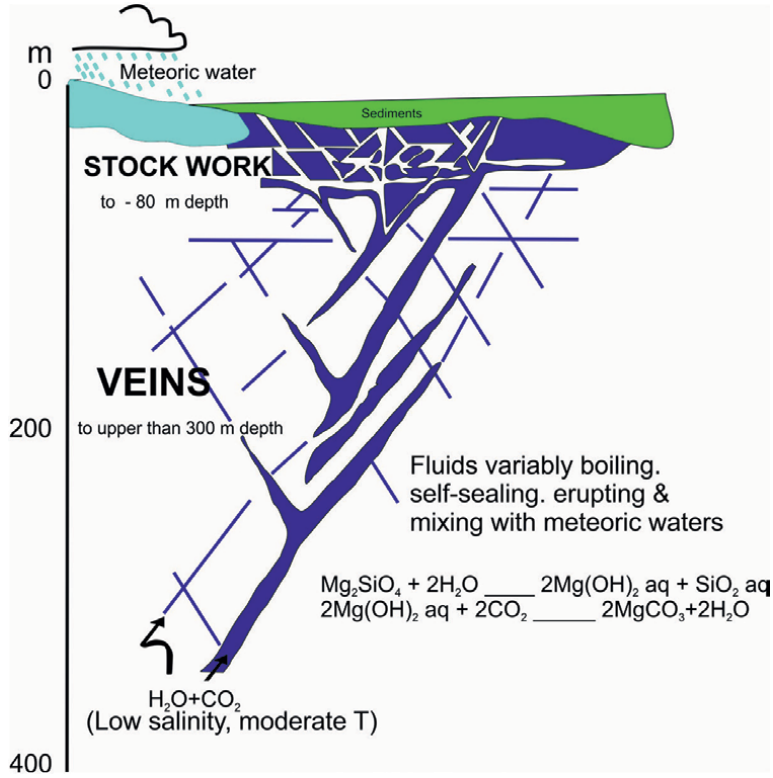

Figure 11.
Kraubath type of magnesite deposit model after [76].

	MgO	CaO	SiO_2	Na_2O	K_2O	P_2O_5
MgO	1					
CaO	**–0.864**	1				
SiO_2	–0.27	0.139	1			
Na_2O	0.36	–0.308	–0.124	1		
K_2O	–0.086	0.138	–0.01	–0.041	1	
P_2O_5	–0.047	0.254	–0.236	–0.316	–0.052	1

Table 3.
Pearson correlations between oxides in magnesite mineralization.

steeply dipping SE invaded the meta-andesite (**Figure 12g**). They are intensively sheared and contain iron oxides in the fissures and cracks (**Figure 12d–f**). The barren quartz veins are nearly vertical and have E-W directions (**Figure 12f**). The highest gold grades are associated with strong arsenopyrite mineralization and in fracture-seal veins.

Mineralized alteration zones trending NW-SE and dipping nearly vertical traverse metagabbro and metavolcanics (**Figure 12f**). They are characterized by the presence

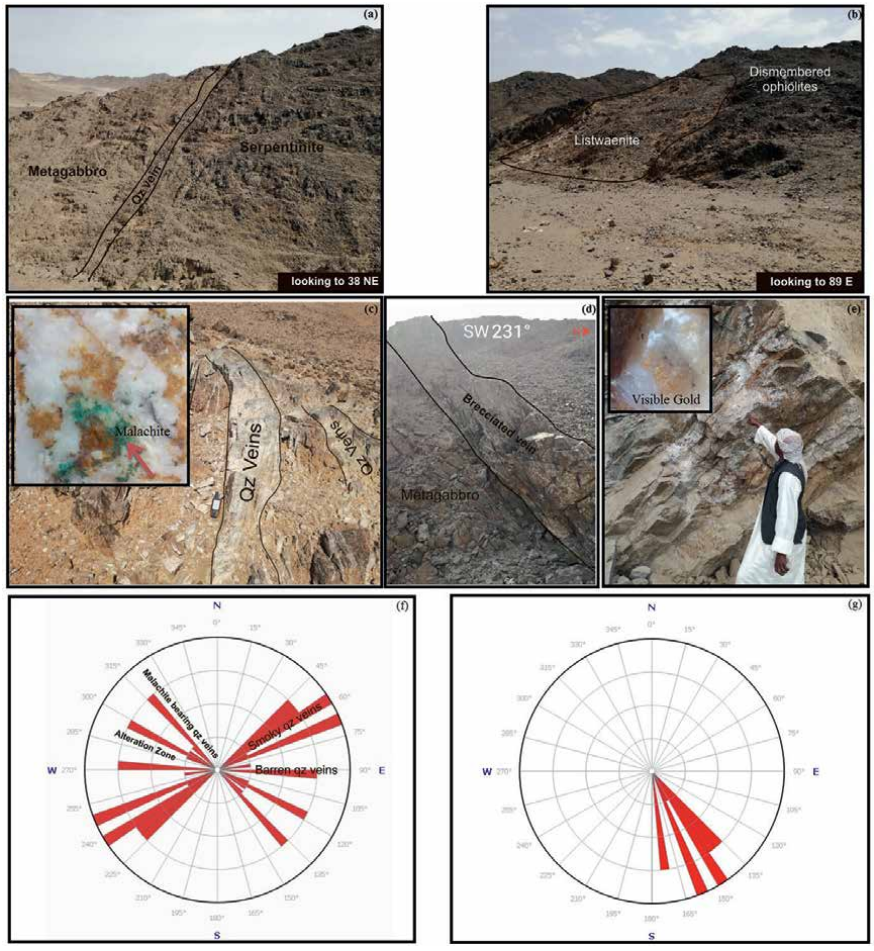

Figure 12.
Field photographs show a) quartz vein between metagabbro and serpentinites, b) the listwaenite within dismembered serpentinite, c) Malachite-bearing quartz veins, d) Brecciated quartz vein containing iron oxides in the fissures, and e) Smoky quartz vein with visible gold. Rose diagram showing f) Alteration zone and various types of quartz veins, and g) the dipping of smoky quartz vein.

of hematite, limonite, goethite and fresh pyrite. They occur either neighboring the auriferous quartz veins. The common types of alteration are silicification, sulphidation, carbonatization, listwaenitization.

10. Conclusions

a. Sol Hamed (SH) area as a part of the ANS ophiolites occurred within Onib-Sol Hamed suture zone in the southern Eastern Desert of Egypt. The ophiolitic assemblages in this area are represented by serpentinite, metagabbro and arc assemblages represented by metavolcanics. They later intruded by gabbroes and granites.

b. Geochemically, the compatible trace elements (Cr-Ni-Co) enrichment in SH serpentinites indicate derivation from a depleted mantle peridotite source. They show affinity to the typical metamorphic peridotites with peridotitic komatiite nature. The normative compositions reflect harzburgitic mantle source. Their Al_2O_3 contents (0.05–1.02 wt. %) are akin to oceanic and active margin peridotites and Pan-African serpentinites. The Cr and TiO_2 contents indicate SSZ environment with tectonic character destructive plate margins and depleted mantle sources. Their Al_2O_3/SiO_2 and MgO/SiO_2 ratios support the SSZ affinity and are similar to ANS peridotites with fore-arc setting. Low value of Al_2O_3/SiO_2 (fore-arc field), suggesting that these rocks were derived from a mantle source with high degrees of partial melting. Moreover, their Al_2O_3 and CaO depletion is typical of fore-arc peridotites. The normative compositions replicate harzburgitic mantle source.

c. Structurally, the area represents four deformational events can be distinguished in the Neoproterozoic rocks (D_1, D_2, D_3 and D_4); D_1: E–W thrust faults and related E–W (F_1) folds; D_2: NW–SE thrust faults and related NW–SE (F_2) folds were formed; D_3: conjugate NNW-trending sinistral and NNE-trending dextral transpression, as well as N–trending tight folds (F_3) and D_4: is E–W dextral strike-slip and dip-slip normal faults striking NNW–SSE to N–S and E–W may be related to Red Sea rifting. There are three major fault sets affected the area. The first set trend mainly NE-SW and is manifested in the volcanic-sedimentary assemblage and Gabal SH. The second set trend E-W affecting all the basement rocks and disturbs the first fault set. The third set trend N-S affected all the rock units.

The associated structural features with shearing are showed as fallowing:

- NNE-SSW normal faults,
- NW-SE reverse faults,
- NE-SW, NW-SE, WNW-ESE, NNE-SSW and EW quartz veins.

The mineralized structures are exemplified by

- Quartz veins have mainly NE-SW and NNW-SSE trends,
- Faults have mainly NE-SW trends,
- Breccia and alteration have mainly NW-SE trend.

d. Magnesite ore deposits in SH serpentinites is cryptocrystalline formed due to hydrothermal alteration of the serpentinite host rocks. It occurs as snow-white veins and stock-works. These characteristics are typical of Kraubath type magnesite deposits.

e. Gold mineralization is confined to malachite-bearing quartz veins, smoky quartz veins and alteration zones. The gold grades increase with arsenopyrite occurrences.

Acknowledgements

The first author is grateful to Shalaten Mineral Resource Company specially, Mr. Sherif El Shahawy (CEO) and Mr. Abdelmagid Mohamed Abdelmagid (Managing Director) also my spiritual father Brigadier General Wael Abu Hamda and my friends in geology section for helping during geologic field work. He also, thanked his mother and his wife for continuous support. And his first baby Seila.

Additional information

Parts of this chapter were previously published in a preprint by the same author: [Tarek Sedki Shehata Ali, Haroun A. Mohamed and Rafat Zaki] [2019]. [Unpublished preprint]. [Minia University]. Available from: [Sedki, T.; Ali, S.; A. Mohamed, H.; Zaki, R. Sol Hamed Ophiolitic Complex, Southern Eastern Desert, Egypt: Petrological, Economic Potentiality and Structural Implications. Preprints 2019, 2019100079. https://doi.org/10.20944/preprints201910.0079.v1 Sedki, T.; Ali, S.; A. Mohamed, H.; Zaki, R. Sol Hamed Ophiolitic Complex, Southern Eastern Desert, Egypt: Petrological, Economic Potentiality and Structural Implications. Preprints 2019, 2019100079. https://doi.org/10.20944/preprints201910.0079.v1].

Author details

Tarek Sedki[1,2,3]*, Haroun A. Mohamed[1], Shehata Ali[1] and Rafat Zaki[1]

1 Geology Department, Faculty of Science, Minia University, El–Minia, Egypt

2 Australian Institute for Mining and Metallurgy (AusIMM), Carlton, Australia

3 Shalatin Mineral Resources Company, Cairo, Egypt

*Address all correspondence to: t.sedki@yahoo.com

References

[1] Stern RJ. Neoproterozoic crustal growth: The solid earth system during a critical episode of earth history. Gondwana Research. 2008;**14**:33-50

[2] Stoeser DB, Camp VE. Pan-African microplate accretion of the Arabian Shield. Geological Society of America Bulletin. 1985;**96**:817-826

[3] Johnson PR, Woldehaimanot B. Development of the Arabian–Nubian Shield: Perspectives on accretion and deformation in the northern East African Orogen and the assembly of Gondwana. In: Yoshida M, Dasgupta S, Windley B, editors. Proterozoic East Gondwana: Supercontinent Assembly and Breakup. Vol. 206. Geological Society of London Special Publications; 2003. pp. 289-325

[4] Stern RJ, Johnson PJ, Kröner A, Yibas B. Neoproterozoic ophiolites of the Arabian–Nubian Shield. In: Kusky T, editor. Precambrian Ophiolites. Developments in Precambrian Geology. Vol. 13. Elsevier; 2004. pp. 95-128

[5] Stern RJ. Crustal evolution in the east African Orogen: A neodymium isotopic perspective. Journal of African Earth Sciences. 2002;**34**:109-117

[6] Abu-Alam TS, Hamdy MM. Thermodynamic modelling of Sol Hamed serpentinite, South Eastern Desert of Egypt: implication for fluid interaction in the Arabian–Nubian Shield ophiolites. Journal of African Earth Sciences. 2014;**99**:7-23

[7] Stern RJ. Arc assembly and continental collision in the Neoproterozoic East African Orogen: implications for the consolidation of Gondwanaland. Annual Reviews of Earth and Planetary Science. 1994;**22**:319-351

[8] Jacobs J, Thomas RJ. Himalayan-type indenter-escape tectonics model for the southern part of the late Neoproterozoic–early Paleozoic East African-Antarctic orogen. Geology. 2004;**32**:721-724

[9] Pallister JS, Stacey JS, Fischer LB, Premo WR. Precambrian ophiolites of Arabia; geologic setting, U–Pb geochronology, Pb-isotope characteristics, and implications for continental accretion. Precambrian Research. 1988;**38**:1-54

[10] Kröner A, Todt W, Hussein IM, Mansour M, Rashwan AA. Dating of late Proterozoic ophiolites in Egypt and the Sudan using the single grain zircon evaporation technique. Precambrian Research. 1992;**59**:15-32

[11] El-Bialy MZ. On the Pan-African transition of the Arabian–Nubian Shield from compression to extension: the post-collision Dokhan volcanic suite of Kid-Malhak region, Sinai, Egypt. Gondwana Research. 2010;**17**:26-43

[12] Abdel-Salam MG, Tsige L, Yihunie T, Hussien B. Terrane rotation during the east African orogeny: Evidence from the Bulbul Shear Zone, South Ethiopia. Gondwana Research. 2008;**14**:497-508

[13] Abdel-Karim AM, El-Shafei SA. Mineral chemistry and geochemistry of ophiolitic metaultramafics from Um Halham and Fawakhir, Central Eastern Desert, Egypt. International Journal of Earth Sciences. 2018;**107**:2337-2355

[14] Abdel-Karim AM, El-Shafei SA. Mineral chemistry and geochemistry of ophiolitic ultramafics from central

Eastern Desert, Egypt: A case for contaminated mantle-derived magma. Geophysical Research Abstracts. 2017;**19**, EGU2017-16680-2

[15] Abdel-Karim AM, Helmy HM, El-Shafei SA. Fore-arc setting of the Gerf ophiolite, Eastern Desert, Egypt: Evidence from mineral chemistry and geochemistry of ultramafites. Lithos. 2016;**263**:52-65

[16] Ahmed AH, Arai S. Characterization of the thermally metamorphosed mantle–crust transition zone of the Neoproterozoic ophiolite at Gebel Mudarjaj, south Eastern Desert, Egypt. Lithos. 2012;**142-143**:67-83

[17] Azer MK, Stern RJ. Neoproterozoic (835-720 Ma) serpentinites in the Eastern Desert, Egypt: Fragments of forearc mantle. Geology. 2007;**115**:457-472

[18] El Bahariya GA. Petrology and origin of Pan-African serpentinites with particular reference to chromian spinel compositions, Eastern Desert, Egypt: Implication for supra-subduction zone ophiolite. In: Third International Conference on the Geology of Africa. Egypt: Assiut University; 2003. pp. 371-388

[19] Zimmer M, Kröner A, Jochum KP, Reischmann T, Todt W. The Gabal Gerf complex: A Precambrian N-MORB ophiolite in the Nubian shield, NE Africa. Chemical Geology. 1995;**123**:29-51

[20] Kröner A. Ophiolites and the evolution of tectonic boundaries in the late Proterozoic Arabian–Nubian Shield of northeast Africa and Arabia. Precambrian Research. 1985;**27**:277-300

[21] Bakor AR, Gass IG, Neary CR. Jabal al Wask Northwest Saudi Arabia: An Eocambrian back-arc ophiolite. Earth and Planetary Science Letters. 1976;**30**:1-9

[22] Abd El-Rahman Y, Polat A, Dilek Y, Fryer BJ, El-Sharkawy M, Sakran S. Geochemistry and tectonic evolution of the Neoproterozoic incipient arc–forearc crust in the Fawakhir area, Central Eastern Desert of Egypt. Precambrian Research. 2009;**175**:116-134

[23] Rm S. Review of late proterozoic sutures, ophiolitic mélanges and tectonics of eastern Egypt and Northeast Sudan. Geologische Rundschau. 1994;**83**:537-546

[24] Abdelsalam M, Stern R. Sutures and shear zones in the Arabian-Nubian Shield. Journal of African Earth Sciences. 1996;**23**(3):289-310

[25] Azer MK. Evolution and economic significance of listwaenites associated with Neoproterozoic ophiolites in south Eastern Desert, Egypt. Geologica Acta. 2013;**11**(1):113-128

[26] Ramadan TM, Ibrahim TM, Said AD, Baiumi M. Application of remote sensing in exploration for uranium mineralization in Gabal El Sela area, south Eastern Desert, Egypt. The Egyptian Journal of Remote Sensing and Space Science. 2013;**16**:199-210

[27] Fitches WR, Graham RH, Hussein IM, Ries AC, Shackleton RM, Price RC. The Late Proterozoic ophiolite of Sol Hamed, NE Sudan. Precambrian Research. 1983;**19**:385-411

[28] Frey FA, Stockman HW. The Ronda high temperature peridotite: Geochemistry and petrogenesis. Geochimica et Cosmochimica Acta. 1985;**49**:2469-2491

[29] Parkinson IJ. Peridotites from the Izu–Bonin–Mariana fore-arc (ODP Leg125): Evidence for mantle melting

and meltmantle interaction in a supra-subduction zone setting. Journal of Petrology. 1998;**39**:1577-1618

[30] Bonatti E. Mantle peridotites from continental rifts to oceanic basins to subduction zones. Earth and Planetary Science Letters. 1989;**9**:297-311

[31] Deschamps F, Godard M, Chauvel C, Andreani M, Hattori K. In situ characterization of serpentinites from forearc mantle wedges: Timing of serpentinization and behavior of fluidmobile elements in subduction zones. Chemical Geology. 2010;**269**:262-277

[32] Stern RJ. Origin of late Precambrian intrusive carbonates, Eastern Desert of Egypt and Sudan: C, O, and Sr isotopic evidence. Precambrian Research. 1990;**46**:259-272

[33] Coleman RG. What is an Ophiolite? In: Ophiolites. Minerals and Rocks. Vol. 12. Berlin, Heidelberg: Springer; 1977. DOI: 10.1007/978-3-642-673-5_1

[34] Pa, F., Oceanic Basalts. Blachie and Son Ltd, New York. 1991

[35] Abdel-Karim AM. Possible origin of the ophiolites of Eastern Desert of Egypt, from geochemical prospectives. Arabian Journal for Science and Engineering. 2010;**34**:1-27

[36] Bodinier JL. Orogenic, ophiolitic, and abyssal peridotites. In: Carlson RW, editor. Treatise on Geochemistry Mantle and Core: Treatise on Geochemistry. 2nd ed. Amsterdam: Elsevier Science Ltd; 2003. pp. 103-170

[37] Azer MK. Petrological and mineralogical studies of Pan-African serpentinites at Bir Al-Edeid area, central Eastern Desert, Egypt. Journal of African Earth Science. 2005;**43**:525-536

[38] Jensen LS. A new cation plot for classifying subalkalic volcanic rocks. Ontario Division Mines Miscellaneous. Ministry of Natural Resources. Vol. 66. 1976

[39] Ishii T, Maekawa H, Fiske R. Petrological studies of peridotites from diapiric Serpentinite Seamounts in the Izu- Ogasawara-Mariana forearc, leg 125. In: Pearce J, Stokking LB, et al., editors. Proceedings of the Ocean Drilling Program, Scientific Results. Ocean Drilling Program. Vol. 125. 1992. pp. 445-485

[40] McDonough WF, Sun S-s. The composition of the earth. Chemical Geology. 1995;**120**:223-253

[41] Salters VJM. Composition of the depleted mantle. Geochemical Geophysical and Geosystem. May 2004;**5**(5)

[42] Jagoutz E, Baddenhausen H, Blum K, Cendales M, Dreibus G, Spettel B, et al. The abundances of major, minor and trace elements in the earth's mantle as derived from primitive ultramafic nodules. Proceedings of the Lunar Planet Conference. 1979;**10**:2031-2050

[43] Hart SR. In search of a bulk-earth composition. Chemical Geology. 1986;**57**:247-267

[44] Pearce JA, Edwards SJ, Parkinson IJ, Leat PT. Geochemistry and tectonic significance of peridotites from the south sandwich arc-basin system, South Atlantic. Contrib Miner Petroleum. 2000;**139**:36-53

[45] Niu Y. Bulk-rock major and trace element compositions of abyssal peridotites: Implications for mantle melting melt extraction and post-melting processes beneath mid-ocean ridges. Journal of Petrology. 2004;**45**(12):2423-2458

[46] Ahmed AH. Heterogeneously depleted Precambrian lithosphere deduced from mantle peridotites and associated chromitite deposits of Al'Ays ophiolite, Northwestern Arabian Shield, Saudi Arabia. Ore Geology Reviews. 2015;**67**:279-296

[47] Hawkins JW. Geology of supra-subduction zones—implications for the origin of ophiolites. In: Dilek Y, Newcomb S, editors. Ophiolite Concept and the Evolution of Geological Thought. Boulder, CO: Geological Society of America Special; 2003. pp. 227-268

[48] Song S, Su L, Niu Y, Lai Y, Zhang L. CH_4 inclusions in orogenic harzburgite: Evidence for reduced slab fluids and implication for redox melting in mantle wedge. Geochimica et Cosmochimica Acta. 2009;**73**(6):1737-1754

[49] Godard M, Lagabrielle Y, Alard O, Harvey J. Geochemistry of the highly depleted peridotites drilled at ODP sites 1272 and 1274 (fifteen-twenty fracture zone, mid-Atlantic ridge): Implications for mantle dynamics beneath a slow spreading ridge. Earth and Planetary Science Letters. 2008;**267**:410-425

[50] Deschamps F, Guillot S, Hattori K. Geochemistry of subduction zone serpentinites: A review. Lithos. 2013;**178**:96-127

[51] El-Sayed MM, Mohamed FH. Geochemical constraints on the tectonomagmatic evolution of the late Precambrian Fawakhir ophiolite, central Eastern Desert, Egypt. Journal of African Earth Science. 1999;**29**:515-533

[52] Farahat ES. Chrome spinels in serpentinites and talc carbonates of the El-Ideid–El Sodmein District, central Eastern Desert, Egypt: Their metamorphism and petrogenetic implications. Chem Erde. 2008;**68**(2):195-205

[53] Khedr MZ. Origin of neoproterozoic ophiolitic peridotites in south Eastern Desert, Egypt, constrained from primary mantle mineral chemistry. Mineralogy and Petrology. 2013;**107**(5):807-828

[54] Boskabadi A, Broman C, Boyce A, Teagle DAH, Cooper MJ, Azer MK, et al. Carbonate alteration of ophiolitic rocks in the Arabian-Nubian shield of Egypt: Sources and compositions of the carbonating fluid and implications for the formation of Au deposits. International Geology Review. 2017;**59**(4):391-419

[55] Ghoneim MF, Hamdy MM. Origin of magnesite veins in serpentinites from Mount El-Rubshi and Mount El-Maiyit, Eastern Desert, Egypt. Achieves in Mineral. 2003;**54**:41-63

[56] Hamdy MM. Metamorphism of ultramafic rocks at Gebel Arais and Gebel Malo Grim, Eastern Desert, Egypt: Mineralogical and O-H stable isotopic constraints. Egypt. Journal of Geology. 2007;**51**:105-124

[57] C, M., Serpentinization of abyssal peridotites at mid-ocean ridges. Comptes Rendus Geoscience, 2003. 335: p. 825-852

[58] Paulick H, Godard M, De Hoog JCM, Suhr G, Harvey J. Geochemistry of abyssal peridotites (Mid-Atlantic Ridge, 15°20′N, ODP Leg 209): Implications for fluid/rock interaction in slow spreading environments. Chemical Geology. 2006;**234**:179-210

[59] Chalot-Prat F, Lombard A. No significant element transfer from the oceanic plate to the mantle wedge during subduction and exhumation of the Tethys lithosphere (Western Alps). Lithos. 2003;**69**:69-103

[60] Hattori KH. Geochemical character of serpentinites associated with high- to ultrahigh-pressure metamorphic rocks in the Alps, Cuba, and the Himalayas: Recycling of elements in subduction zones. Geochemistry, Geophysics, Geosystems. Sep 2007;**8**(9)

[61] Nockolds SR. The relation between chemical composition and paragenesis in the biotites of micas of igneous rocks. American Journal of Science. 1947;**245**(5):401-420

[62] Gokhale NW. Chemical composition of biotite as a guide to ascertain the origin of granites. Bulletin Society Geology. 1968;**40**:107-111

[63] Wood DA. The application of a Th–Hf–Ta diagram to problems of tectonomagmatic classification and to establishing the nature of crustal contamination of basaltic lavas of the British Tertiary Volcanic Province. Earth Planet Science. 1980;**50**:11-30

[64] Pearce JA, Lippard SJ, Roberts S. Characteristics and tectonic significance of supra-subduction ophiolites. In: Kokelaar BP, Howells MF, editors. Geological Society of London. Vol. 16. Special Publication; 1984. pp. 777-794

[65] Geng HY, Sun M, Yuan C, Zhao GC, Xiao WJ. Geochemical and geochronological study of early carboniferous volcanic rocks from the West Junggar: Petrogenesis and tectonic implications. Journal of Asian Earth Sciences. 2011;**42**:854-866

[66] Shervais JW. Ti –V plots and the petrogenesis of modern and ophiolitic lavas. Earth Planetary Science Letters. 1982;**59**:101-118

[67] Flower MFJ, Levine HM. Petrogenesis of a tholeiite–boninite sequence from Ayios Mamas, Troodos ophiolite: Evidence for splitting of a volcanic arc contribution to. Mineralogy and Petrology. 1987;**97**:509-524

[68] Streckeisen A. Classification of common igneous rocks by mean of their chemical composition. A provisional attempt. Neues Jahrbuch für Mineralogie – Abhandlungen. Neues Jahrbuch für Mineralogie, Monatsh, DTSCH; 1976:1-15

[69] Khalil K. Chromite mineralization in ultramafic rocks of the Wadi Ghadir area, Eastern Desert, Egypt: Mineralogical, microchemical and genetic study. Neues Jahrbuch für Mineralogie Abhandlungen. 2007;**183**:283-296

[70] Ohanley DS. Serpentinites, records of tectonic and petrological history. Oxford Monographs on Geology and Geophysics. 1996 (no 34.):741-742

[71] Snow JE. Pervasive magnesium loss by marine weathering of peridotite. Geochimica et Cosmochimica Acta. 1995;**59**:4219-4235

[72] Kusky TM, Ramadan TM. Structural controls on Neoproterozoic mineralization in the South Eastern Desert, Egypt: An integrated field, Landsat TM, and SIR-C/X SAR approach. Journal of African Earth Sciences. 2002;**35**(1):107-121

[73] Ren D, Abdelsalam MG. Tracing along-strike structural continuity in the Neoproterozoic Allaqi-Heiani Suture, southern Egypt using principal component analysis (PCA), fast Fourier transform (FFT), and redundant wavelet transform (RWT) of ASTER data. Journal of African Earth Sciences. 2006;**44**(2):181-195

[74] Abdeen MM, Abdelghaffar AA. Syn-and post-accretionary structures in the Neoproterozoic central Allaqi-Heiani suture zone, Southeastern Egypt. Precambrian Research. 2011;**185**(3-4):95-108

[75] Ibrahim W, Watanabe K, Ibrahim M, Yonezu K. Neoproterozoic Tectonic Evolution of Gabal Abu Houdied Area, South Eastern Desert, Egypt: As a Part of Arabian–Nubian Shield Tectonics. Arabian Journal for Science and Engineering. 2015;**40**(7):1947-1966

[76] Pohl W. Genesis of magnesite deposits—Models and trends. Geologische Rundschau. 1990;**79**(2):291-299

[77] Allegre CJ, Humler E, Hofmann AW. The chemical composition of the earth. Earth and Planetary Science Letters. 1995;**134**:515-526

[78] Arif M. Goechemistry of serpentinized peridotites from the Indus Suture ophiolite in Swat, NW Pakistan. Geological Bulletin University of Peshawar. 2003;**36**:1-10

[79] Dardir AA, Elshimi KAM. Geology and geochemical exploration for gold in the banded iron formation of Um Nar area, Central Eastern Desert, Egypt. Annals of the Geological Survey of Egypt. 1992;**18**:381-409

[80] Takla MA, Suror AA. On the occurrence of Ni-sulphides and arsenides in some Egyptian serpentinites. Egyptian Minerals. 1996;**8**:1-18

[81] Botros NS. Geological and Geochemical Studies on Some Gold Occurrences in the North Eastern Desert, Egypt. PhD thesis. Zagazig, Egypt: Zagazig Univ.; 1991. 146 pp

[82] Oweiss KA, El Naggar AA, Abdel Razik KA, Moselhy N, Ali AB. Gold exploration at the Heianai area, south Eastern Desert, Egypt. Annals of the Geological Survey of Egypt. 2001;**24**:435-450

Chapter 5

Why the Pounamu? Low- to Medium Grade Metabasites and Metaultrabasites of New Zealand from a Geoheritage Perspective

Károly Németh, Tamás Sági and Sándor Józsa

Abstract

Pounamu plays a very important role in Māori culture (New Zealand) and is a taonga (treasure) of the people. Pounamu is a result of the intricate, unique geological context of the Zealandia microcontinent in the SW Pacific successfully separated from Gondwana in the Late Mesozoic but cut half in a NE-SWE trending right-lateral strike-slip dominated plate boundary separating the Indo-Australian and Pacific Plates within the continental lithospheric segment of Zealandia. Along this nearly 500 km onshore structural zone, a set of narrow Paleozoic to Mesozoic lithospheric terrains assembled among ophiolite belts such as the Dun Mountain Terrain. Metasomatic influence on the ancient seafloor in combination with high-grade regional metamorphic forces along the evolving plate boundaries, a globally unique region with high geodiversity formed, giving way to the assemblage of metamorphosed ultramafic bodies to generate great variety of greenstones, referred as pounamu by Māori. The perfect physicochemical conditions of this rock made it to become a key geomaterial for tool-making and trade subjects within the Māori culture.

Keywords: ophiolite, ultramafic, geological terrain, metasomatic, basalt, amphibole

1. Introduction

The most famous and well-known Māori symbolic tools of geologic origin are the polished stone tools (dominantly adzes and chisels), pendants, etc., made from pounamu: a very esthetic, yet elegant looking rock, geologically nephrite and/or bowenite [1, 2]. Nephrite in mineralogical sense is a rock type of a combination of a variety of the calcium, magnesium, and iron-rich amphibole minerals (double chain silicate group) tremolite and/or actinolite (https://www.mindat.org/min-29085.html [Accessed: November 15, 2023]). Chemically it can be expressed as $Ca_2(Mg, Fe)_5Si_8O_{22}(OH)_2$ indicating a molecular water-rich mineral species with a potential gradual assemblage of mineral combinations of Mg to Fe ratio. In the contrary, bowenite is a hard, compact variety of the serpentinite species (it is a rock composed

predominantly of one or more serpentine group minerals, and its name refers to the texture of a snakeskin) such as antigorite that is best to express chemically as $Mg_3(Si_2O_5)(OH)_4$ (https://www.mindat.org/min-260.html [Accessed: November 15, 2023]). Nephrite is commonly grouped into the informal but commonly used "stone" group of jade that itself is not a unique rock type. It can be either a nephrite that is dominantly a silicate of calcium and magnesium in the amphibole group of minerals or jadeite which is a rock dominantly composed of a silicate of sodium and aluminum in the pyroxene group of minerals that is dominated by a single chain silicate group (pyroxene) mineral. Another common informal name used in New Zealand for 7 is "greenstone," which is a major umbrella term for anything that is gemstone quality "green" stone.

According to Tamati Te Otatu, a Māori chief from the eighteenth century, pounamu has the same value for the Māori as gold for the "white people": "Let the gold be worked by the white men. It was not a thing known to our ancestors. My only treasure is the pounamu (Kati ano taku taonga nui i te pounamu). Fern-root may be found. When my ko strikes against a fern-root, I break that root and see if it is of a good mealy kind, but that [the gold], a sandfly is larger than it." [1].

Why did the Māori choose this particular type of rock as the most sacred material representing nature for their ornaments? What geological factors influenced the first inhabitants of New Zealand to turn their attention to this (or other) type of rock and, indeed, to make it the most prized of all? The questions above shed light on the development of (late Neolithic) human societies from a perspective that few people attach much importance to. Namely, the extent to which the development of human society is influenced by the inanimate natural environment regarding local (or even remotely collected) rock types.

2. Geoarchaeological context of pounamu

In general, the rock types that could be used to create everyday objects of use in a neolithic society are important to distinguish from those collected primarily to make tools with no practical use. To produce practical tools (e.g., adzes, perforated axes, flat chisels, elongated axes, or maces), mechanical resistance, good machinability, easy availability and/or common occurrence are important aspects of the raw material. The combination of excellent mechanical properties and the high frequency of occurrence of the raw materials is a very rare phenomenon. In most cases, the raw material is either particularly common or has very good physical properties; however, both are strongly related to the geological background (i.e., frequency and types of occurrences of raw materials and their physical characteristics).

For polished stone tools of everyday use, the best rock types are the following. (1) Dominantly, but not necessarily equigranular igneous rocks containing minerals entangled with each other in a non-directed fabric (e.g., ophitic gabbro, subophitic dolerite, microholocrystalline phonolite). (2) Non-foliated high-grade metamorphic rocks containing minerals entangled with each other (e.g., hornfels, contact metabasite basic rocks affected by two distinct metamorphic events, firstly a regional and after that a contact metamorphism). (3) Dominantly equigranular and monomineralic rocks with minerals of high hardness and resistance to weathering processes (e.g., Na-pyroxenite (a high-pressure metaophiolitic rock). Some common rock types, like quartzites (various grade monomineralic metamorphic rocks) and sandstones, are made of very hard and resilient minerals; however, this is not enough as

other factors, like foliation or weak cohesion between crystals, deteriorate the quality of the raw material and make machinability difficult. On the other hand, there is another group of common rock types, the carbonates *sensu lato* (e.g., limestone, dolomite, marl, and marble), that are easy to process, but they are neither mechanically nor chemically resistant, both at the level of the rocks and the minerals forming them. In summary, the selection of rock types for tool making is rather based on the fine textural appearance of the rock types than their mineral assemblages. Minerals with relatively "pure" physical characteristics such as serpentine can create homogeneous microtextures making the rock like serpentinite extremely hard and resistant, suitable for tool making. Serpentine for instance is a group of minerals that are usually attractive green in color. Serpentinite, however, is a rock composed mainly of serpentine minerals. It is used as gemstone, architectural stone, and carving material despite the minerals, serpentine "soft" physical property, the interlocking microfabric of the rock creates a hard rock suitable for tool making.

3. Geological context of pounamu

Māori people took the method of preparation of stone tools from the East Polynesian homeland [3]. They may have a wide petrological knowledge as the most valued rock types for adzes (both sedimentary, igneous, and metamorphic in origin) are related to specific regions (a specific argillite from D'Urville Island/Rangitoto ki te Tonga; a rare, aphanitic basalt from the Coromandel Peninsula in the North Island of New Zealand; and especially greenstones/pounamu found in very distinct and remote areas of the South Island) [4]. In addition to these three important and widely used rock types, each Māori tribe used the rocks found in their territory (e.g., flint and quartzite) to make adzes, as the more noble raw materials required invasion of enemy territory or trade [2].

From these rock types the sedimentary (argillite) and the igneous (basalt) were chosen because of their quite easy machinability and these were used as adzes in everyday life. On the other hand, greenstones are harder to polish and are often particularly difficult to access, while polished stone tools made from them have symbolic rather than practical significance. Green-colored rock types ("greenstones") are very often used for stone tools in many parts of the world such as in Neolithic Europe [5, 6]. Perhaps to be able to develop a "greenstone" usage within an early human community required relatively easy access and understanding of the source region's geological assets [6].

These rocks are almost without exception metamorphic rocks, dominantly metabasites and metaultrabasites (eclogite, Na-pyroxenite, omphacite/jadeite schists, metabasalt, metadolerite, nephrite, serpentinite) hence their source regions had to be associated with some sort of (meta)ophiolite belts [5] or ancient suture zones [7] that are common mostly in the Eastern Mediterranean region [8], Apennine Peninsula in Italy [5, 9, 10], in the older cratonic regions such as Fennoscandia [11–14] or associated with a low viscosity Archean lava flows of komatiites [15]. In the formation of greenstone, the post-emplacement seafloor processes as well as the long-lasting hydrothermal effect in the mafic to ultramafic, mostly oceanic crustal material together with subsequent regional metamorphism generate a very diverse rock assemblage [16]. The pounamu occurrences within New Zealand follow major ultramafic belts such as the Dun Mountain Ophiolite Belt (**Figures 1**–**3**), which runs across the South Island of New Zealand on the

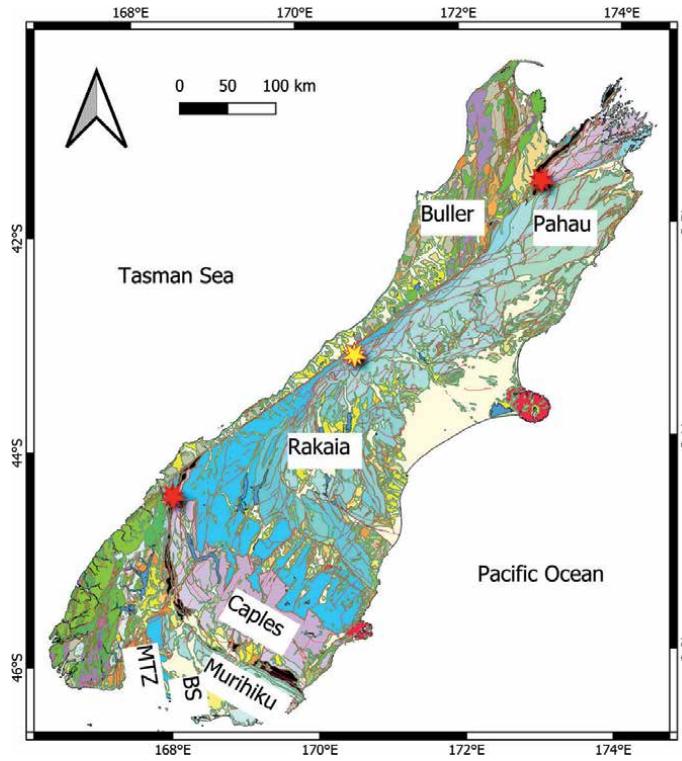

Figure 1.
The geological features of the South Island of New Zealand based on the 1 to 1-million scale geological map (https://www.gns.cri.nz/data-and-resources/geological-map-of-new-zealand/). Note the Dun Mountain Terrain (marked black) displaced spatial distribution along the right-lateral transform of the Alpine Fault. In the west of the Alpine Fault, older Paleozoic rocks are on the surface (green, brown, purple fields), and broad alluvial fans (beige) cover them (Buller Terrain). In the east from the Alpine Fault, younger Mesozoic terrains with a gradually decreasing metamorphic overprint (dark blue to light blue) form the basement from Brook Street and Murihiku Terrain (narrow bands with bluish color in the south) in an older system while Caples (pink), Rakaia (blue) and Pahau (light blue) Terrains represented by younger Mesozoic dominantly greywacke terrains. Dun Mountain Terrain represents an ophiolite zone (red stars are two key localities). Along the Alpine Fault within the Alpine Schist, ultramafic rocks (yellow star) are the source assemblages of pounamu that are eroded from the bedrock into broad riverbeds around the township of Hokitika.

surface. Tracing pounamu in a geological sense helped significantly establish the New Zealand Terrain concept, and it is a clear indicator of plate boundary processes and terrain amalgamation [17].

The New Zealand greenstones are dominantly nephrites [18–24]. About New Zealand greenstone heritage a digital library provides vital information and inventory (https://www.greenstone.org/ [Accessed: February 19, 2024]) [25]. In contrast, the Greenstone resources and their indigenous, Māori legislative aspects are clearly outlined [26]. These New Zealand greenstones are mono- or bimineralic rocks composed of crypto- or microcrystalline amphiboles of the tremolite-actinolite series (https://www.mindat.org/min-29085.html [Accessed: November 15, 2023]). These metaophiolitic rocks occur in three large geological units of the South Island (**Figure 1**): The Dun Mountain-Maitai-, the Caples-Waipapa, and the Torlesse Terrane in Westland and West Otago [27].

The other, much rarer greenstone is a special type of serpentinite, which is a fine-grained metaultrabasite called bowenite, and it is composed by a variety of antigorite. It can be found only in a very small area in the Fiordland region (**Figures 1**–**3**) of the

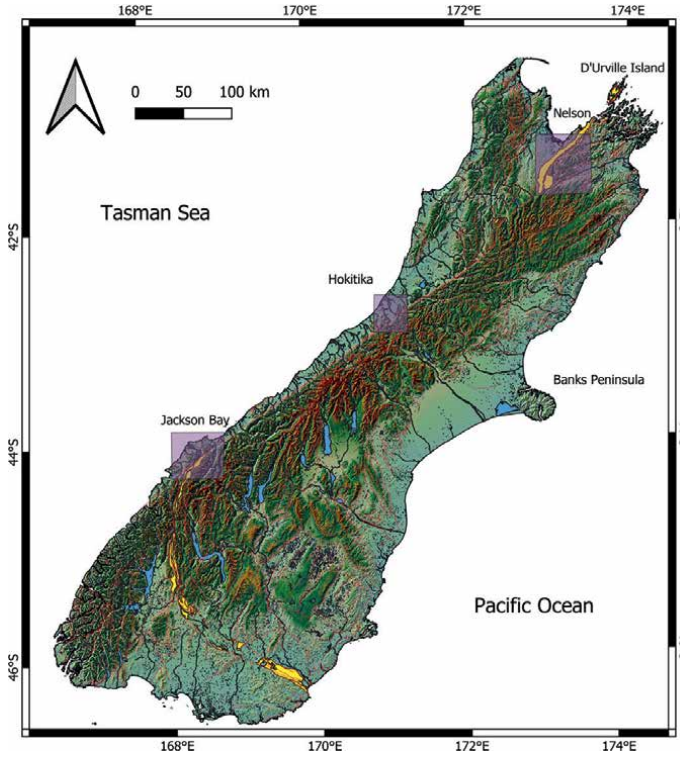

Figure 2.
Digital terrain model (DEM) of the South Island of New Zealand based on the Land Information New Zealand (LINZ) 8-m resolution topographic data clearly showing the position of the Alpine Fault (steep topographic escarpment running across the western side of the South Island) where ultramafic pods hosting pounamu showed by a box near Hokitika. The map also showing the displaced Dun Mountain Terrain mafic and ultramafic rocks at Jackson Bay and the Nelson area (light purple boxes).

South Island [28, 29] (https://www.mountainjade.co.nz/blogs/news/exploring-the-pounamu-bearing-rivers-of-new-zealand [Accessed: November 15, 2023]).

4. New Zealand pounamu

Pounamu is generally found in rivers in specific parts of the South Island as nondescriptive boulders and stones (https://www.mountainjade.co.nz/blogs/news/exploring-the-pounamu-bearing-rivers-of-new-zealand [Accessed: November 15, 2023]). Pounamu has been formed in New Zealand in four main locations: the West Coast (**Figure 4**), Fiordland, western Southland (**Figure 5**), and the Nelson district (**Figure 6**) [30–32]. It is typically recovered from rivers and beaches where it has been transported after being eroded from the mountains. The group of rocks from which pounamu comes are called ophiolites. Ophiolites are slices of the deep ocean crust and part of the mantle. When these deep mantle rocks (serpentinite) and crustal rocks (mafic igneous rocks) are heated up (metamorphosed) together, pounamu can be formed at their contact [28, 33–37].

Most New Zealand greenstones (nephrites) are made dominantly (≫99%) of microcrystalline amphiboles that are characteristic of low grade metabasites [28]. New Zealand nephrites were formed in two phases related to the regional

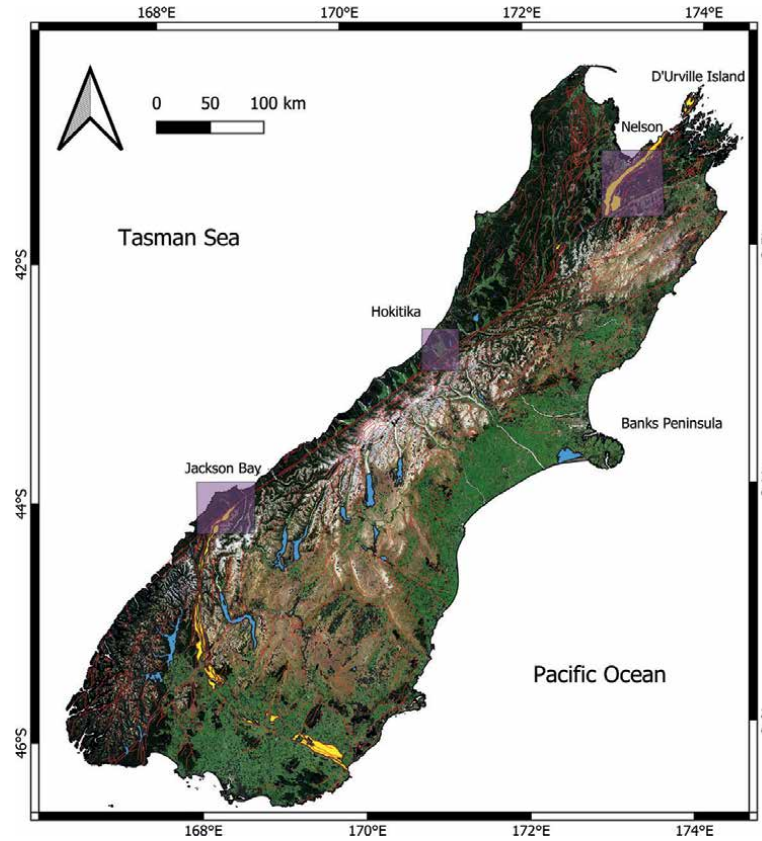

Figure 3.
LINZ 10-m resolution satellite imagery marking the major westward tributary of rivers from the steep escarpment of the Alpine Fault promoting rapid erosion and weathering out of the hard pounamu into the alluvial plains, mostly around the Hokitika region. Yellow fields mark the Dun Mountain Terrain ultramafic successions.

metamorphism of ultrabasic-basic igneous rocks of oceanic origin, e.g., oceanic crustal material gone through regional scale metamorphic processes [27, 29, 30]. First the igneous rocks (harzburgite, gabbro, dolerite) were serpentinized, and after that in a narrow zone along the boundary of metabasic and adjacent metasedimentary formations amphiboles were formed during local metasomatic reactions. The petrogenetic processes took place under the following conditions. Low grade metamorphic reactions (prehnite-pumpellyite—actinolite facies; 250–300°C) are more common in the Dun Mountain-Maitai terrane (**Figure 7**) and in some parts of the Caples terrane, while low- to medium grade metamorphic reactions (pumpellyite-actinolite—lower greenschist; 300–470°C) are characteristic for the Haast Schist (Caples, Torlesse, Waipapa Terranes). Based on Sr-isotopic data of Adams et al. (2007) the Ca came from the metasedimentary rocks instead of an early metasomatism by serpentinization fluids, which can explain the extremely limited (and small-scale) occurrence of the nephrites. This process also explains the rarity of nephrites in general, and their common placer deposit appearance within riverbeds in the Hokitika region (**Figure 2**). Another limitation of nephrite formation is the proximity of mylonitic shear zones which act as migration channels for metasomatic fluids [27]. Most probably local shear is responsible for the felted fabric of amphiboles.

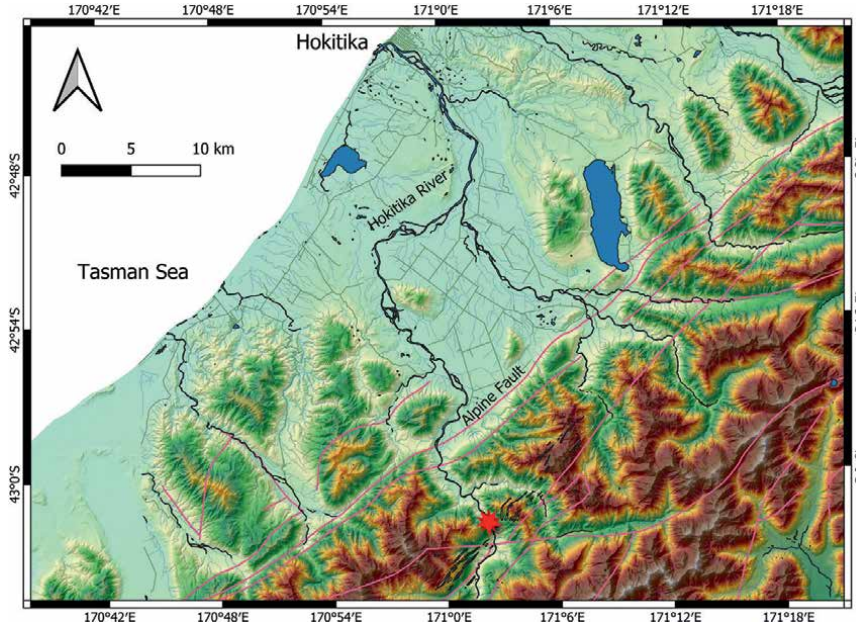

Figure 4.
The main pounamu sources are dominantly derived from the Pounamu Ultramafic Belt (red star) within the Alpine Schist along the Alpine Fault that is shown on a LINZ 8-m resolution DEM. Note the orographic setting and its relationship with the narrow band of metaserpentine and metabasite as the source of pounamu (yellow and black lines parallel to the main faults near the red star).

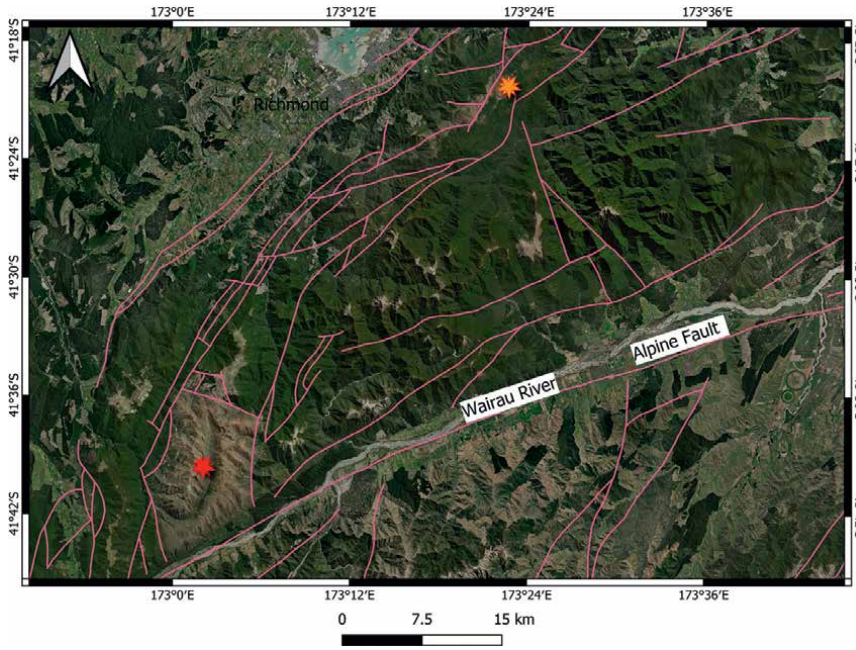

Figure 5.
Red Hill on a Bing Satellite Image in the Nelson—Marlborough—Tasman region of the northern part of the South Island. Note the reddish hills of the Red Hill (red star) and Dun Mountain (yellow star) where major mafic rocks such as dunite crop out.

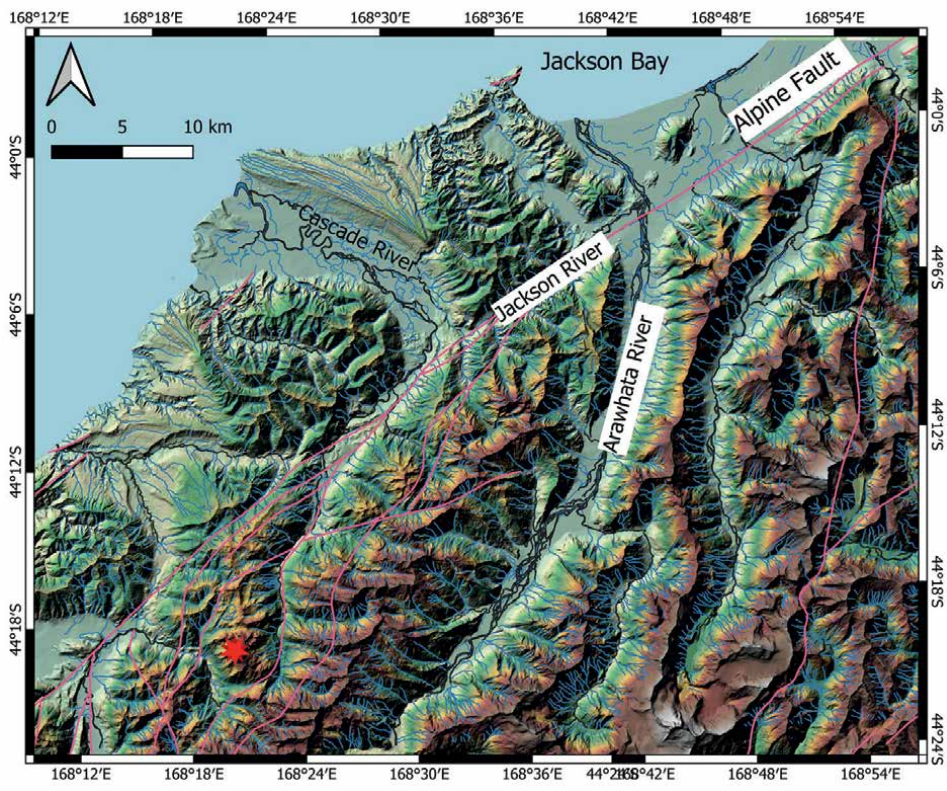

Figure 6.
Complex geotectonic situation within Fiordland (on LINZ 8-m resolution DEM) where the Dun Mountain Terrain rocks (Red Mountain—red star) narrowly connecting other terrains converging to the Alpine Fault. Greenstone derived from the main tributaries of the Cascade River and accumulating in alluvial fans close to the Tasman Sea.

Figure 7.
The large fan of the Cascade River in the Fiordland represents a common source of pounamu and other dunite and serpentine rock varieties. The Red Mountain is in the far left of the image visually similar like the Red Hill in the Nelson area about 500 km in the north.

The Dun Mountain Ophiolite Belt (**Figure 1**) has been metamorphosed in western Southland and pounamu from this belt is found along the eastern and northern edge of Fiordland [38, 39]. The Anita Bay Dunite near Milford Sound is a small but highly prized source of pounamu. In the Southern Alps, the Pounamu Ultramafic Belt in the Haast Schist occurs as isolated pods which are eroded and found on West Coast rivers and beaches [33]. One source of inanga pounamu at the head of Lake Wakatipu is possibly the only jade mining site in the world with Government protection [40].

The formation of various greenstones including the highly valued pounamu is associated with the unique geotectonical evolution of New Zealand within the Zealandia geotectonic context [41–43]. New Zealand's high-order stratigraphy framework shows well the geotectonic context of the Late Paleozoic-Mesozoic tectonic evolution of the basement rocks forming distinct lithospheric terrains that amalgamated over 100 million of year time scale [44–46]. In this process, plate margin processes and closure of ocean basins lead to the formation of narrow bands of wrapped oceanic crustal components into mafic to ultramafic lithological zones following more or less the plate boundary along convergence then collision took place [33, 36, 43]. On the tectonic map of New Zealand, the distribution pattern of the onshore basement rocks based on exposures and various geophysical data extraction highlights the long light lateral displacement zone along the Alpine Fault System in the South Island (**Figure 1**). In both ends of the major displacement zone, the main basement tectonic units are exposing typical ophiolites with the full spectrum of the base of an oceanic crust to the deep marine successions locked into the Dun Mountain and Maitai Terrain (commonly mentioned together). This interrelationship in continental scale is remarkably shown by the existence of the Red Hill area in the Nelson region in the north and the Red Mountains in the south in Fiordland [47–49]. These locations are the original places where the name dunite was derived, referring to the Dun Mountain in the north, and the redingote, which refers to the name of the Roding River in the north [50, 51]. These rocks show low metamorphic grades, but intense metasomatic processes rather formed during syn- or slightly post-accumulation times, creating sporadic zones of rodingite as a metasomatic rock assemblage [52] recording mafic to ultramafic intrusive zones in the ancient Late Paleozoic-Mesozoic oceanic realms. Between these nearly 500-km long displacement zone metamorphic processes affected the typical greywacke basin rocks. Along this transform plate boundary narrow (10 to 100 m wide) zones of ultramafic to mafic rocks with mild metamorphic imprint formed metabasites and metaserpentinite [37]. This zone is commonly referred to as the Pounamu Ultramafic Belt or Terrain, indicating its significance as a completely wrapped former oceanic basin preserved within the zone of the plate boundary. The Alpine Schists that are located right in proximity to the Alpine Fault (**Figure 8**) recognized including unusual metavolcanic rocks, cherts, and marbles all typical for an ofiolite-type rock zone [39, 53–55]. This type of rock is far more abundant in this rock assemblage than those forming the greywacke-dominated Torlesse rocks to the east. What is more distinct and convincing to look at this zone as an independent tectonic terrain is that the Alpine Schists also host a great variety of metaperidotite pods, referred to as the Pounamu Ultramafic Belt (PUB) [54]. High-quality but isolated pounamu is located only in very few locations in situ. In contrast, due to differential erosion caused by the significant hardness difference between nephrite and the host meta-ultramafics, boulders and gravelly bars within high-energy river systems preserved gemstone quality greenstones and formed the traditional source of pounamu in New Zealand (**Figure 9**) somehow, in a similar context but in a far more complicated geotectonic realm pounamu known from alluvial and glacial fans

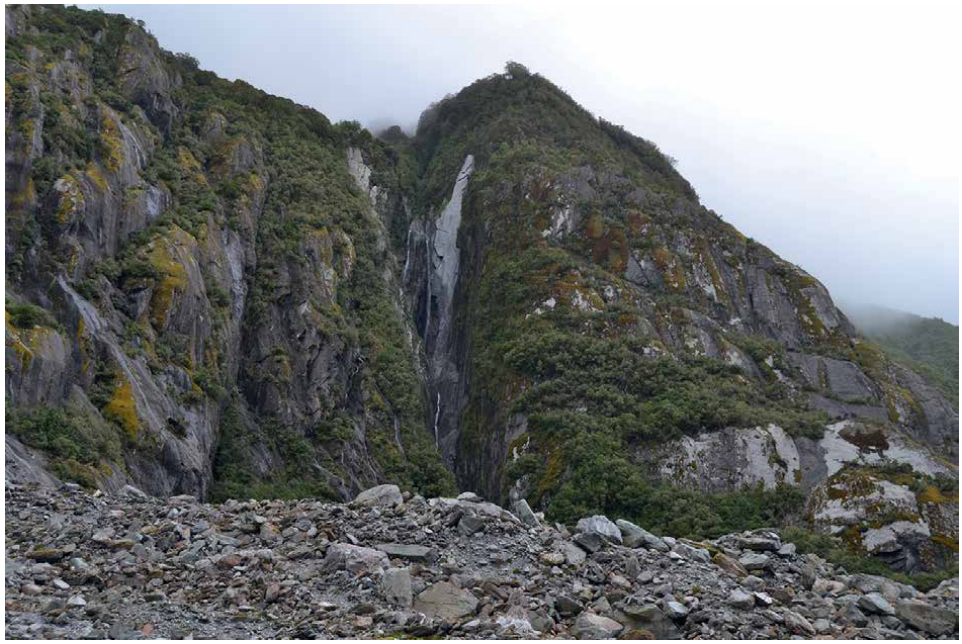

Figure 8.
Alpine Schist outcrop near Fox Glacier along the Alpine Fault composed of garnet-facies metamorphic rocks. Following the same zone sporadic metabasite and metaserpentinite form the Pounamu Ultramafic Terrain.

Figure 9.
Main fluvial outflow valleys are the main arteries pounamu carried out westward to the narrow West Coast coastal plains.

exciting the region where narrow Paleozoic and Mesozoic Terrain belt congregate into the Alpine Fault system in the Fiordland.

5. Geoheritage value and global comparison

What makes Greenstone so special that it is worth the effort to find and process it? Several factors can be considered, but they all have one thing common: all are somehow related to geology! In no particular order of importance, these are the following.

1. *Rarity*. Nephrite occurs only as bedrock in narrow zones in the metaophioloites of the South Island and can be found mostly as pebbles in glacial and alluvial deposits. This may have contributed to the "divine" origin of Pounamu in particular since while the Māori could encounter the material of other pebbles and boulders relatively easily in the surrounding mountains, nephrites were hardly to be found in situ as bedrock.

2. *"Purity*." Nephrites are monomineralic rocks; they are composed almost only of amphiboles of the tremolite-actinolite series; in most cases, other minerals are less than 1 m/m% of the rock. There are only few rock types in New Zealand that are monomineralic; however, they are much less special in other ways. For example, quartzite is dominantly a monomineralic rock type but has a very wide range of colors, minor constituents, and thus appearance; limestone is composed almost only of calcite, despite the fact that it has many varieties depending on the origin of the rock (e.g., fossiliferous, oolithic, stylolithic). Aphanitic igneous rock may look uniform too; however, in other important external characteristics, they do not come close to the uniqueness of nephrite; obsidian would be the most likely candidate.

3. *Hardness and toughness*. As composed dominantly of amphiboles, which are 5–6 on the Mohs Scale (https://en.wikipedia.org/wiki/Mohs_scale), nephrite is hard enough to keep well-polished long enough, while not too hard to process. The rock-forming minerals are fine-grained and fibrous, and they are either felted due to the high strain rate of shear zones or unoriented and interwoven. Whether it is the first or the second type, the rock will be very tough and physically resistant.

4. *Resistance to weathering*. Because it is monomineralic, it has a uniform weathering profile. It is quite resilient to weathering processes, which means that a polished surface of the rock will keep its appearance. In several thousand years, only a few cm wide weathering profiles could form on nephrite despite the particularly wet climate of Westland, South Island [9].

5. *Color, luster, transparency*. New Zealand nephrites have various appearances, commonly greenish, more- or less translucent, especially if they are cut and polished and have a bright luster. Based on optical properties observed by the naked eye, there are several types of pounamu, which arise from fine impurities and/or weathering processes of the rocks [8]. Inanga: pearly white, grayish green, green, bluish green; it can be very translucent or quite opaque. Kawakawa: light- to dark green, even almost black with small black dots (opaque mineral inclusions), moderately translucent. Auhunga: pale green and opaque,

color between kawakawa and inanga. Kahotea: green with white flakes. Kahurangi: apple green, highly translucent (and often flawless). Kōkopu: light to dark brown, light blue, olive- to yellow-green, golden yellow; always brownish mottled. Pīpīwharauroa: green and light green/white banded, causing chatoyant effect. Raukaraka: orange crust on green pounamu: an oxidized version of kawakawa. Totokweka: Like kawakawa, mineral inclusions are reddish, most probably due to oxidation processes. Tangiwai is not nephrite but bowenite; however, it is also called pounamu. It has an olive, brown, yellowish to bluish-green color, and it is moderately translucent.

All the above physicochemical features made pounamu a highly valuable geocultural treasure that influenced the Māori culture and vividly shaped the contemporary art and identity of New Zealand well beyond the traditional Māori aspects. Pounamu is part of New Zealand culture, and the usage of stones as guardians following original symbolic carvings provides the people a sense of the land that most New Zealanders highly appreciate. Pounamu, therefore, could be looked at as a significant geocultural element of the geoheritage of the West Coast of the South Island of New Zealand. As proposed earlier, the West Coast could form a key globally significant geopark that potentially could be listed as a UNESCO Global Geopark [56]. Within such geopark the pounamu and the geocultural aspect of it as a messenger of the terrain accretion of Zealandia should be considered seriously.

6. Conclusion

As in Europe or Asia, the nephrites gained a special position in polished stone implements, and it was the same in New Zealand. Only geological and mineralogical-petrological properties could mark nephrites a unique rock, a divine gift for the Māori people. In the eyes of the Māori people, pounamu is of great spiritual importance. It has become fully intertwined with Māori culture, an inseparable and identity-forming part of it. Even its collection and sale are highly regulated. Overcoming the fact that esthetics has always played an important role in the selection of symbolic tools in human societies, it is easy to see that the "rising" of pounamu happened almost exclusively due to geological factors. This finding goes a long way, as it clearly shows the influence that geological diversity and the inanimate natural environment have on us: preserving geodiversity, transfer of basic geological knowledge to future generations are an essential part of preserving our culture and traditions.

Acknowledgements

This report is a direct result of the Erasmus+ International Credit Mobility (2019–2022, 2024–2025) research program conducted between Eötvös University, Budapest, Hungary, and Massey University, Palmerston North, New Zealand.

Author details

Károly Németh[1,2,3,4*], Tamás Sági[5] and Sándor Józsa[5]

1 Massey University, Palmerston North, New Zealand

2 Saudi Geological Survey, Jeddah, Kingdom of Saudi Arabia

3 Institute of Earth Physics and Space Science, Sopron, Hungary

4 The Geoconservation Trust Aotearoa Pacific, Opotiki, New Zealand

5 Eötvös Lóránd University (ELTE), Budapest, Hungary

*Address all correspondence to: knemeth@geoconservation.org

References

[1] Best E. The Stone Implements of the Māori. Digital ed A.R. Shearer, Government Printer: Wellington, New Zealand. 1974. p. 440. Available from: https://nzetc.victoria.ac.nz/tm/scholarly/tei-BesSton.html

[2] Turner FJ. Geological investigations of the nephrites, serpentines, and related "green stones" used by the Maoris of Otago and South Canterbury. Transactions and Proceedings of the Royal Society of New Zealand. 1936;**65**:187-210

[3] Moore P, McFadgen B. 'Kōhatu—Māori use of stone—Stone tools', Te Ara—The Encyclopedia of New Zealand. Available from: http://www.TeAra.govt.nz/en/kohatu-maori-use-of-stone/page-1 [Accessed: November 15, 2023]. In: Story by Phil Moore and Bruce McFadgen, published 12 Jun 2006. 2023

[4] Anonymus. Blood, Earth, Fire: Whangai, Whenua, Ahi Ka. The Transformation of Aotearoa New Zealand. (Te Papa exhibition). Text originally published in Tai Awatea, Te Papa's onfloor multimedia database (2006). 2023. Available from: https://collections.tepapa.govt.nz/topic/1439: [Accessed: November 15, 2023]

[5] D'Amico C. Neolithic 'greenstone' axe blades from northwestern Italy across Europe: A first petrographic comparison. Archaeometry. 2005;**47**(2):235-252. DOI: 10.1111/j.1475-4754.2005.00199.x

[6] Dolfini A. From the Neolithic to the Bronze Age in Central Italy: Settlement, burial, and social change at the dawn of metal production. Journal of Archaeological Research. 2020;**28**(4):503-556. DOI: 10.1007/s10814-019-09141-w

[7] Claesson S, Bibikova E, Bogdanova S, Skobelev V. Archaean terranes, Palaeoproterozoic reworking and accretion in the Ukrainian Shield, East European Craton. Geological Society Memoir. 2006;**32**:645-654. DOI: 10.1144/GSL.MEM.2006.32.01.38

[8] Sotiriou P, Polat A. Comparisons between Tethyan anorthosite-bearing ophiolites and Archean anorthosite-bearing layered intrusions: Implications for Archean geodynamic processes. Tectonics. 2020;**39**(8):e2020TC006096. DOI: 10.1029/2020TC006096

[9] Váczi B, Szakmány G, Starnini E, Kasztovszky Z, Bendó Z, Nebiacolombo FA, et al. High-pressure meta-ophiolite boulders and cobbles from northern Italy as possible raw-material sources for "greenstone" prehistoric tools: Petrography and archaeological assessment. European Journal of Mineralogy. 2019;**31**(5-6):905-917. DOI: 10.1127/ejm/2019/0031-2859

[10] Giustetto R, Perrone U, Compagnoni R. Neolithic polished greenstone industry from Castello di Annone (Italy): Minero-petrographic study and archaeometric implications. European Journal of Mineralogy. 2016;**28**(5):889-905. DOI: 10.1127/ejm/2016/0028-2558

[11] Nilsson C, Muotka T, Timm H, Malmqvist B. Chapter 12 - The Fennoscandian Shield. In: Tockner K, Zarfl C, Robinson CT, editors. Rivers of Europe. 2nd ed. Elsevier; 2022. pp. 455-496. DOI: 10.1016/B978-0-08-102612-0.00012-2

[12] Sayab M, Molnár F, Aerden D, Niiranen T, Kuva J, Välimaa J. A succession of near-orthogonal horizontal tectonic shortenings in

the Paleoproterozoic Central Lapland Greenstone Belt of Fennoscandia: Constraints from the world-class Suurikuusikko gold deposit. Mineralium Deposita. 2020;**55**(8):1605-1624. DOI: 10.1007/s00126-019-00910-7

[13] Molnár F, Middleton A, Stein H, O'Brien H, Lahaye Y, Huhma H, et al. Repeated syn- and post-orogenic gold mineralization events between 1.92 and 1.76 Ga along the Kiistala Shear Zone in the Central Lapland Greenstone Belt, northern Finland. Ore Geology Reviews. 2018;**101**:936-959. DOI: 10.1016/j.oregeorev.2018.08.015

[14] Eilu P, Pankka H, Keinänen V, Kortelainen V, Niiranen T, Pulkkinen E. Characteristics of gold mineralisation in the greenstone belts of northern Finland. Special Paper of the Geological Survey of Finland. 2007;**2007**(44):57-106

[15] Gangopadhyay A, Walker RJ, Hanski E, Solheid PA. Origin of Paleoproterozoic komatiites at Jeesiörova, Kittilä greenstone complex, Finnish Lapland. Journal of Petrology. 2006;**47**(4):773-789. DOI: 10.1093/petrology/egi093

[16] German CR, Seyfried WE. In: Holland HD, Turekian KK, editors. Treatise on Geochemistry. 2nd ed. Oxford: Elsevier; 2014. pp. 191-233

[17] Johnston Mike R. Chapter 2 The Path to Understanding the Central Terranes of Zealandia. Memoirs. Vol. 49, No. 1. London: Geological Society; 2019. pp. 15-30. DOI: 10.1144/M49.2

[18] Nathan S, Rattenbury MS, Suggate RP. Geology of the Greymouth area. Institute of Geological and Nuclear Sciences 1:250,000 Geological Map. 2002;**12**:1-62

[19] Turnbull IM. Geology of the Wakatipu area. Institute of Geological and Nuclear Sciences 1:250,000 Geological Map. 2000;**2000**(January(18)):1-72

[20] Cooper AF. Nephrite and metagabbro in the Haast Schist at Muddy Creek, northwest Otago, New Zealand. New Zealand Journal of Geology and Geophysics. 1995;**38**(3):325-332. DOI: 10.1080/00288306.1995.9514660

[21] Turnbull IM. Structure and interpretation of the Caples Terrane of the Thomson Mountains, Northern Southland, New Zealand. New Zealand Journal of Geology and Geophysics. 1980;**23**(1):43-62. DOI: 10.1080/00288306.1980.10424191

[22] Bishop DG, Bradshaw JD, Landls CA, Turnbull IM. Lithostratigraphy and structure of the Caples Terrane of the Humboldt Mountains, New Zealand. New Zealand Journal of Geology and Geophysics. 1976;**19**(6):827-848

[23] Kawachi Y. Geology and petrochemistry of weakly metamorphosed rocks in the upper Wakatipu district, southern New Zealand. New Zealand Journal of Geology and Geophysics. 1974;**17**(1):169-208. DOI: 10.1080/00288306.1976.10420742

[24] Tennant WC, Claridge RFC, Mc Cammon CA, Smirnov AI, Beck RJ. Structural studies of New Zealand pounamu using Mössbauer spectroscopy and electron paramagnetic resonance. Journal of the Royal Society of New Zealand. 2005;**35**(4):385-398. DOI: 10.1080/03014223.2005.9517790

[25] Bainbridge D, Witten IH. Greenstone digital library software: Current research. In: Proceedings of the 2004 Joint ACM/IEEE Conference on Digital Libraries, 2004, Tucson, AZ, USA. IEEE - Institute of Electrical and Electronics Engineers; 11 June 2004. p. 416. DOI: 10.1145/996350.996483

[26] Wheen NR. Legislating for indigenous peoples' ownership and management of minerals: A New Zealand case study on pounamu. Management of Environmental Quality: An International Journal. 2009;**20**(5):551-565. DOI: 10.1108/14777830910981212

[27] Adams CJ, Beck RJ, Campbell HJ. Characterisation and origin of New Zealand nephrite jade using its strontium isotopic signature. Lithos. 2007; **97**(3-4):307-322. DOI: 10.1016/j.lithos.2007.01.001

[28] Scott JM. An updated catalogue of New Zealand's mantle peridotite and serpentinite. New Zealand Journal of Geology and Geophysics. 2020;**63**(4):428-449. DOI: 10.1080/00288306.2020.1776738

[29] Coleman RG, New Zealand Geological Survey. New Zealand Serpentinites and Associated Metasomatic Rocks. Wellington, N.Z.: Dept. of Scientific and Industrial Research, New Zealand Geological Survey; 1966

[30] Prokhor SA. The genesis of nephrite and emplacement of the nephrite-bearing ultramafic complexes of east Sayan. International Geology Review. 1991;**33**(3):290-300. DOI: 10.1080/00206819109465694

[31] Beck R. Jade in the South Pacific. In: Keverne R, editor. Jade. Boston, MA: Springer US; 1991. pp. 221-258. DOI: 10.1007/978-1-4615-3922-3_12

[32] Grapes RH, Yun ST. Geochemistry of a New Zealand nephrite weathering rind. New Zealand Journal of Geology and Geophysics. 2010;**53**(4):413-426. DOI: 10.1080/00288306.2010.514929

[33] Cooper AF, Reay A. Lithology, field relationships, and structure of the pounamu ultramafics from the Whitcombe and Hokitika rivers, Westland, New Zealand. New Zealand Journal of Geology and Geophysics. 1983;**26**(4):359-379. DOI: 10.1080/00288306.1983.10422254

[34] Cooper AF, Reay A, Ireland TR, Norman MD. Cretaceous molybdenite in metasomatic epidosite associated with the Pounamu ophiolite, New Zealand. New Zealand Journal of Geology and Geophysics. 2020;**63**(2):227-236. DOI: 10.1080/00288306.2019.1691018

[35] Grapes R, Palmer K. (Ruby-sapphire)—Chromian mica-tourmaline rocks from Westland, New Zealand. Journal of Petrology. 1996;**37**(2):293-315. DOI: 10.1093/petrology/37.2.293

[36] Ireland TR, Reay A, Cooper AF. The Pounamu ultramafic belt in the Diedrich Range, Westland, New Zealand. New Zealand Journal of Geology and Geophysics. 1984;**27**(3):247-256. DOI: 10.1080/00288306.1984.10422295

[37] McClintock MK, Cooper AF. Geochemistry, mineralogy, and metamorphic history of kyanite-orthoamphibole-bearing Alpine Fault mylonite, South Westland, New Zealand. New Zealand Journal of Geology and Geophysics. 2003;**46**(1):47-62. DOI: 10.1080/00288306.2003.9514995

[38] Shao Y, Prior DJ, Toy VG, Negrini M, Scott JM. Does second phase content control the evolution of olivine CPO type and deformation mechanisms? A case study of paired harzburgite and dunite bands in the Red Hills Massif, Dun Mountain Ophiolite. Lithos. 2021;**406-407**:106532. DOI: 10.1016/j.lithos.2021.106532

[39] Tarling MS, Smith SAF, Scott JM, Rooney JS, Viti C, Gordon KC. The internal structure and composition of

a plate-boundary-scale serpentinite shear zone: The Livingstone Fault, New Zealand. Solid Earth. 2019;**10**(4):1025-1047. DOI: 10.5194/se-10-1025-2019

[40] Hanna MN, Hanna DM. Pounamu New Zealand Jade. Jade Press; 1995. p. 28. ISBN: 978-0473030124

[41] Mortimer N, van den Bogaard P, Hoernle K, Timm C, Gans PB, Werner R, et al. Late Cretaceous oceanic plate reorganization and the breakup of Zealandia and Gondwana. Gondwana Research. 2019;**65**:31-42. DOI: 10.1016/j.gr.2018.07.010

[42] Mortimer N. Zealandia (including New Zealand and New Caledonia). In: Alderton D, Elias SA, editors. Encyclopedia of Geology. 2nd ed. Oxford: Academic Press; 2021. pp. 631-641. DOI: 10.1016/B978-0-08-102908-4.00065-5

[43] Mortimer N, Rattenbury MS, King PR, Bland KJ, Barrell DJA, Bache F, et al. High-level stratigraphic scheme for New Zealand rocks. New Zealand Journal of Geology and Geophysics. 2014;**57**(4):402-419. DOI: 10.1080/00288306.2014.946062

[44] Mortimer N, Charlier BLA, Rooyakkers SM, Turnbull RE, Wilson CJN, Negrini M, et al. Crustal basement terranes under the Taupō Volcanic Zone, New Zealand: Context for hydrothermal and magmatic processes. Journal of Volcanology and Geothermal Research. 2023;**440**:107855. DOI: 10.1016/j.jvolgeores.2023.107855

[45] Mortimer N, Lee J, Stockli DF. Terrane and core complex architecture of the Otago Schist in the Dunstan and Cairnmuir Mountains, New Zealand, from U-Pb and (U-Th)/He zircon dating. New Zealand Journal of Geology and Geophysics. 2023. DOI: 10.1080/00288306.2023.2176892

[46] Mortimer N, Williams S, Seton M, Calvert A, Waight T, Turnbull R, et al. Reconnaissance basement geology and tectonics of North Zealandia. Tectonics. 2023;**42**(10):e2023TC007961. DOI: 10.1029/2023TC007961

[47] Challlis GA. The origin of New Zealand ultramafic intrusions. Journal of Petrology. 1965;**6**(2):322-364. DOI: 10.1093/petrology/6.2.322

[48] Lauder WR. The geology of Dun Mountain, Nelson, New Zealand. New Zealand Journal of Geology and Geophysics. 1965;**8**(3):475-504. DOI: 10.1080/00288306.1965.10426418

[49] Coombs DS, Landis CA, Norris RJ, Sinton JM, Borns DJ, Craw D. Dun Mountain Ophiolite Belt, New Zealand, its tectonic settings, constitution, and origin, with special reference to the southern portion. American Journal of Science. 1976;**276**(5):561-603. DOI: 10.2475/ajs.276.5.561

[50] Davis TE, Johnston MR, Rankin PC, Stull RJ. The Dun mountain ophiolite belt in East Nelson, New Zealand. In: Proceedings of the International Ophiolite Symposium, Nicosia, Cyprus, 1979. Republic of Cyprus, Ministry of Agriculture and Natural Resources, Geological Survey Department; 1980. pp. 480-496

[51] Reed JJ. Mineralogy and petrology in the New Zealand Geological Survey 1865-1965. New Zealand Journal of Geology and Geophysics. 1965;**8**(6):999-1087. DOI: 10.1080/00288306.1965.10428155

[52] Hu CN, Santosh M, Yang QY, Kim SW, Nakagawa M, Maruyama S. Magmatic and metasomatic imprints in a long-lasting subduction zone: Evidence from zircon in rodingite and serpentinite of Kochi, SW Japan. Lithos.

2017;**274-275**:349-362. DOI: 10.1016/j.lithos.2017.01.008

[53] Roser BP, Cooper AF. Geochemistry and terrane affiliation of Haast Schist from the western Southern Alps, New Zealand. New Zealand Journal of Geology and Geophysics. 1990;**33**(1):1-10. DOI: 10.1080/00288306.1990.10427567

[54] Cooper AF, Ireland TR. The Pounamu terrane, a new Cretaceous exotic terrane within the Alpine Schist, New Zealand; tectonically emplaced, deformed and metamorphosed during collision of the LIP Hikurangi Plateau with Zealandia. Gondwana Research. 2015;**27**(3):1255-1269. DOI: 10.1016/j.gr.2013.11.011

[55] Cooper AF, Price RC, Reay A. Geochemistry and origin of a Mesozoic ophiolite: The Pounamu ultramafics, Westland, New Zealand. New Zealand Journal of Geology and Geophysics. 2018;**61**(4):444-460. DOI: 10.1080/00288306.2018.1494005

[56] Németh K, Palmer J. Westland geoheritage of a rifted Gondwana margin—A potential UNESCo Global gfeopark. Geoscience Society of New Zealand Miscellaneous Publications. 2018;**151A**:194

Edited by Károly Németh

This book is a collection of works on new research in metamorphic geology. The chapters cover a broad range of subjects, including new advances as well as field-based approaches to and novel technologies for solving metamorphic geology problems, including micromineralogy, microanalytical, geostatistical, microtextural, Geographical Information Systems (GIS), and remote sensing methods.

Published in London, UK

IntechOpen

ISBN 978-0-85466-495-5